



Università Politecnica delle Marche

Master's Degree in Environmental Engineering

**Application of a hydrokinetic turbine along the Misa River
(Senigallia, Italy): a numerical investigation**

**Applicazione di una turbina idro-cinetica lungo il fiume Misa
(Senigallia, Italia): un'analisi numerica**

Advisor

Dr. Matteo Postacchini

Co-advisors

Dr. Gianluca Zitti

Dr. Eleonora Perugini

Student

Riccardo Rossetti

ACADEMIC YEAR 2021/2022

Contents

1	INTRODUCTION.....	6
1.1	Fluvial and estuary hydraulics	8
1.2	Hydrokinetic turbine: state of the art	11
1.3	Description of the area	16
1.4	Available data	20
1.4.1	Hydrometric data acquisition	20
1.4.2	Tidal stage data acquisition	23
2	MATERIALS AND METHODS.....	27
2.1	HEC-RAS software description.....	28
2.1.1	Steady flow analysis.....	28
2.1.2	Unsteady flow analysis	37
2.1.3	Software interface	39
2.2	Hydrokinetic technology principles.....	50
2.2.1	The ductless Archimedes turbine	52
3	RESULTS	63
3.1	Selection of the typical year.....	63
3.2	Model implementation and calibration	74



3.2.1	Model setup	74
3.2.2	Calibration of the model.....	84
3.3	Energetic analysis	104
3.3.1	Cross sections selection.....	105
3.3.2	Turbines configuration	112
3.3.3	Energetic production calculations	115
4	DISCUSSION	124
5	CONCLUSIONS.....	128
6	REFERENCES.....	131
7	ACKNOWLEDGMENTS.....	133

Abstract

This thesis is devoted to the assessment of the potential power production of a hydrokinetic turbine, object of study in the Hydraulics laboratory of UNIVPM in the recent years. The turbine is supposed to be applied along the final stretch of the Misa River, on the basis of the results coming from the hydraulic modelling performed through the use of the HEC-RAS software. Firstly, a preliminary statistical analysis of the available hydrometric data (collected by the Civil Protection of the Marche Region) has been performed in order to select the typical year, for which the data have been extracted with the aim to build up the model. Afterwards, the model has been calibrated, acting mostly on input parameters, such as Manning coefficients and boundary conditions. Finally, the results of the simulated year, such as channel velocity and river stage along the whole river stretch, have been used to choose possible locations and configurations of hydrokinetic Archimedes screw turbines, in order to perform an energy production assessment.

Sommario

Questa tesi è dedicata alla stima della possibile produzione di energia di una turbina idro-cinetica, già oggetto di studio nel laboratorio di Idraulica e Costruzioni Marittime dell'UNIVPM. Si è ipotizzato di applicare la turbina lungo la parte finale del fiume Misa, sulla base dei risultati provenienti dalla modellazione idraulica realizzata mediante il software HEC-RAS. Inizialmente, è stata fatta un'analisi statistica preliminare dei dati idrometrici (raccolti dalla Protezione Civile della Regione Marche), in modo da poter selezionare l'anno tipico, per il quale sono stati estratti i dati necessari alla costruzione del modello numerico. Successivamente, il modello è stato calibrato, agendo su diversi parametri di input, come i coefficienti di Manning e le condizioni al contorno. Dopo la modellazione, i risultati di tutto l'anno simulato, come la velocità del flusso e il livello idrometrico di tutto l'arco di fiume studiato, sono stati utilizzati per scegliere alcuni possibili luoghi di installazione e relative configurazioni di un sistema di turbine idrocinetiche a vite di Archimede, così da valutarne la produzione di energia.

1 INTRODUCTION

The aim of this work lies on the assessment of the energy production of a hydrokinetic turbine in the Misa River, which is a river that flows through the Marche Region and that ends in Senigallia municipality, on the basis of a numerical-model simulation.

The hydraulic model implementation is very important, both from a scientific and from a practical point of view: in fact, it allows to perform a preliminary analysis, a starting point for many further analyses of different aspects relative to the river, such as any environmental potential problems (e.g. floods, banks erosion), or for the evaluation of the feasibility of any developing technologies, which is, in particular, the key aspect of this work.

The model construction requires different data, such as cross-sections coming from field surveys, river discharges, tidal ranges, bathymetric surveys and so on: the accuracy of the model strictly depends on the precision of these data. Thus, the more the data are updated, accounting for any changes that the river basin could be subjected with time, the more the results will be accurate.

In this thesis, a hydraulic model has been developed by using the HEC-RAS software, one of the most used open-source software in this field: it allows to model one and two dimensional natural and anthropic channel networks, performing different types of analyses (e.g. steady simulations, unsteady simulations, sediment transport). In this work, the modelling phase started from a previously constructed model and the focus was on the calibration of it.

The second phase of the work was the evaluation, based on the results of the hydraulic model, of the possible energy production using a hydrokinetic turbine, which is object of study in the Hydraulics department of the UNIVPM: the innovative aspect of this technology is that this turbine works with lower river discharges and velocities in respect to the conventional turbines used in traditional hydropower plants: this implies a lower amount of energy production but, on the other hand, a much lower environmental impact and much lower costs, as these micro turbines don't need important engineering constructions, such as dams. Moreover, this type of technology does not require any specific geomorphological characteristics of the river area, as it doesn't need a high hydraulic jump or any additional construction facilities.

The thesis is organised as follows: after a description of the state of the art, materials and method used are reported (Chapter 2) and the results (Chapter 3) have been divided into three main parts, such as the data analysis (phase 1), the numerical model implementation and calibration (phase 2) and the energy production assessment (phase 3), followed by the discussion (Chapter 4) and the conclusions (Chapter 5).

1.1 Fluvial and estuary hydraulics

A river is a natural flowing watercourse, usually freshwater, flowing towards an ocean, sea, lake or another river: they can flow down mountains, through valleys or along plains, and can create canyons or gorges.

The river channel typically contains a single stream, but some rivers flow as several interconnecting streams, producing a braided river; flowing in its channel, it is a source of energy that acts on the river channel to change its shape and form.

In the middle reaches where a river flows over flatter land, meanders may form through erosion of the river banks and deposition on the inside of bends.

Throughout the course of the river, the total volume of water transported downstream will often be a combination of the free water flow together with a substantial volume flowing through sub-surface rocks and gravels that underlie the river and its floodplain.

In coastal environments, two types of river mouth, depending on the way the river flows into the sea, exist, i.e. river estuary and river delta. Focusing on the former classification, “an estuary is a partially enclosed coastal body of brackish water with one or more rivers or streams flowing into it, and with a free connection to the open sea” (Pritchard, 1967). Figure 1 shows both types of river mouth.



Figure 1 – Types of river mouth: river delta (left) and river estuary (right)

Estuarine environments are dynamically complex, with the hydrodynamics being triggered by many factors, such as nonlinear interactions between the bathymetry, the river current and many sea forcing actions. The sediment transport and related morphodynamics derives from such complexity and act in the estuarine region by shaping the riverbed and sometimes leading to interesting morphological features, like river mouth bars that, after being generated, migrate and evolve in proximity of the river mouth.

Another classification of the estuaries can be made according to the water circulation, thus including salt-wedge estuaries, partially mixed estuaries, well-mixed estuaries, inverse estuaries and intermittent estuaries: this classification depends on the interactions between freshwater and seawater, in terms of both physical and chemical characteristics (tidal forcing, salt concentration, etc.).

Further, estuaries can be split out depending on the tidal range extent: in particular, micro-tidal (less than 2 m), meso-tidal (between 2 m and 4 m), and macro-tidal (higher

than 4 m) may occur. In Mediterranean climates, micro-tidal estuaries generally have narrow mouths, are poorly flushed and have relatively long water residence times, i.e., typically weeks to months, whereas macro-tidal estuaries are generally funnel-shaped and well-flushed, with relatively short residence times, i.e., typically hours to days.

1.2 Hydrokinetic turbine: state of the art

When we talk about “hydrokinetic turbine”, we talk about an emerging class of renewable energy technology, strongly recognized as a unique and unconventional solution feasible for both in-land water resources and marine energy.

The process of hydrokinetic energy conversion implies utilization of kinetic energy contained in river streams, tidal currents, or other man-made waterways for generation of electricity (Khan, 2009).

The main difference with conventional hydroelectric plants, where an artificial water-head is created using dams and/or penstocks (for large-hydro and micro-hydro, respectively), is basically that hydrokinetic converters can be constructed without significantly altering the natural pathway of the water stream: thus, this kind of systems is expected to be more environmentally friendly when compared to the conventional ones or tidal barrage systems and, furthermore, with characteristics of modularity and scalability, which are attractive features under different points of view.

On the other hand, scepticism on the technological viability is very strong: in addition to several fundamental inquiries (resource availability, definition of technologies, field of application, etc.), a number of technology-specific questions (e.g. what converter type is best suited, whether duct augmentation is worth attempting, how to place a turbine in a channel) are issues that have been put forward for many years.

Now, the climatic changes and the worldwide environmental crisis impose to study and solve these problems, looking for the most efficient solutions (this is the corner stone of this work as well).

As exploitation of this, different interrelated concepts categorized in two broader classes (turbine/non turbine systems, Figure 2 and 3) have been developed or, as in case of non-turbine systems, are mostly at the proof-of-concept stage.

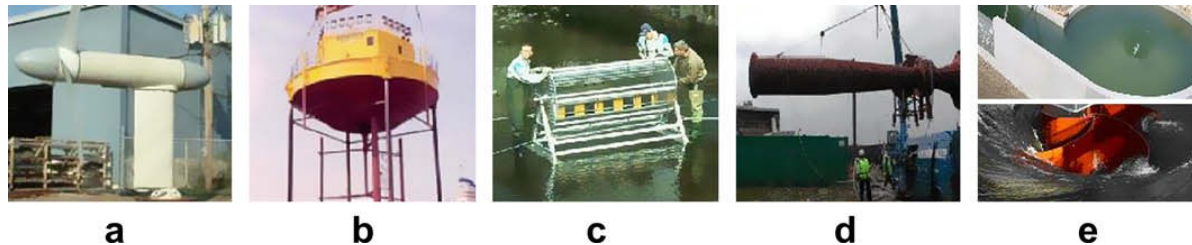


Figure 2 - Example of turbine systems: (a) Free Flow; (b) Kobold; (c) Atlantisstrom; (d) HydroVenturi; (e) Neo-Aerodynamic (Khan, 2009)

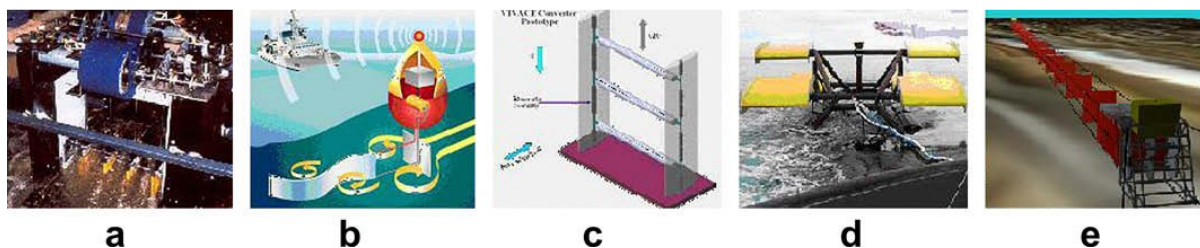


Figure 3 - Example of non-turbine systems: (a) OCPS; (b) EEL; (c) VIVACE; (d) Seasnail; (e) Tidal Sails (Khan, 2009)

The term “Hydrokinetic Turbine” has long been interchangeably used with other synonyms, such as: “Water Current Turbine” (WCT), “Ultra-low-head Hydro Turbine”, “Free Flow/Stream Turbine” (implying use of no dam, reservoir or augmentation), “Zero Head Hydro Turbine”, or “In-stream Hydro Turbine”. They are used in tidal application and, as our case, rivers or artificial waterways application: the converters of the first technology are often termed as “Tidal In-stream Energy Converter” (TISEC) or simply “Tidal Current Turbine”, whereas, for the latter one, they are generally identified as “River Current Turbine (RCT)”, “River Current Energy Conversion System” (RCECS), “River Instream Energy Converter” (RISEC) or, in brief, “River Turbine”.

In order to better understand the field of study, in the following are reported a couple of definitions given by the US Department of Energy (USDoE):

- “Low pressure run-of-the-river ultra-low-head turbine that will operate on the equivalent of less than 0.2 m of head” (1981);
- a more recent (2006) assessment has classified these devices as “Low Power/Unconventional Systems that may use hydro resources with less than 8 feet head”.

Moreover, the USDoE reported the hydropower potential and working hydraulic head of a potential project as measures of technology classification: this also indicates that the conventional hydroelectric plants use higher head and/or capacity in sharp contrast to the unconventional low-head/hydrokinetic schemes, as shown in Figure 4.

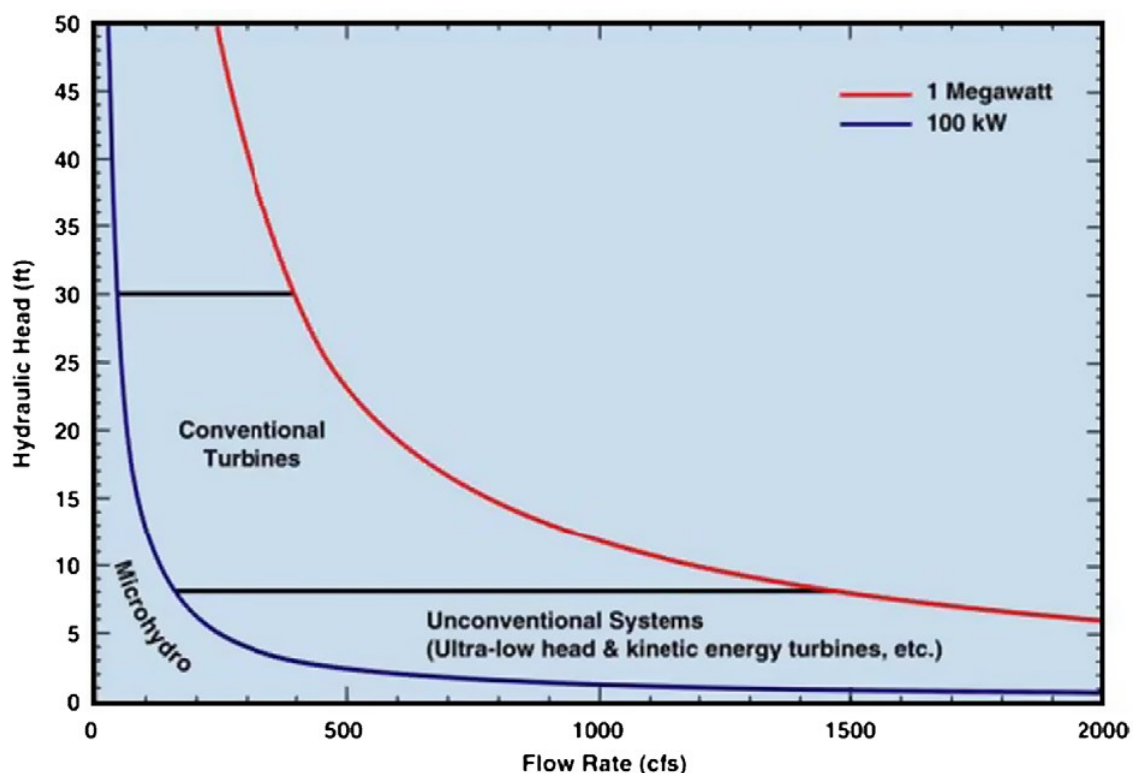


Figure 4 - Conventional hydro versus hydrokinetic energy conversion schemes

All the hydrokinetic devices operated on the same conversion principles regardless of their areas of application and, focusing on the river applications, some design and operational features are reported.

Design

- *Size*: river turbines are being considered in the range of few kW to several hundred kW;
- *Directionality*: river flow is unidirectional and this eliminates the requirement for rotor yawing;
- *Placement*: depending on the channel cross-section, a river current turbine may be placed at the seafloor/riverbed or in other arrangements (floating or mounted to a near-surface structure).

Operation

- *Flow characteristics*: the flow characteristic of a river stream has strong stochastic variation (seasonal to daily);
- *Control*: the stochastic variation typical of river turbines implies an impossibility to operate in forecasted condition, so an active dynamic control system may need to be synthesized.

End-use

- *Grid-connectivity*: hydrokinetic converters used in river streams may become feasible in powering remote areas or stand-alone loads. Depending on how the technology evolves, this type of schemes may also fall within the distributed generation scenarios in the near future;

- *Other purposes:* hydrokinetic turbines can potentially be used in conjunction with an existing large hydroelectric facility, where the tailrace of a stream can be utilized for capacity augmentation (i.e, resource usage maximization). Other potential areas of end-use may be direct water pumping for irrigation, desalination of seawater and space heating.

1.3 Description of the area

The Misa River is a river of the Marche region and it is entirely comprised in the Ancona province (Figure 5): its length is about 45 kilometres, with a catchment (Figure 6) of approximately 383 km² and a discharge of 400, 450 and 600 m³/s for return periods of 100, 200, and 500 years, respectively (Brocchini, et al., 2017); the average stage is slightly lower than 1 m and the average hydraulic gradient “*i*” is 11.34% (Regione Marche - Autorità di Bacino Regionale, 2016).

The Misa River flows into an estuary which is, following the water circulation classification, characteristic of a salt-wedge estuary.

The River basin is bounded by the Cesano watershed north-westward, by the Esino river watershed south-eastward and by the Sentino stream (an Esino river tributary) sub-basin southward.



Figure 5 - Misa River location

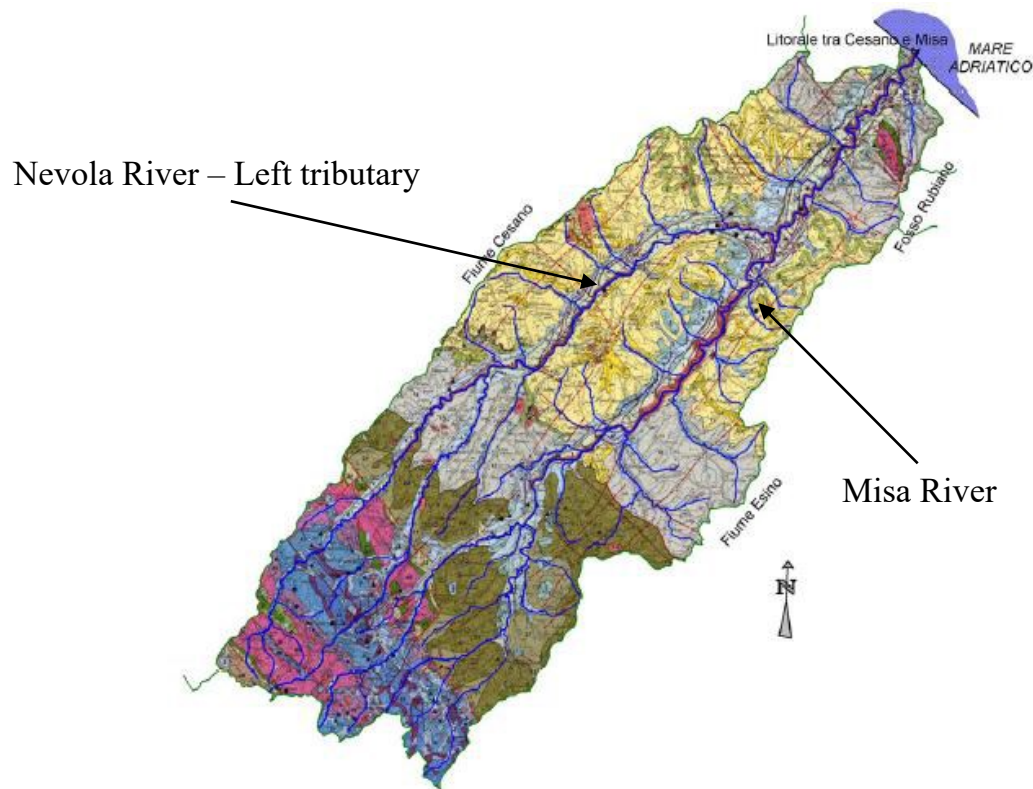


Figure 6 - Misa River catchment

The Misa River watershed is enclosed between the following municipalities: Arcevia, Barbara, Belvedere Ostrense, Castelleone di Suasa, Corinaldo, Genga, Mergo, Montecarotto, Ostra, Ostra Vetere, Poggio San Marcello, Rosora, Sassoferrato, Senigallia, Serra dei Conti, Serra San Quirico, Trecastelli (Castelcolonna and Ripe).

The river, born on the south-west slope of the Arcevia' anticlinal, is of Apennine origin and has its estuary in Senigallia. The direction of the flow is SW-NE and it ends into the Adriatic Sea. The last portion of the river is bounded by two reinforced concrete walls, with jetties stick out on the shoreline longitudinal profile for about 250 m.

The main Misa River left tributary is the Nevola River, which, in turn, generates from the confluence between the Fenella stream and the Acquaviva stream, and joins the Misa River at about 9 km before its end, thus ensuring a remarkable increase of both

solid and liquid flows (Figure 6). The Nevola River, along with the Acquaviva stream, point in the same direction as the Misa River (SW-NE).

As most of the rivers of the Marche Region, the Misa river has a torrential regime, with poor or null flows during dry periods and very high flows (order of hundreds of cubic meters per second) during rainy periods: this is due to the geological, geomorphological, lithological and climatic characteristics of the watershed. In particular, the basin is composed mainly by clayey rocks (around 85%), thus it has a low permeability degree, except for the most inner area, where it is made up of calcareous rocks, which has, thanks to fracturing, a secondary permeability. In general, this lithology leads to a fairly high runoff coefficient, with low subsoil infiltration and very fast meteoric water discharges along the slope, with relatively short times of concentration.

The basin, as shown in Figure 6, is significantly asymmetric: the left tributaries are more developed in respect to the right ones, and they predominantly participate to the river discharge.

The river presents many meander-like shape flow paths, with a strong influence of a number of anthropic structures, such as:

- many roads that cross the channel transversally, with their relative bridges (23 bridges and 2 traverses, in specific), the majority of whom are located upstream of Pianello di Ostra, thus implying a strong vertical erosion;
- numerous transversal and longitudinal river banks protections, such as protecting walls (stone gabions, concrete cubes, concrete slabs, reinforced Jersey

barriers), bank strengthening (using soft approach, i.e. bioengineering) and cliffs (gigantic calcareous boulders, concrete hexapods and tetrapods).

The watershed has narrow deep valleys in the upstream section and enlargements moving downstream, with the presence also of alluvial terraces (most developed on the hydrographic left).

From a geological point of view, the alluvial terraces in the middle section of the catchment are made of gravel and calcareous boulders intertwined with gravelly-sandy lenses. On the other side, for what regards the alluvial deposits, they are characterized by an increased clayey fraction.

1.4 Available data

1.4.1 Hydrometric data acquisition

The hydrometric data have been downloaded from the **SIRMIP**¹ (Sistema Informativo Regionale Meteo-Idrio-Pluviometrico) website, which is a database belonging to the “Centro Funzionale Multirischi” of the Civil Protection of the Marche Region: through it, it is possible to have free access to different hydro-meteorological data, such as hydrometry, pressure, precipitation, humidity, temperature, snow, solar radiation and wind data.

These data, which were originally managed by the Servizio Idrografico e Mareografico Nazionale (SIMN) and only later by the Civil Protection (2002), are based on two distinct networks, which are:

- a mechanical network, developed by the SIMN in the 1916, that owned thermometers, rain gauges and hydrometers as sensors. When these tasks have been managed by the Civil Protection, the network was composed by 21 thermometers and 83 rain gauges;
- a telemetric network, consisting of 53 thermometers, 77 rain gauges, 13 anemometers, 15 barometers, 30 hygrometers, 7 snow-meters and 70 hydrometers along with a hydrometric rod for the calibration measures, which were installed in Marche Region following the strengthening program for the weather, hydro, pluviometric monitoring stations. Since January 2019, this type of network fully replaced the mechanical one and both the number and the types

¹ SIRMIP website: <http://84.38.48.145/sol/indexjs.php?lang=it>

of the sensor increased. In the past 15 years, some hydrometric stations have been equipped with sensor able to estimate discharges in continuous.

Through the use of this database, the data for the hydraulic analysis of the Misa River have been downloaded: in particular, data of the hydrometric level and relative rating curves have been selected and organized in excel files.

The stations of interest for the purpose of the work, reported in Figure 7, are:

- Bettollelle, which is the upstream cross-section, i.e. the initial boundary condition for the numerical model: in particular, the downloaded data from this sensor are the ones related to the hydrometric level and the relative rating curves;
- Ponte Garibaldi, which is a section near to the river estuary, that has been use as “check section” for the model calibration. In this case, only hydrometric level data have been downloaded (rating curves for this sections were not available).



Figure 7 - Station locations: RG1 (Ponte Garibaldi) and RG2 (Bettollelle)

As shown in Figure 8, on the SIRMIP website, there's the possibility of choosing either the basin and/or the province and/or the municipality where the data acquisition is required. Then, it is also possible to select the needed sensors (the place of the stations) together with the type of data to download, that can be directly downloaded in both text file and excel format, depending on their availability.

Bacino: **Misa** Provincia: (Tutte) Comune: **Senigallia** 2 sensori trovati
 Seleziona sensore, tipo dato, elaborazione e periodo.

Seleziona sensori ▾

Tipo dato: ☒ Dato Validato ☐ Dato Originale

Elaborazione: ☒ Livello idrometrico [m] ☐ Livello idrometrico min/max [m] ☐ Livello idrometrico ore 12 [cm]

☐ Portata massima [m3 s-1] ☐ Portata media giornaliera [m3 s-1] ☐ Scala di deflusso

☐ Portata media mensile [m3 s-1] ☐ Portata media annuale [m3 s-1] ☐ Portata [m3 s-1]

☐ Presenza in Annali Idrologici 2 ☐ Coordinate ☐ Afflussi meteorici mensili ed annuali

☐ Caratteristiche idrologiche

Data inizio (AAAA-MM-GG hh:mm) 2018-01-01 00:00 Data fine 2018-05-31 23:30

Premere un tasto per estrarre i dati:

Figure 8 - SIRMIP website data download interface

Note that data can be downloaded as “Original data” or “Validated data”, which is an aspect that will be discussed chapter 3.1.

Then, the rating curves, only available for Bettolle station, have been downloaded and reported in Table 1.

Validity beginning					Validity end					Validity range [m]		
Year	M	D	H	Min	Year	M	D	H	Min	Min	Max	Discharge [m ³ /s]
2005	1	1	0	30	2006	1	1	0	0	0.56	4.34	$Q = 8.39 * [H - (0.55)]^{2.323} + 0$
2006	1	1	0	30	2007	1	1	0	0	1.02	5.01	$Q = 23.351 * [H - (1.011)]^{1.659} + 0$
2007	1	1	0	30	2008	12	13	7	0	0.77	4.33	$Q = 9.4265 * [H - (0.76)]^{2.137} + 0$
2008	12	13	7	30	2011	1	1	0	0	0.77	4.01	$Q = 11.4929 * [H - (0.76)]^{1.8516} + 0$
2011	1	1	0	30	2011	3	1	10	30	0.77	9999	$Q = 11.4929 * [H - (0.76)]^{1.8516} + 0$
2011	3	5	0	30	2015	5	23	6	30	0.55	4.39	$Q = 6.195 * [H - (0.517)]^{2.576} + 0$
2011	3	5	0	30	2015	5	23	6	30	4.4	6.35	$Q = 185.568 * [H - (4.39)]^{1.138} + 202.776$
2015	5	23	7	0	2017	3	7	16	0	0.2	1.51	$Q = 5.9 * [H - (0.148)]^{2.934} + 0$
2015	5	23	7	0	2017	3	7	16	0	1.52	3.01	$Q = 27.549 * [H - (1.51)]^{1.188} + 14.609$
2015	5	23	7	0	2017	3	7	16	0	3.02	6.5	$Q = 101.284 * [H - (3.01)]^{1.061} + 59.209$
2017	3	7	16	30	2018	3	5	0	0	0.95	3.02	$Q = 14.388 * [H - (0.942)]^{1.974} + 0$
2017	3	7	16	30	2018	3	5	0	0	3.03	6.5	$Q = 100.396 * [H - (3.02)]^{1.068} + 60.954$
2019	12	15	0	0	2030	1	1	0	0	0.85	1.03	$Q = 2.33 * [H - (0.84)]^{0.79} + 0$
2019	12	15	0	0	2030	1	1	0	0	1.04	2.1	$Q = 19.68 * [H - (1.03)]^{1.24} + 0.6$
2019	12	15	0	0	2030	1	1	0	0	2.11	3.8	$Q = 64.05 * [H - (2.1)]^{1.26} + 22.01$
2019	12	15	0	0	2030	1	1	0	0	3.81	5.5	$Q = 155.87 * [H - (3.8)]^{1.16} + 146.7$

Table 1 - Bettolle station rating curves with relative range of validity

Each equation reported is referred to a specific range of validity, in terms of both time (i.e. initial and ending date of validity) and space (i.e. the hydrometric level range of validity). The reason why there are a number of different equation is that they are strictly dependant on the geometry of the cross-section.

1.4.2 Tidal stage data acquisition

The “Servizio Mareografico Nazionale” (SMN) of the “Istituto Superiore per la Protezione e la Ricerca Ambientale” (ISPRA), is aimed at taking care of all the aspects related to the marine climate, the coast status and the marine levels, providing the publication of the observed and elaborated data, accompanied by cartography, standards and collection methods. In the marine environment, the SMN has assumed the management of the “Rete Ondametrica Nazionale” (RON), which has led to the empowerment and development of the “Rete Mareografica Nazionale” (RMN).

The RMN is composed of 36 measuring stations, which are evenly distributed on the national territory, and mainly located within the port facilities.

For almost all stations of the RMN, the hydrometric level is monitored by using a microwave sensor (radar) that owns a millimetric accuracy, and it is coupled with a second floating gauge. Moreover, also the historical ultrasound hydrometric sensor is in operation. By comparing the outputs coming from these three sensors, where the ultrasound one is used as verification, the ISPRA is able to efficiently calibrate the radar sensor, in order to achieve an excellent accuracy in stage data.

Each stage sensor computes the reading with respect to an oceanographic rod whose height has been set in relation to the “Istituto Geografico Militare” (I.G.M.) altimetric network, by connecting to the closest I.G.M. cornerstone. The stations are also equipped with an anemometric sensor which gathers wind direction and velocity data at 10 meters above ground level, a barometric sensor, an air temperature sensor and a water temperature sensor along with a relative moisture sensor. Furthermore, 10 stations come with a multiparametric probe aimed at evaluating the water quality: the measured parameters are the water temperature, pH, conductivity and redox.

All stations are provided with local system for the management and the storage of data, and with a transmission apparatus (UMTS) linked directly to the SMN headquarter in Rome. In addition, for 9 strategic stations addressed to particular phenomena measurements (rogue waves), is present a second satellite transmission data system, which ensures the connection even in the case of UMTS system black-out events.

All the data collected by the SMN are available and can be easily download from the ISPRA website²: through it, it is possible to choose different stations on the left and then select the desired data for a specific time interval (starting from 1st January 2010).

Regarding the present work, tidal stages data have been used as final boundary condition of the HEC-RAS model. At first, data coming from Ancona station have been used, which is located at a latitude of 43°37'29.16'' and at a longitude of 13°30'23.46'' and it is placed right on the S.Primiano harbor. The station is equipped with altimetric cornerstones, where each of them is set with the average sea level measured at Genova municipality by the ancient Thomson tidal gauge.

The downloaded data, since they are recorded every ten minutes, are given with this time interval, so they have been arranged similarly to the hydrometric level data, i.e. with the same time interval of 30 minutes, in order to make possible a comparison between the two datasets. This operation has been done filtering the tidal stage data, removing the values relative to intermediate time steps (i.e. relative to 10, 20, 40 and 50 minutes of each hour).

Then, also data coming from a recently installed tide gauge at Senigallia harbour have been used in the final calibration step of the model. These data are slightly different from the Ancona station data for two main reasons, such as:

- the distance between the two tide gauges;

² ISPRA website:

<https://www.mareografico.it/?session=0S287294898082H88C85Z6672&syslng=ita&sysmen=-1&sysind=-1&syssub=-1&sysfnt=0&code=RETE&idr=1>

- the different reference systems used for the two datasets: in particular, the difference from the zero of the Ancona tide gauge and the zero of the Senigallia tide gauge (which has been used as average sea level reference system of the numerical model), determined on the results of last surveys, is equal to 0.078 m.

The tidal stage datasets of Senigallia tide gauge and Ancona tide gauge are shown in Figure 9.

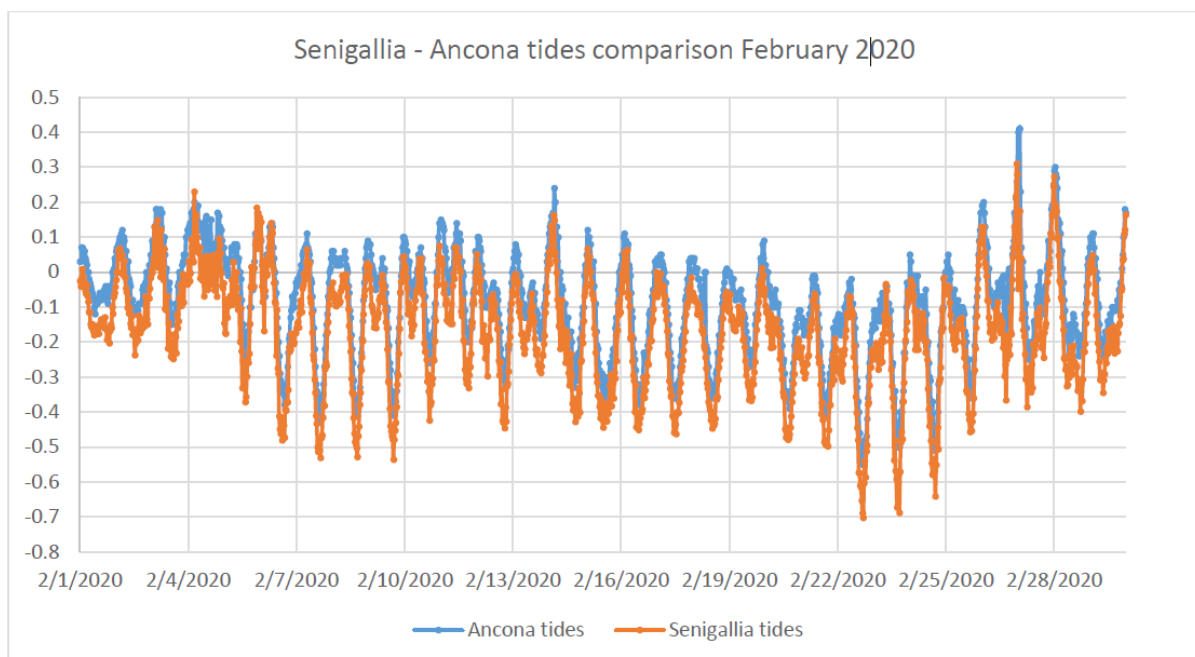


Figure 9 - Comparison between Ancona and Senigallia tidal motion

2 MATERIALS AND METHODS

The present work is divided into three main phases:

1. Initially, hydrometric data of the Misa River have been analysed: in particular, the whole dataset of fifteen years (from 2005 to 2020) has been downloaded from the SIRMIP website. By means of statistical analysis, the “typical year” has been selected and its data have been used as a boundary condition for the hydraulic numerical model;
2. then, data have been implemented into the software HEC-RAS, in an existing hydraulic model (Martinelli, 2021; Ilari, 2021): once all its parameters (boundary conditions, bathymetry, etc.) have been arranged for the typical year, the model has been calibrated, comparing the model results with the measured data (i.e. hydrometric level in a check cross-section, near the river estuary) and evaluating the Root Mean Square Error (RMSE) between them;
3. finally, with the help of the hydraulic simulation results, a number of hypothetical cross-sections have been selected, which were the ones with the most suitable characteristics for the application of a system of hydrokinetic turbine with different dimensions and setup parameters. For each of these configurations, the available power and the extracted power have been assessed, and the results have been critically analysed and discussed.

2.1 HEC-RAS software description

HEC-RAS is an open-source software developed by the US Army Corps of Engineers in 1995 at the Hydrologic Engineering Centre (HEC) in Davis, California, and it is one of the most famous software codes for the modelling of one and two-dimensional natural and anthropic channel networks (River Analysis System, RAS).

It allows to carry out simulations of different phenomena in different conditions, such as:

- steady flow condition, either in sub-critical and/or super-critical and/or mixed regimes, in order to analyse mild slope flows in a single channel or in channel networks;
- unsteady flow condition;
- solid transport hydrodynamic processes simulations (e.g. erosion and/or deposition);
- water quality simulations (water temperature analysis, dissolved oxygen or organic materials transport).

The employed version is the 6.0, which allows, in particular, to perform two-dimensional hydraulic simulations in unsteady flow environments, which are key aspect of this work.

2.1.1 Steady flow analysis

The software, performing a steady flow analysis, is able to return water profiles relative to steady or quasi-steady flow conditions: these results are elaborated by the software

applying the law of conservation of energy to two consecutive cross-sections (Figure 10) through the “standard step method”, which consist of an iterative process.

The law of conservation of energy is represented by the following equation:

$$Z_2 + Y_2 + \frac{\alpha_2 V_2^2}{2g} = Z_1 + Y_1 + \frac{\alpha_1 V_1^2}{2g} + h_e \quad (1)$$

Where:

Z_1, Z_2 = thalweg of the two cross-sections;

Y_1, Y_2 = water depth (stage) at the two cross-sections;

V_1, V_2 = average velocity of the two cross-sections (total discharge/total flow area);

α_1, α_2 = velocity weighting coefficients of the two cross-sections;

g = gravitational acceleration;

h_e = energy head loss.

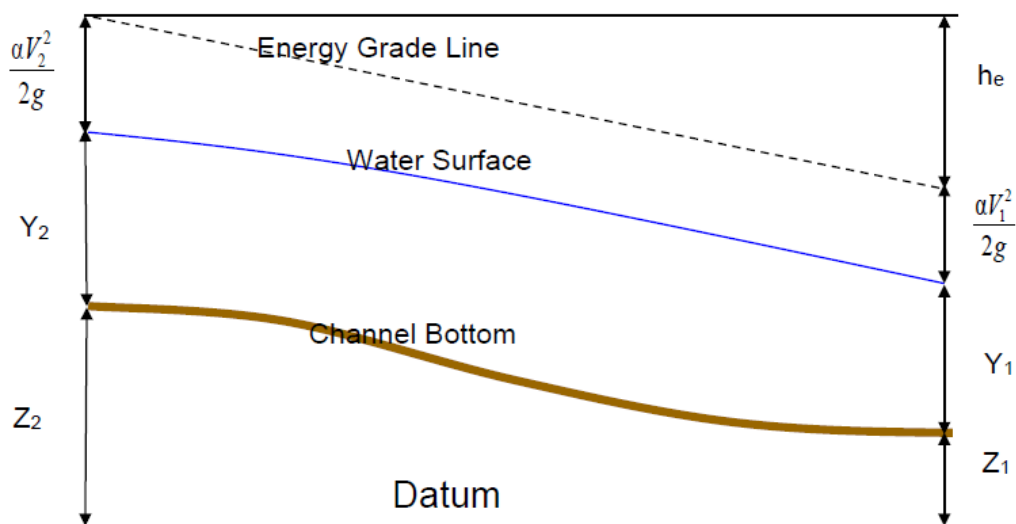


Figure 10 - Representation of the terms of the energy equation

More in details, the last term h_e , the head loss between the two cross-section, takes into account both the friction losses due to roughness and contraction/expansion losses; it is calculated by the following equation:

$$h_e = L\bar{S}_f + C \left| \frac{a_2 V_2^2}{2g} - \frac{a_1 V_1^2}{2g} \right| \quad (2)$$

Where:

\bar{S}_f = friction slope (slope of the energy grade line) between the two cross-sections;

C = expansion (or contraction) loss coefficient;

L = average length of the reach between the two cross-sections weighted with respect to the discharge distribution in the cross-sections, which is evaluated as:

$$L = \frac{L_{lob}\bar{Q}_{lob} + L_{ch}\bar{Q}_{ch} + L_{rob}\bar{Q}_{rob}}{\bar{Q}_{lob} + \bar{Q}_{ch} + \bar{Q}_{rob}} \quad (3)$$

Where L_{lob} , L_{ch} , L_{rob} are referred to the cross-sections reach lengths specified for flow in the left overbank (“lob”), main channel (“ch”), and right overbank (“rob”), respectively, while \bar{Q}_{lob} , \bar{Q}_{ch} , \bar{Q}_{rob} are the arithmetic averages of the flows between sections for the left overbank, main channel, and right overbank, respectively.

As natural stream channels are usually composed of very heterogeneous materials and different type of vegetation as well, the cross-sections are considered composed of different parts, each of them with a specific roughness coefficient, called Manning coefficient “ n ” (Figure 11).

Thus, the total conveyance (flow per unit of head loss per unit of length) is calculated, in order to determine the slope of the energy grade line S_f , through the use of Manning equation for each subdivision of the cross section:

$$Q = KS_f^{\frac{1}{2}} \quad (4)$$

$$K = \frac{1.486}{n} AR^{\frac{2}{3}} \quad (5)$$

where:

K = conveyance for each subdivision;

n = Manning coefficient for each subdivision;

A = flow area for subdivision;

R = hydraulic radius for subdivision (A/P, with P = wet perimeter);

S_f = slope of the energy grade line.

These values of the conveyance factor are summed up by the software in order to get three final values for:

- K_{lob} = conveyance factor for the left overbank;
- K_{rob} = conveyance factor for the right overbank;
- K_{ch} = conveyance factor for the main channel, computed as a single element.

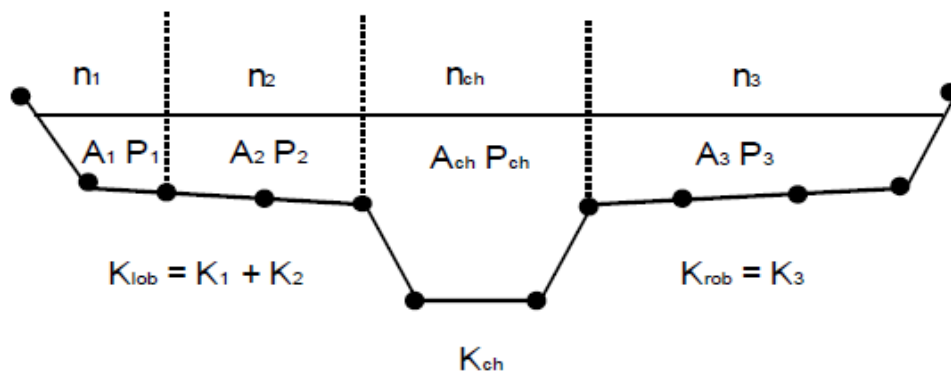


Figure 11 - Default conveyance factor subdivision method

The total conveyance for the whole section is obtained by summing up all the three subdivision conveyances (K_{lob} , K_{rob} , and K_{ch}): this method is the default one in HEC-RAS for calculating the conveyances throughout the cross-sections.

An alternative procedure is also available, in which the conveyance is evaluated between every point in the overbanks, instead of calculating it within just the subdivision, as shown in Figure 12.

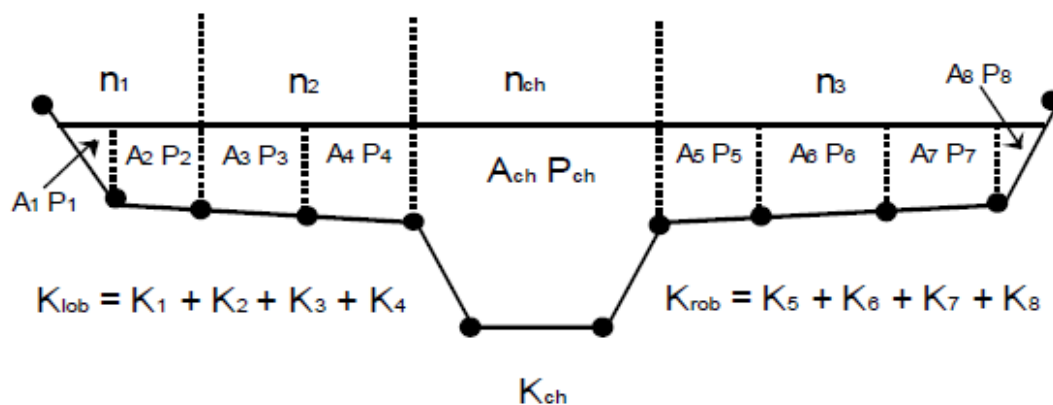


Figure 12 - Alternative conveyance factor calculation method

With this method, the conveyance factors are summed up in order to get the total K_{lob} and K_{rob} .

These two methods give different results whenever some portions of the overbanks have ground sections with significant vertical slopes: in general, the default approach provides a lower value for the total conveyance considering the same water surface elevation. On the other hand, the HEC-RAS default method is more consistent with the Manning equation and the concept of separate flow elements.

Then, the velocity weighting coefficient (α), is evaluated with respect to the conveyances of the left, right and main channel overbanks:

$$\alpha = \frac{(A_t)^2 \left[\frac{K_{lob}^3}{A_{lob}^2} + \frac{K_{ch}^3}{A_{ch}^2} + \frac{K_{rob}^3}{A_{rob}^2} \right]}{K_t^3} \quad (6)$$

where:

A_t = total flow area of cross section;

A_{lob} , A_{ch} , A_{rob} = flow areas of left overbank, main channel overbank and right overbank, respectively;

K_t = total conveyance of the cross-section;

K_{lob} , K_{ch} , K_{rob} = conveyances of left overbank, main channel overbank and right overbank, respectively.

The conveyance factor is used by the software to determine the friction loss, that is part of the total head loss h_e as mentioned before: it is a simple product of the slope of the energy grade line S_f and the average length of the reach between the two cross-sections weighted with respect to the discharge distribution in the cross-sections (L), which was determined previously. Regarding the first term S_f , it is calculated as an exploitation of the Manning equation:

$$S_f = \left(\frac{Q}{K} \right)^2 \quad (7)$$

In HEC-RAS there are four different alternatives for the estimation of S_f :

- Average Conveyance Equation

$$\bar{S}_f = \left(\frac{Q_1 + Q_2}{K_1 + K_2} \right)^2 \quad (8)$$

- Average Friction Slope Equation

$$\bar{S}_f = \frac{S_{f1} + S_{f2}}{2} \quad (9)$$

- Geometric Mean Friction Slope Equation

$$\bar{S}_f = \sqrt{S_{f1} \times S_{f2}} \quad (10)$$

- Harmonic Mean Friction Slope Equation

$$\bar{S}_f = \frac{2(S_{f1} \times S_{f2})}{S_{f1} + S_{f2}} \quad (11)$$

where the subscripts 1 and 2 refer to the two subareas the river cross-section is divided into.

Unless differently specified, the equation (8) is the default method used by the software.

The last contribute to be determined in the calculation of the total head loss h_e is the contraction/expansion coefficient (C), which represents the contraction or expansion to which the flow can be subjected, causing additional losses due to the changes in subsequent cross-sections.

Considering a sub-critical flow regime:

- With a mild change in cross section, values of 0.1 and 0.3 for the contraction/expansion coefficients, respectively, should be considered;
- in case of bridge section, with a sudden change in cross section, higher values should be assumed, i.e. 0.3 for the contraction and 0.5 for the expansion;
- in the presence of abrupt transitions, these values should be even higher, such as 0.6 for the contraction and 0.8 for the expansion.

In general, these coefficients are never greater than 1 and, on the other hand, if there is the presence of identic cross-section or anytime this further energy loss does not want to be taken into consideration, both coefficients can be set to 0.

In the case of super-critical flows, lower values of contraction/expansion coefficient should be adopted, because, since the dynamic head ($\alpha V^2/2g$) varies exponentially, to small stages variations correspond high variations of the total head, with the consequent overestimation of the head losses.

For this reason, considering super-critical flows:

- with a mild cross-section variation, suitable contraction/expansion coefficient values are 0.01 and 0.03, respectively;
- in case of sudden geometry variation, typically, values of 0.05 for the contraction coefficient and 0.2 for the expansion coefficient are usually recommended.

The software considers the presence of a contraction whenever the downstream flow velocity is higher than the upstream one. On the contrary, if the upstream velocity is greater than the downstream one, the program considers the presence of an expansion.

Then, in order to run the simulation, the boundary conditions must be introduced into the software, following these rules:

- downstream for sub-critical flow;
- upstream for super-critical flow;
- both upstream and downstream for mixed regime.

The software gives the possibility to select different types of boundary conditions, such as water surface elevation, critical depth, normal depth and rating curves.

Finally, here is reported the iterative computation procedure used by HEC-RAS in order to evaluate the water surface elevation:

1. assumption of a water surface elevation at the first cross-section (the most upstream one) in case of subcritical regime or, in case of supercritical regime, in the downstream cross-section;
2. determination of the corresponding total conveyance and velocity head;
3. calculation of the friction loss and development of the head loss equation h_e ;
4. Once the values of the point 2 and 3 are known, these are used to find out a new value of the water surface elevation by using the law of conservation of energy equation;
5. The two values of the water surface elevations, the assumed one and the calculated one, are compared: if there is a difference between them less than 0.003 m, the iterative procedure ends up; on the other hand, if the difference is higher than 0.003 m, the iterative procedure continues until the latter value is satisfied.

Note that the law of conservation of energy is not applicable if the water surface elevation passes through the critical state (caused by, for example, a significant variation in the channel bed slope, a hydraulic jump, an overflow, the presence of a bridge piles and junctions), as it is valid only for sub-critical flow regimes.

In those cases, the momentum equation must be taken into account by the implementation of the unsteady flow analysis.

2.1.2 Unsteady flow analysis

As mentioned, the unsteady flow analysis takes into account both the principle of conservation of mass and the principle of conservation of momentum: the first one states that, for a control volume, the net rate of flow into the volume must be equal to the rate of change of storage inside the volume, whereas, the latter states that, for a control volume, the net rate of momentum entering the volume (momentum flux) plus the sum of all external forces acting on the volume must be equal to the rate of accumulation of momentum.

The relative equations are:

- Continuity equation:

$$\frac{\delta A_t}{\delta t} + \frac{\delta Q}{\delta x} - q_l = 0 \quad (12)$$

- Momentum equation:

$$\frac{\delta Q}{\delta t} + \frac{\delta QV}{\delta x} - gA \left(\frac{\delta z}{\delta x} + S_f \right) = 0 \quad (13)$$

where:

Q = channel flow;

A_T = total flow area (sum of the active area and the off-channel storage area);

q_l = lateral inflow per unit length;

A = cross-sectional area;

g = gravitational acceleration;

S_f = friction slope;

Università Politecnica delle Marche

V = average flow velocity;

$\frac{\delta z}{\delta x}$ = water surface slope.

These equations are solved by the software simultaneously, by means of “finite difference” method, i.e. transforming the partial derivatives into finite differences obtaining, as a result, an algebraic equation system.

2.1.3 Software interface

In this section, a brief description of the software interface is reported (US Army Corps of Engineers Institute for Water Resources Hydrologic Engineering centre, 2020).

The HEC-RAS main window (Figure 13) is structured in three sections, where at the top there is the menu bar, while moving downward there are the button bar and the and the part devoted to the project information.

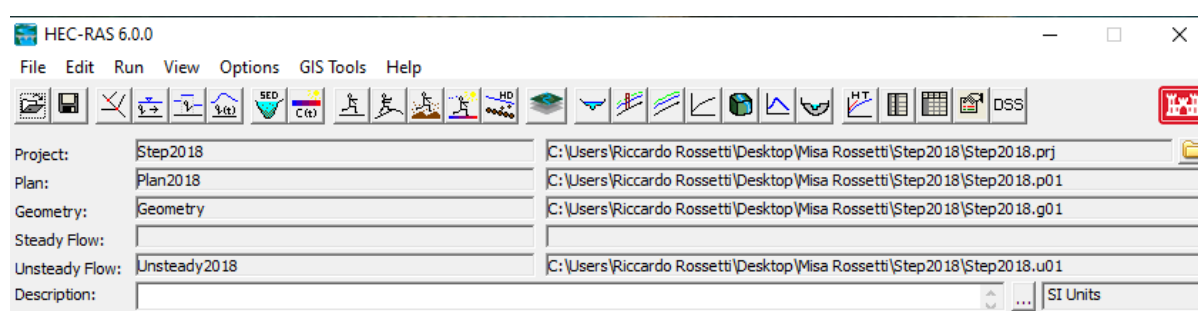


Figure 13 - HEC-RAS main window

The menu bar, is essentially composed of the following options:

- File: option used for file management;
- Edit: option used for entering and editing data;
- Run: option used to perform hydraulic calculations;
- View: option containing a set of tools used to display the model output by means of graphs and tables;
- Options: menu item used to change program setup options;
- GIS tools: option used to enter the HEC-RAS Mapper tool, which allows the creation of terrain models with the subsequent visualization of inundations mapping and flood animations;
- Help: option used to get on-line help.

For what regards the main window button bar, all the functions are illustrated in Figure 14:

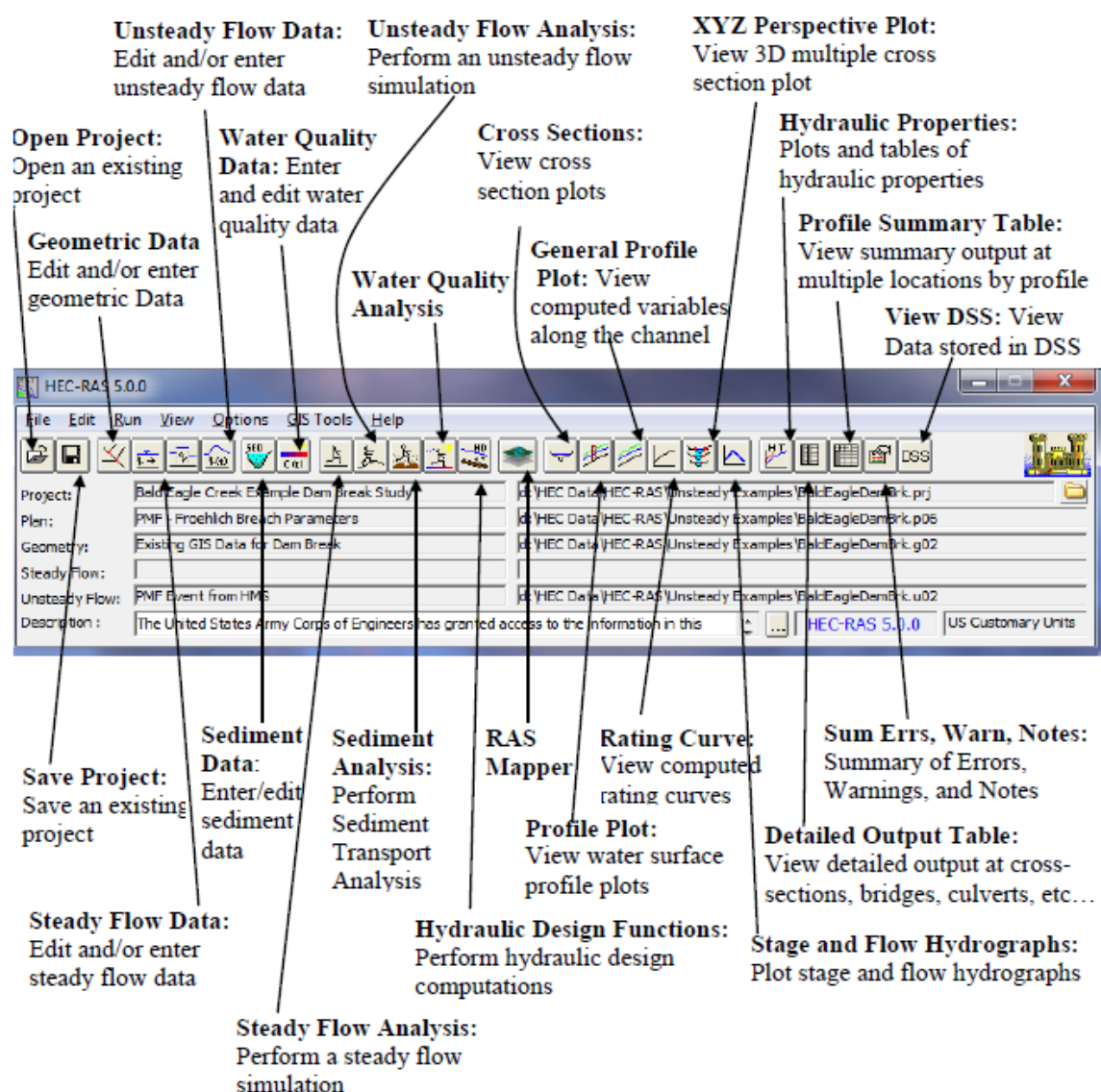


Figure 14 - HEC-RAS main window button bar

When either a new project or an existing one is opened, it is possible to enter the “Geometric Data” button to have an overview of the river path (Figure 15).

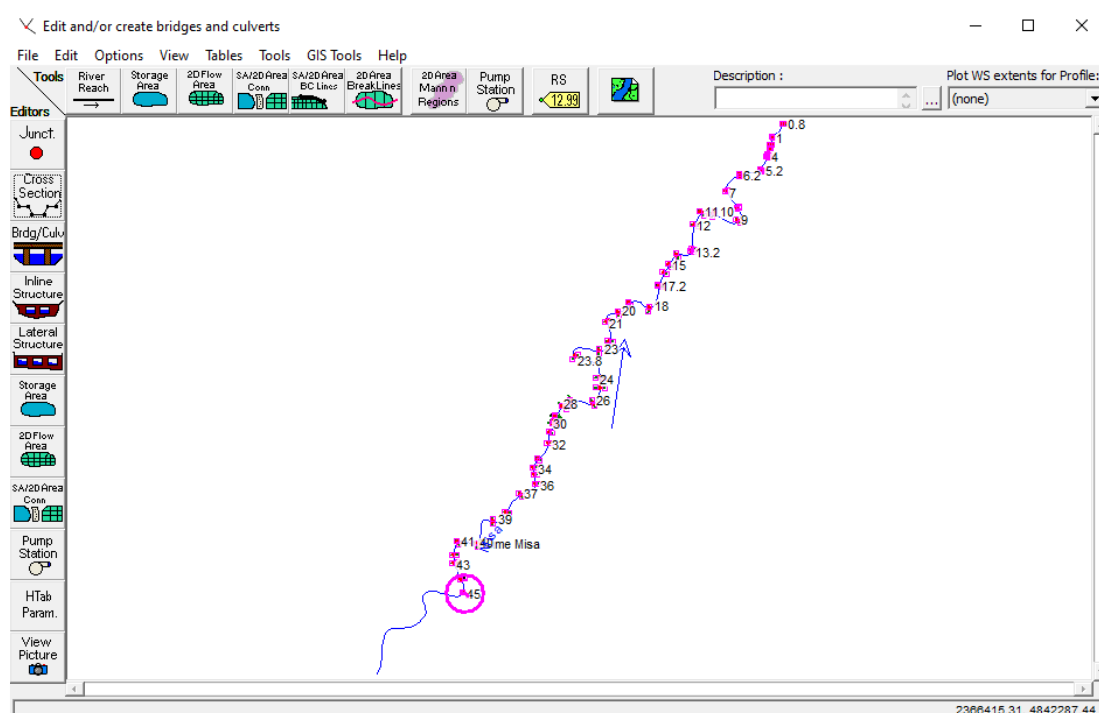


Figure 15 - Geometric data window

In this window, pressing the “Cross section” button, the cross-sections relative to the river are shown in detail one by one (Figure 16).

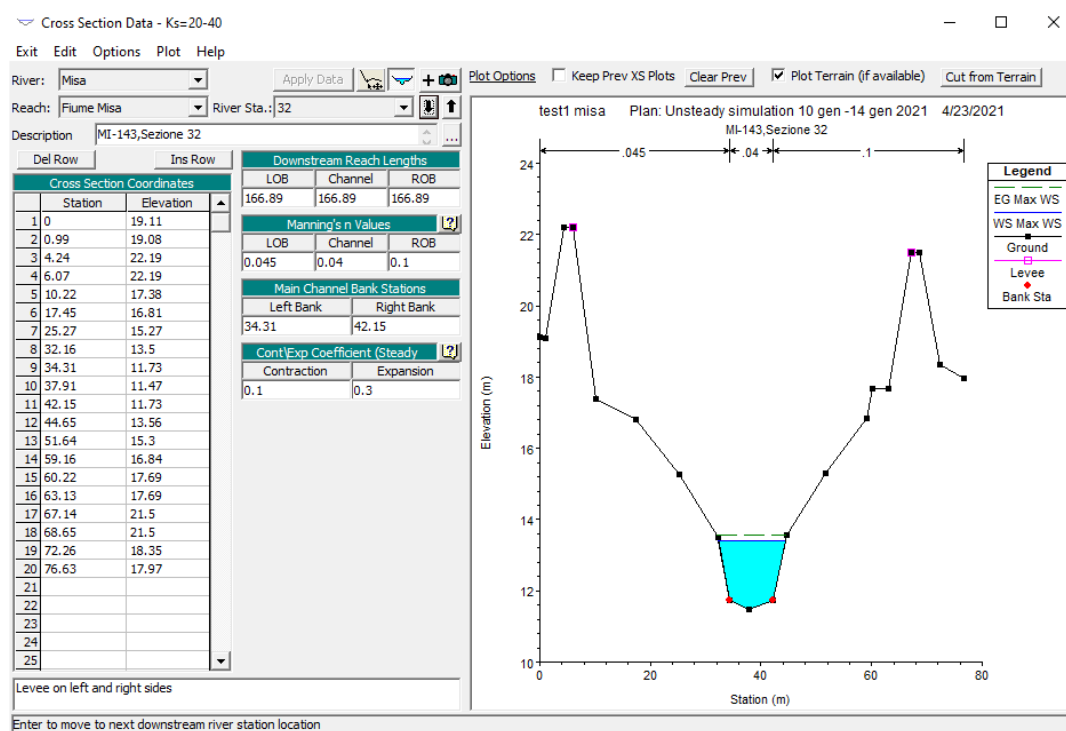


Figure 16 - Cross-section data editor

From the window shown in Figure 16, several details about the selected cross-sections are displayed. In the top part, there are the cross-section general information, such as the name of both the river and the reach, the river station (which has a decreasing numbering moving downstream) and a brief description of the current cross section. Each cross-section is composed of different points, which are defined through the use of the “Cross Sections Coordinates” table. In particular, the station column, indicates the progressive distance that each point has with respect to the origin (along the x-axis), whereas, the elevation column stands for the elevation that each point of the cross-section has with respect to the average sea level. With the table “downstream Reach Lengths” it is possible to define the distance between the cross-section and the following one. Specifically, the terms “LOB” and “ROB” indicate the left-over bank and the right-over bank, respectively, and are used to identify the distance of both the leftmost point and the rightmost point of the cross-section from the following section, while “Channel” indicates the distance between the cross-section thalweg and the following section.

Another important table is that relative to the “Main Channel Bank Station”, where the points of the cross-section belonging to the to the main channel (red points Figure 16), which represent the low flow conditions, are chosen.

From the options menu, it is also possible to add levees to the cross-section along with the ineffective flow areas, which are portions of the cross-section where water has no conveyance.

For what concerns the Manning table, it is possible to insert three different roughness coefficients, one for the left-over bank, one for the main channel and one for the right-over bank.

In particular, the Manning coefficients must be added in relation to the type of both the channel and the flood plains.

2.1.3.1 Unsteady simulation setup

To perform an unsteady flow analysis, the first thing to do is the implementation of the boundary conditions (Figure 17).

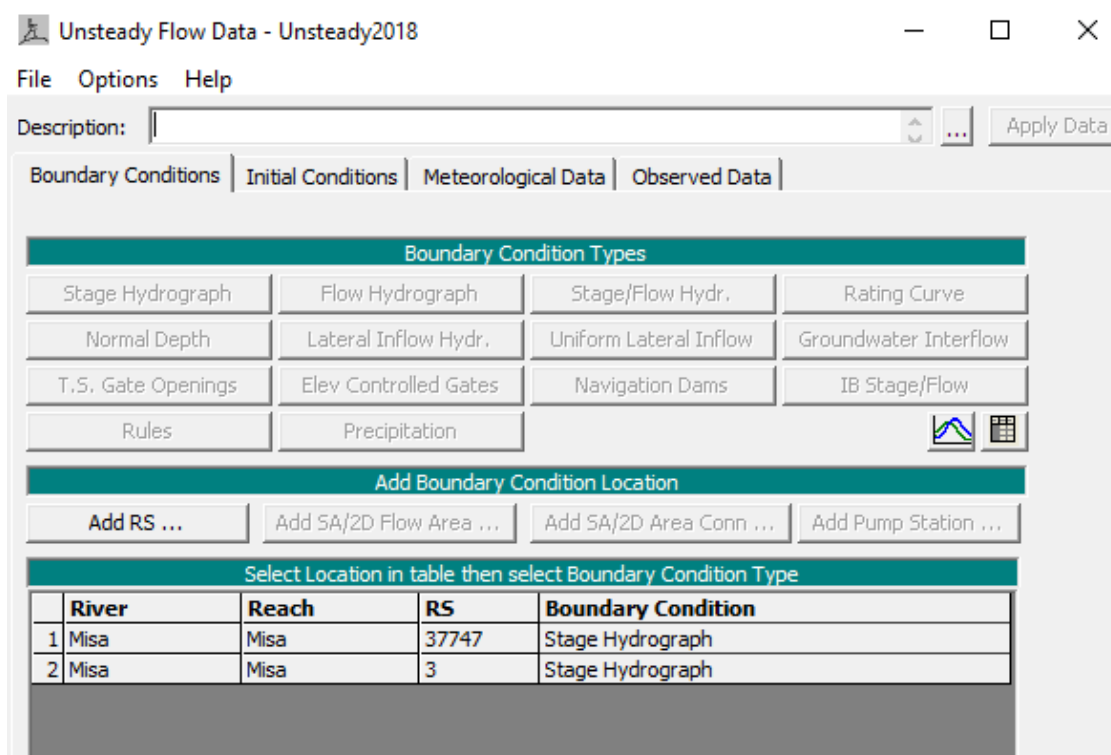


Figure 17 - Unsteady flow data boundary conditions

Boundary conditions that must be assigned on both the most upstream section and the most downstream one: the most used boundary conditions are the following:

- stage hydrograph: where there is the possibility to add different water elevation values (referred to the average sea level) related to the considered time series;
- flow hydrograph: where there is the possibility to add different flow data for the considered time series;
- stage/flow hydrograph: where it is possible to enter both values of stage and flow for the considered time series.

In each of these types of boundary conditions, there is the possibility to set the period of analysis along with the “Data time interval”, which is the interval of time over which the stage/flow data will be inserted into the software (Figure 18).

Flow Hydrograph

River: Misa Reach: Misa RS: 39110

☐ Read from DSS before simulation Select DSS file and Path

File:

Path:

☒ Enter Table Data time interval: 30 Minute

Select/Enter the Data's Starting Time Reference

☐ Use Simulation Time: Date: 04FEB2017 Time: 0000

☒ Fixed Start Time: Date: 04FEB2017 Time: 0000

No. Ordinates Interpolate Missing Values Del Row Ins Row

Hydrograph Data			
	Date	Simulation Time (hours)	Flow (m ³ /s)
1	03Feb2017 2400	00:00	5.266
2	04Feb2017 0030	00:30	5.266
3	04Feb2017 0100	01:00	5.266
4	04Feb2017 0130	01:30	5.428
5	04Feb2017 0200	02:00	5.428
6	04Feb2017 0230	02:30	5.428
7	04Feb2017 0300	03:00	5.594
8	04Feb2017 0330	03:30	5.428
9	04Feb2017 0400	04:00	5.107
10	04Feb2017 0430	04:30	5.594
11	04Feb2017 0500	05:00	5.763
12	04Feb2017 0530	05:30	5.428
13	04Feb2017 0600	06:00	5.266
14	04Feb2017 0630	06:30	5.266
15	04Feb2017 0700	07:00	5.266

Time Step Adjustment Options ("Critical" boundary conditions)

☐ Monitor this hydrograph for adjustments to computational time step

Max Change in Flow (without changing time step):

Min Flow: Multiplier:

Plot Data OK Cancel

Figure 18 - Flow hydrograph edit window

Once the boundary conditions are set, the unsteady flow data can be saved in order to be immediately recalled.

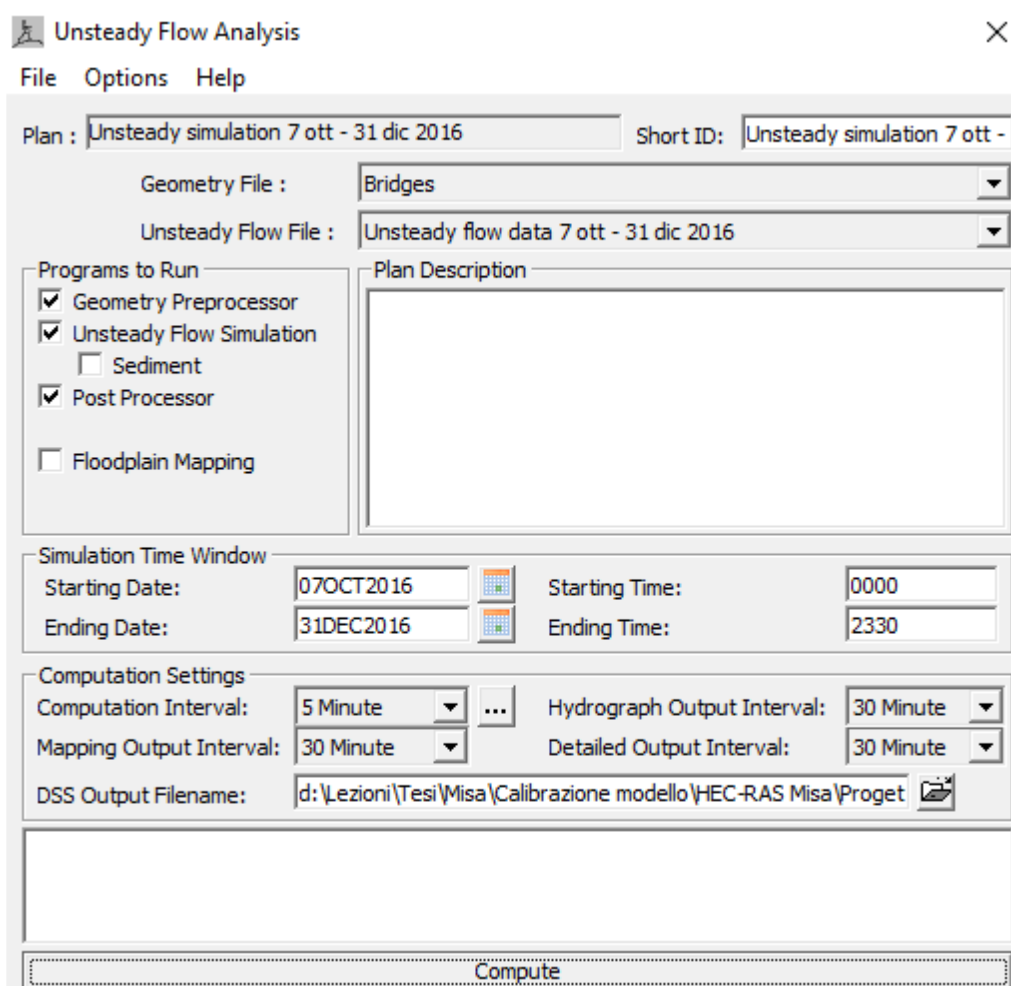
To run the unsteady simulation, the first step is the definition of a plan which defines both the geometry and the unsteady flow data to be analysed. Afterwards, it is possible to select the components which will be used for the unsteady flow analysis and that are: a geometric data pre-processor, the unsteady flow simulator and an output post-processor.

In order to correctly set up the unsteady simulation, it is required entering both the start and the end of the simulation period from the “Simulation Time Window” in the “Unsteady Flow Analysis”. This time interval can be either equal or less than the time period associated to the “Unsteady Flow Data”.

For what regards the “Computation Setting” table (Figure 19), it is composed of different options such as:

- Computation interval: this represents the simulation time-step. Firstly, it should be small enough to accurately describe both the rise and the fall of the hydrograph. Generally, a good estimate is to consider a computation interval which is equal or less than the time of rise of the hydrograph divided by 20. Secondly, it should follow the Courant condition criteria, i.e., the computation interval should be equal or less than the time required by water to travel from one cross-section to the next;
- Mapping output interval: this field is used to enter the interval at which it is possible to visualize mapping output within HEC-RAS Mapper;

- Hydrograph output interval: this interval must be equal or large than the selected computation interval and is set in order to give a suitable number of points to define the shape of the computed hydrograph without losing information regarding the peaks or volume of the hydrograph;
- Detailed output interval: this option allows to set the time interval on which the simulation results will be shown. The selected time interval must always be equal or higher than the computational interval.



Unsteady Flow Analysis [Close]

File Options Help

Plan : Unsteady simulation 7 ott - 31 dic 2016 Short ID: Unsteady simulation 7 ott -

Geometry File : Bridges

Unsteady Flow File : Unsteady flow data 7 ott - 31 dic 2016

Programs to Run

- ☒ Geometry Preprocessor
- ☒ Unsteady Flow Simulation
 - ☐ Sediment
- ☒ Post Processor
- ☐ Floodplain Mapping

Plan Description

Simulation Time Window

Starting Date: 07OCT2016 Starting Time: 0000

Ending Date: 31DEC2016 Ending Time: 2330

Computation Settings

Computation Interval: 5 Minute Hydrograph Output Interval: 30 Minute

Mapping Output Interval: 30 Minute Detailed Output Interval: 30 Minute

DSS Output Filename: d:\Lezioni\Tesi\Misa\Calibrazione modello\HEC-RAS Misa\Proget

Compute

Figure 19 - Unsteady flow analysis window

2.1.3.2 Unsteady simulation results

Once the simulation has been run, the obtained results can be consulted in different ways. One of these consists in the visualization of the results by means of a table which can be organized in relation to either the desired cross-sections and/or the desired profiles (Figures 20 and 21).

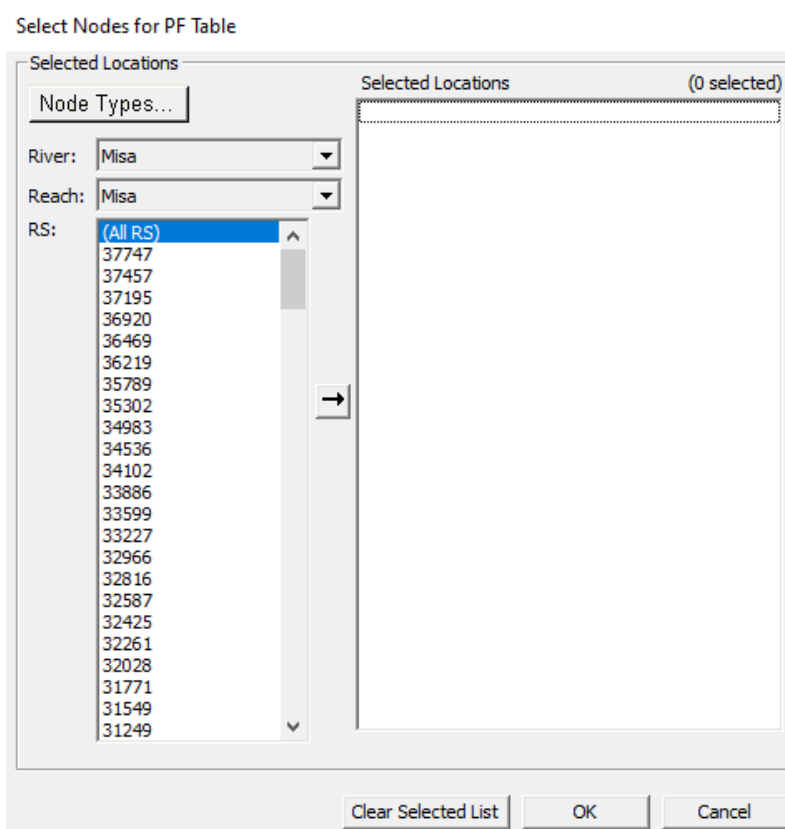


Figure 20 - Selection of the cross-section

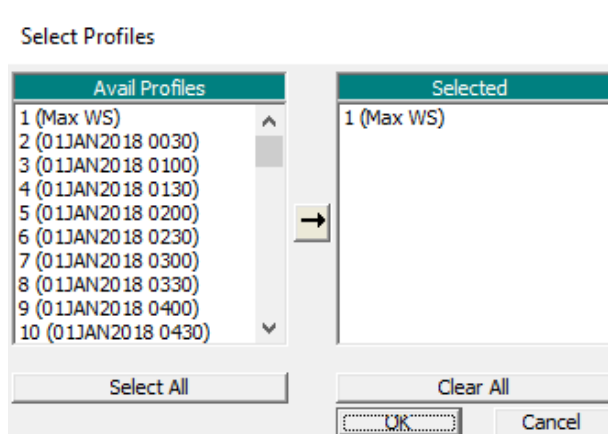


Figure 21 - Selection of the profile

As both the cross-sections and the profiles are selected, all the information concerning the cross-sections, profiles, total flow, minimum channel elevation, water surface elevation, critical water surface, energy grade line elevation, energy grade line slope, channel velocity, flow area, top width and Froude number, are displayed as in Figure 22.

Profile Output Table - Standard Table 1

File Options Std. Tables Locations Help

HEC-RAS Plan: 2018all River: Misa Reach: Misa Profile: Max WS Reload Data

Reach	River Sta	Profile	Q Total (m3/s)	Min Ch El (m)	W.S. Elev (m)	Crit W.S. (m)	E.G. Elev (m)	E.G. Slope (m/m)	Vel Chnl (m/s)	Flow Area (m2)	Top Width (m)	Froude # Chl
Misa	37747	Max WS	192.60	19.58	22.39		22.55	0.001507	1.90	110.36	65.85	0.37
Misa	37457	Max WS	192.37	19.51	22.24		22.40	0.001820	2.11	111.49	79.70	0.42
Misa	37195	Max WS	192.16	19.33	22.17		22.28	0.001019	1.55	129.10	69.15	0.30
Misa	36920	Max WS	191.97	19.16	22.08		22.20	0.001026	1.58	123.88	57.53	0.30
Misa	36469	Max WS	191.66	18.58	21.97		22.08	0.000936	1.65	133.09	74.54	0.30
Misa	36219	Max WS	191.44	18.32	21.95		22.02	0.000498	1.26	170.02	83.90	0.22
Misa	35789	Max WS	191.15	18.17	21.60		21.91	0.002624	2.80	80.62	44.97	0.50
Misa	35302	Max WS	190.29	17.73	21.38		21.58	0.001896	2.51	103.76	78.59	0.43
Misa	34983	Max WS	190.40	17.48	21.14		21.42	0.002211	2.62	85.52	48.18	0.45
Misa	34536	Max WS	190.54	17.35	20.80		21.10	0.002524	2.73	82.21	45.28	0.48
Misa	34102	Max WS	190.56	17.04	20.39		20.77	0.003155	3.01	73.54	40.77	0.54
Misa	33886	Max WS	190.48	16.84	20.21		20.58	0.003379	3.23	78.96	58.64	0.57
Misa	33599	Max WS	190.41	16.58	20.02		20.28	0.002323	2.69	88.45	53.59	0.47
Misa	33227	Max WS	190.41	16.12	19.86		20.07	0.001460	2.19	100.44	50.02	0.37
Misa	32966	Max WS	190.34	16.01	19.77		19.94	0.001740	2.30	94.74	48.41	0.41

Figure 22 - Results table

Another way to access the simulation results is by checking directly either each cross-section or the entire river profile (Figures 23 and 24), where it is even possible to see an animation of the water surface elevation trend over time.



2.2 Hydrokinetic technology principles

Hydrokinetic (or water current) turbines produce electricity directly from the flowing water of the stream: the turbine blades would turn the generator and capture the energy due to the water motion (Vermaak, 2013).

The amount of electricity that can be generated from this energy source depends on the volume and velocity of the water resource: in fact, it can be installed in a flow with water velocity equal or greater than 0.5 m/s.

Similar to wind energy converters, the total available power (measured in Watt) captured by a hydrokinetic is calculated as follow:

$$P_a = \frac{1}{2} \times A \times \rho \times V^3 \times C_p \quad (14)$$

Where:

A = cross-sectional turbine area (m²);

ρ = water density (1000 kg/m³);

V = water current velocity (m/s);

C_p = turbine power coefficient (or efficiency) which is $16/27=0.592$ (theoretical maximum power available coming from the well-known Betz law).

The advantage is that the water is approximately 800 times denser than air, and this implies that the amount of energy generated by a hydrokinetic turbine is much greater than the one produced by a wind turbine of equal diameter and velocity: this is why, even with lower velocities, this technology is studied and potentially viable.

Hence, in general, the extracted power for a hydrokinetic turbine is calculated as:

$$P_e = \frac{1}{2} \times \pi \times r^2 \times \rho \times V^3 \times C_p(\lambda, \beta) \times \eta_D \quad (15)$$

Where, in addition to the previous terms:

r = radius of the turbine (m);

η_D = efficiency of the drive train (e.g. generator, gearbox, etc.)

λ = tip speed ratio (TSR), expressed as $\lambda = \frac{w \times r}{V}$ with w = angular velocity of the turbine (rad/s);

β = pitch angle (degrees) of the turbine.

The two most common small-scale hydrokinetic turbine concepts are axial-flow turbine and cross-flow turbine.

Focusing on the axial flow turbine, which is the type of the one chosen in this work, they can be arranged with various configurations, as shown in Figure 25.

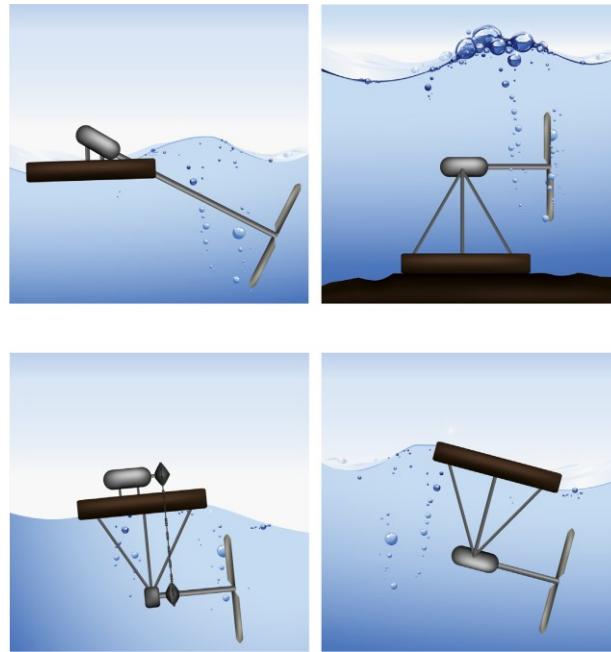


Figure 25 - Horizontal axis turbines configurations: (i) inclined axis; (ii) Rigid Mooring, (iii) Non-submerged Generator, (iv) Submerged generator

2.2.1 The ductless Archimedes turbine

The turbine chosen for this study is the ductless Archimedes screw turbine: in this chapter, the main characteristics and parameters, in terms of geometry and efficiency, will be briefly illustrated, with particular attention for the ones used in this work.

Various reviews on hydrokinetic power systems are available in literature, but especially in the field of micro-hydropower plants and in ducted systems, in which this kind of technology showed a very high efficiency.

In this scenario, the study of the Hydraulics research group of UNIVPM aims to evaluate the performance of the turbine and to optimize the fundamental design parameters of the Archimedes screw turbine as an axial hydrokinetic turbine, i.e. arranging the screw in the fluid flow without any supply or protection system, typical of the traditional or ducted conditions in which this turbine usually operates (Zitti G. ,

Fattore, Brunori, Brunori, & Brocchini, 2019). The idea of an effective Archimedean-type Hydrokinetic Turbine aimed at producing a device that:

1. is simple and cheap, therefore it can be used in location with limitation, such as in shipping areas;
2. reduces environmental impacts;
3. does not require the construction of civil infrastructures (barrages, reservoirs);
4. works also in small water depths;
5. maximizes the flow energy exploitation.

Notwithstanding the geometrical differences among the various hydrokinetic turbines, the evaluation of the efficiency of a hydrokinetic turbine is based on Betz' one-dimensional model, shown in Figure 26.

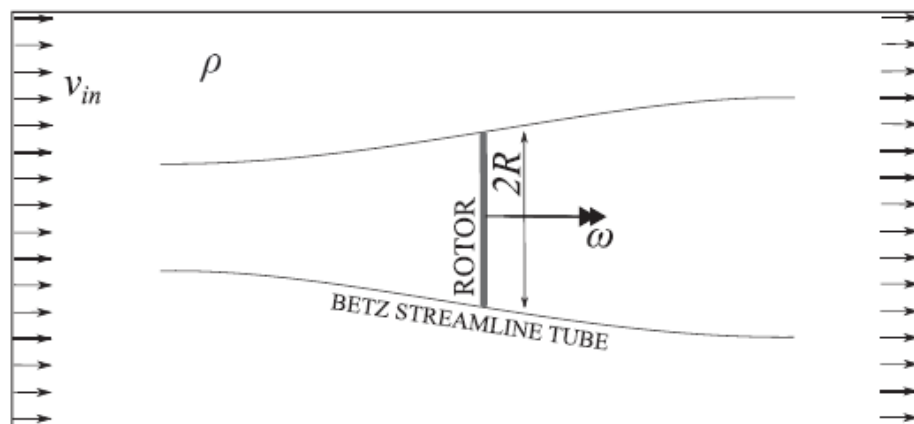


Figure 26 - Sketch of Betz' model

Based on this model and on the equations of the Betz' theory (14) and (15), laboratory experiments and numerical simulations have been performed in order to evaluate efficiency parameters in respect to the geometry and configuration of the turbine itself, as well as in respect to external conditions.

The screw turbine used for the tests (and later on in this work) is shown in Figure 27(a) and 27(b).

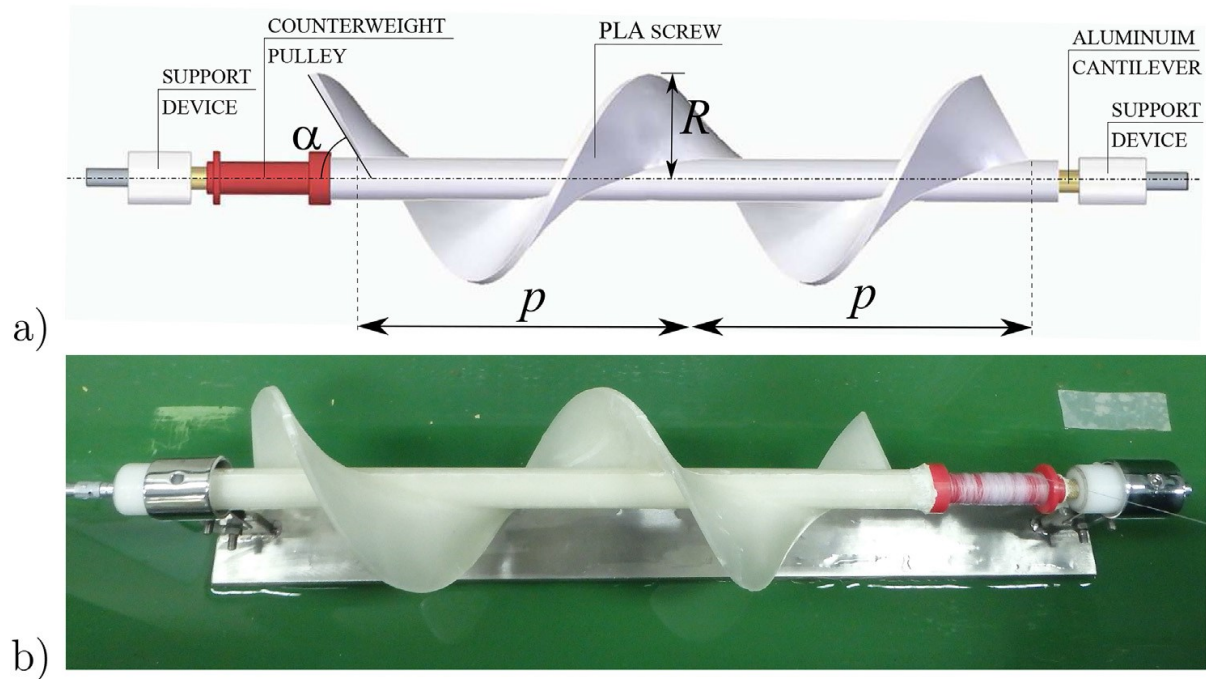


Figure 27 - The screw turbine used for the experiments. a) sketch of the screw turbine model with main components; b) top view of the turbine in the support system

The laboratory tests have been developed with a fixed geometry of the turbine, which is reported in Table 2.

Parameter	symbol	value
Turbine radius	R	50 mm
Axle radius	—	20 mm
Axle length	L	320 mm
Blade stride	p	160 mm
Blade inclination with respect to axle	α	70°

Table 2 - Geometric parameters of the turbine

The available power of flow P_a (equation (14)) was evaluated with Betz' law, where the rotor area (A) was approximated by the projection of the turbine volume on a plane perpendicular to the flow, which means:

- if the axis of the turbine is parallel to the flow ($\theta=0$), the cross section area is that of a circle of radius R;
- if the angle of the turbine axis with the flow direction is $\theta \neq 0$, the cross section area is

$$A = R^2\pi\cos\theta + 2RL\sin\theta \quad (16)$$

Where L is the turbine length.

Therefore, varying the angle θ , the flow power increases because of the increase in A.

In Table 3 and in the graphs of Figure 28, 29 and 30, some of the results are reported.

ID ($\theta - \omega$) grad-rads ⁻¹	TSR [adim]	\bar{M}_t [Nm]	P_t [mW]	C_p
0-0.5	0.125	$4.94 \cdot 10^{-3}$	2.47	0.079
0-1	0.25	$4.46 \cdot 10^{-3}$	4.46	0.142
0-1.5	0.375	$3.72 \cdot 10^{-3}$	5.59	0.178
0-2	0.5	$3.21 \cdot 10^{-3}$	6.42	0.204
0-2.5	0.625	$2.90 \cdot 10^{-3}$	7.23	0.231
0-3	0.75	$2.49 \cdot 10^{-3}$	7.47	0.238
0-3.5	0.875	$2.07 \cdot 10^{-3}$	7.24	0.231
0-4	1	$1.69 \cdot 10^{-3}$	6.76	0.215
0-4.5	1.125	$1.31 \cdot 10^{-3}$	5.89	0.188
0-5	1.25	$0.97 \cdot 10^{-3}$	4.83	0.154
0-5.5	1.375	$0.62 \cdot 10^{-3}$	3.42	0.109
0-6	1.5	$0.29 \cdot 10^{-3}$	1.76	0.056
10-0.5	0.125	$4.74 \cdot 10^{-3}$	2.37	0.045
10-1	0.25	$4.46 \cdot 10^{-3}$	4.46	0.084
10-1.5	0.375	$3.95 \cdot 10^{-3}$	5.92	0.111
10-2	0.5	$3.43 \cdot 10^{-3}$	6.87	0.129
10-2.5	0.625	$2.95 \cdot 10^{-3}$	7.38	0.139
10-3	0.75	$2.54 \cdot 10^{-3}$	7.63	0.144
10-3.5	0.875	$2.19 \cdot 10^{-3}$	7.67	0.144
10-4	1	$1.85 \cdot 10^{-3}$	7.39	0.139
10-4.5	1.125	$1.49 \cdot 10^{-3}$	6.72	0.126
10-5	1.25	$1.13 \cdot 10^{-3}$	5.66	0.106
10-5.5	1.375	$0.78 \cdot 10^{-3}$	4.29	0.081
10-6	1.5	$0.44 \cdot 10^{-3}$	2.62	0.049

Table 3 - Summary of the conditions used for the numerical simulations and related results

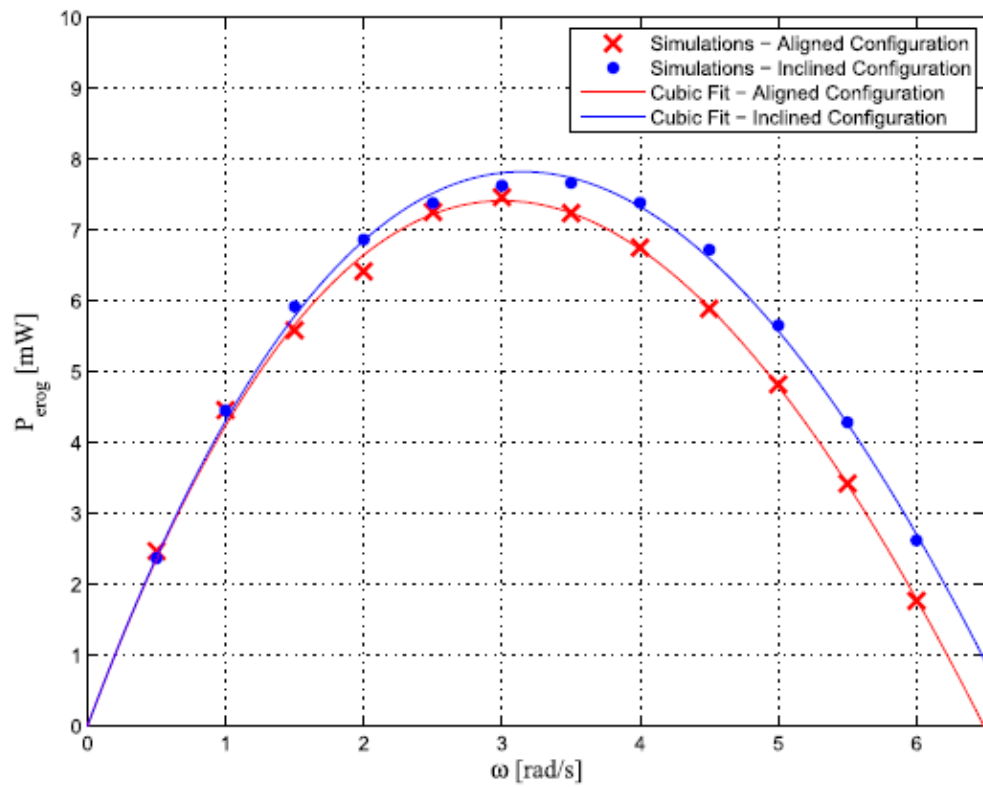


Figure 28 - Generated power from numerical simulations, as function of the corresponding angular velocity w

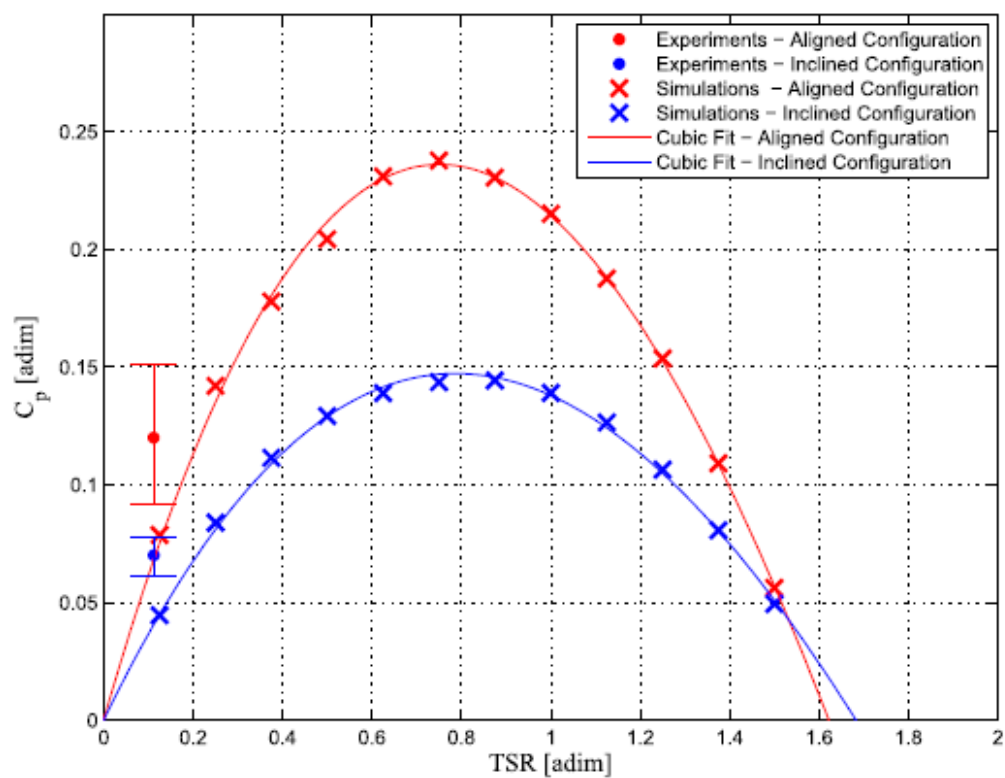


Figure 29 - Power coefficient C_p as a function of the tip speed ratio for the laboratory experiments and for the numerical simulations

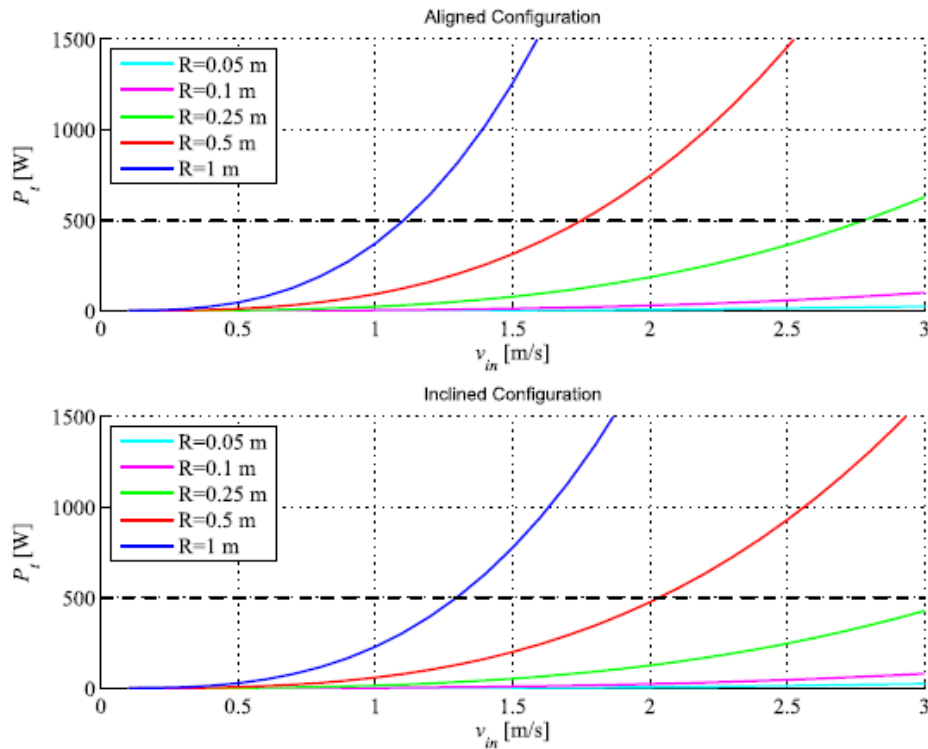


Figure 30 - Power generated by Archimedean- Hydrokinetic turbines, with different radii R and for different water flow v_{in}

These results show the variability of the Power extracted in respect to the angular velocity for both aligned and inclined configurations (Figure 28) and relative power coefficients variability (Figure 29), as well as the variability of the power extracted depending on the flow velocity v_{in} (Figure 30).

Results of laboratory experiments and numerical simulations showed that the performance coefficients of the hydrokinetic Archimedes turbine are in line with the performances of other hydrokinetic turbines.

Even if these results show better performances for the aligned configuration, comparison between laboratory tests and numerical analysis suggested that possible blockage and wall effects, which characterize laboratory tests, could affect the results: so, further experiments have been exploited, in order to analyse the effects of the pitch

angle on the efficiency of an Archimedean-type turbine (Zitti G. , Fattore, Brunori, Brunori, & Brocchini, 2019).

The results of this study have been reported through the use of different parameters:

- $A_B = \pi R^2$, intended as the cross sectional area, and relative power from Betz formula $P_{fB} = 0.5 \rho A_B v^3$, from which the performance coefficient C_{pB} which is more representative of the dependence of the generated power on the incidence angle;
- $A_S = R^2 \pi \cos(\theta) + 2RL \sin(\theta)$, intended as the area adapted for the inclined screw and relative $P_{fS} = 0.5 \rho A_S v^3$, from which the performance coefficient C_{pS} , which is more representative of the efficiency.

In Figure 31 and 32, the results are shown for different configuration, i.e. with different pitch angle and different TSR.

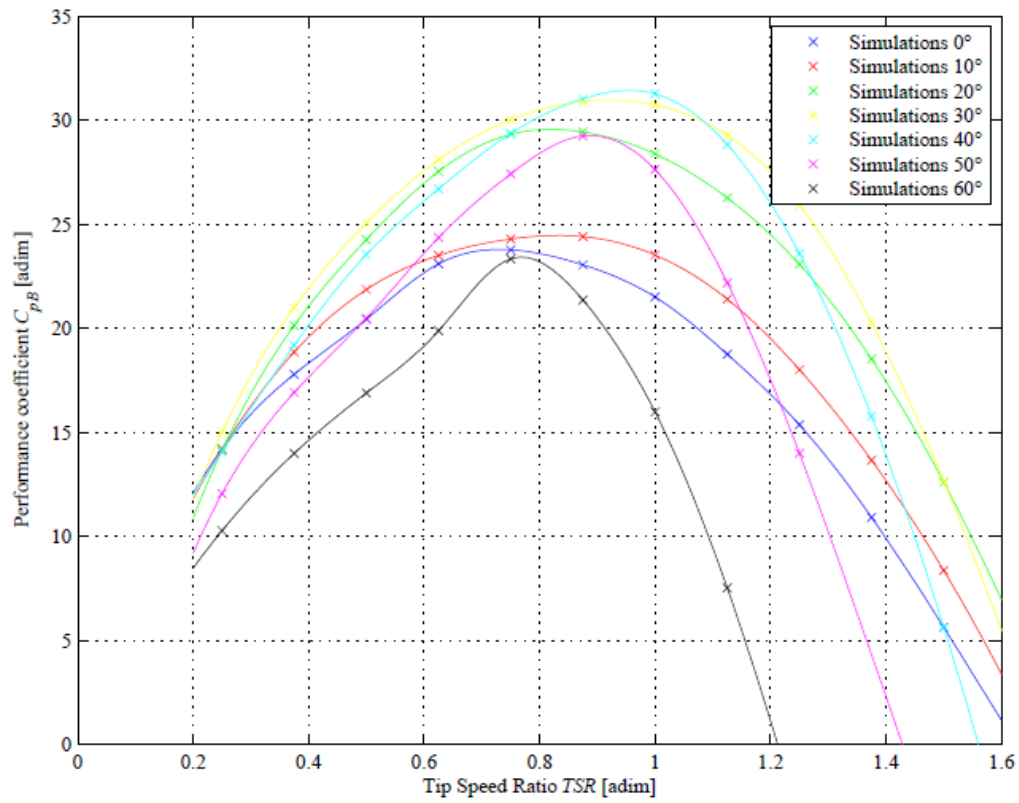


Figure 31 - Performance coefficient C_{pB} , evaluated with the fixed cross sectional area A_B

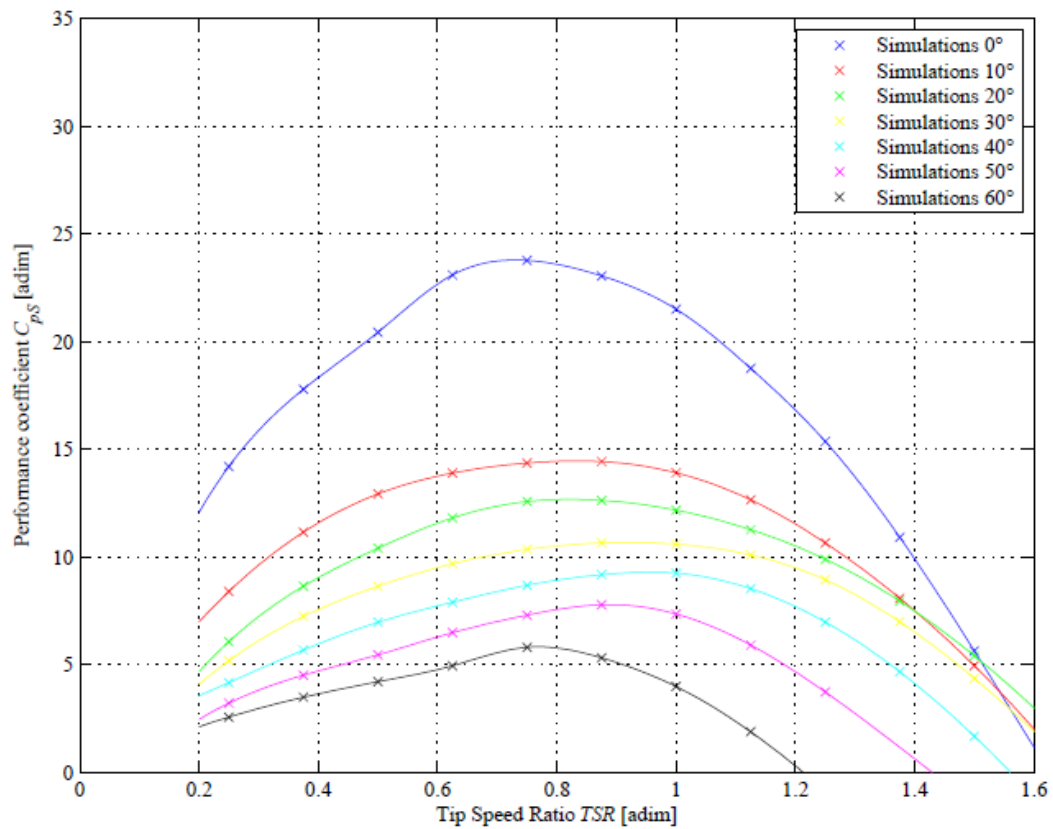


Figure 32 - Performance coefficient C_{pS} , evaluated with the screw adapted cross-sectional area A_S

In summary, the best performance C_{pS} is obtained when the axis of the turbine is aligned with the stream flow (Figure 31), but the power provided C_{pB} in inclined configurations with incidence angle lower than 50° is larger than that provided in aligned configuration (Figure 32). This suggests that the lower performances in the inclined configurations are mainly due to the increase of the cross section area A_s .

More in details, in Table 4 are reported the specific values of the results obtained, that will be useful later on in the present work: in fact, these parameters will be recalled when the possible configurations of the turbines will be discussed and chosen.

ID (θ , TSR)	P_t [mW]	C_{pB}	C_{pS}
0, 0.250	4.461	14.2%	14.2%
0, 0.375	5.587	17.8%	17.8%
0, 0.500	6.418	20.4%	20.4%
0, 0.625	7.256	23.1%	23.1%
0, 0.750	7.468	23.8%	23.8%
0, 0.875	7.242	23.1%	23.1%
0, 1.000	6.756	21.5%	21.5%
0, 1.125	5.891	18.8%	18.8%
0, 1.250	4.825	15.4%	15.4%
0, 1.375	3.425	10.9%	10.9%
0, 1.500	1.765	5.6%	5.6%
10, 0.250	4.456	14.2%	8.4%
10, 0.375	5.924	18.9%	11.1%
10, 0.500	6.869	21.9%	12.9%
10, 0.625	7.384	23.5%	13.9%
10, 0.750	7.631	24.3%	14.4%
10, 0.875	7.668	24.4%	14.4%
10, 1.000	7.390	23.5%	13.9%
10, 1.125	6.724	21.4%	12.6%
10, 1.250	5.657	18.0%	10.6%
10, 1.375	4.289	13.7%	8.1%
10, 1.500	2.623	8.3%	4.9%
20, 0.250	4.439	14.1%	6.1%
20, 0.375	6.326	20.1%	8.6%
20, 0.500	7.623	24.3%	10.4%
20, 0.625	8.653	27.5%	11.8%
20, 0.750	9.212	29.3%	12.6%
20, 0.875	9.248	29.4%	12.6%
20, 1.000	8.918	28.4%	12.2%
20, 1.125	8.252	26.3%	11.3%
20, 1.250	7.250	23.1%	9.9%
20, 1.375	5.817	18.5%	7.9%
20, 1.500	3.955	12.6%	5.4%
30, 0.250	4.717	15.0%	5.2%
30, 0.375	6.596	21.0%	7.2%
30, 0.500	7.872	25.1%	8.6%
30, 0.625	8.827	28.1%	9.7%
30, 0.750	9.434	30.0%	10.3%
30, 0.875	9.712	30.9%	10.6%
30, 1.000	9.657	30.7%	10.6%
30, 1.125	9.199	29.3%	10.1%
30, 1.250	8.146	25.9%	8.9%
30, 1.375	6.367	20.3%	7.0%
30, 1.500	3.970	12.6%	4.4%
40, 0.250	4.417	14.1%	4.2%
40, 0.375	6.026	19.2%	5.7%
40, 0.500	7.396	23.5%	7.0%
40, 0.625	8.388	26.7%	7.9%
40, 0.750	9.226	29.4%	8.7%
40, 0.875	9.748	31.0%	9.2%
40, 1.000	9.827	31.3%	9.2%
40, 1.125	9.057	28.8%	8.5%
40, 1.250	7.412	23.6%	7.0%
40, 1.375	4.952	15.8%	4.7%
40, 1.500	1.762	5.6%	1.7%
50, 0.250	3.784	12.0%	3.2%
50, 0.375	5.313	16.9%	4.5%
50, 0.500	6.435	20.5%	5.4%
50, 0.625	7.652	24.4%	6.5%
50, 0.750	8.615	27.4%	7.3%
50, 0.875	9.189	29.2%	7.8%
50, 1.000	8.680	27.6%	7.3%
50, 1.125	6.971	22.2%	5.9%
50, 1.250	4.394	14.0%	3.7%
60, 0.250	3.225	10.3%	2.5%
60, 0.375	4.391	14.0%	3.5%
60, 0.500	5.305	16.9%	4.2%
60, 0.625	6.244	19.9%	4.9%
60, 0.750	7.332	23.3%	5.8%
60, 0.875	6.710	21.4%	5.3%
60, 1.000	5.020	16.0%	4.0%
60, 1.125	2.360	7.5%	1.9%

Table 4 - Results of performance coefficients in dependence of θ and TSR

In this thesis, different configurations have been hypothesized, with a varying radius, depending on the inspected cross-section, following the same proportion L/R of Table 1, i.e. the length of the turbine equal to six times the radius.

In addition to the radius, the other parameters that have been imposed in the next are the flow velocity (v_{in}) and the angular velocity (w) of the turbine, with implies different “Tip Speed Ratio” (TSR).

Furthermore, both aligned configuration and inclined configuration have been analysed, i.e. different pitch angles (θ) have been imposed.

3 RESULTS

3.1 Selection of the typical year

As the aim of this work is to assess the energy production in medium-long terms, the modelling and the following analysis have been performed on the basis of the typical year, which is defined following these steps:

- download of hydrometric level datasets of at least 10 years;
- construction, for each year, of the duration curve, which represents the discharge, calculated from the hydrometric level using the relative rating curve, vs the probability of exceedance, i.e. it represents the percentage of time that a specified discharge will be equated or exceeded;
- calculation of the average duration curve of the whole dataset;
- calculation of the (RMSE) of each duration curve in respect to the average one;
- selection of the typical year, which is the one with the lower RMSE.

Hence, the dataset of the stage values has been downloaded from the Bettolle station, with a range from 2003 to 2020, which are, essentially, all the years which were available.

These data, downloaded in excel format, are displayed and organized as shown in Table 5 and 6.

The first column identifies the sensor (1112 stays for Bettolle sensor), the subsequent five columns identify the date and the time of data acquisition, the seventh column the

stage and the last two columns the water level in dry conditions and the station, respectively. In order to better managing the data, both the date (year, month, and day) and the time have been concatenated. This operation allows the creation of serial numbers (last column in Table 6, “Time tot”) which have turned out to be useful for the graphical representation of the simulation results. The data are recorded and then provided with a time step of 30 minutes: the values of the last column represent univocally an exact instant of time, as they are the sum of values of the column “Data value” (which are integers that are referred to a specific day) plus the values of the column “Time value” (which are decimals, referred to a specific hour of the day).

Codice sensore	Data: Anno	Mese	Giorno	Ora	Minuto	Livello idrometrico [m]	Livello idrometrico interpolato [0/1]	Codice stazione
1112	2018	1	1	0	30	1.29	0	26
1112	2018	1	1	1	0	1.29	0	26
1112	2018	1	1	1	30	1.28	0	26
1112	2018	1	1	2	0	1.28	0	26
1112	2018	1	1	2	30	1.29	0	26
1112	2018	1	1	3	0	1.28	0	26
1112	2018	1	1	3	30	1.28	0	26
1112	2018	1	1	4	0	1.28	0	26
1112	2018	1	1	4	30	1.29	0	26
1112	2018	1	1	5	0	1.29	0	26
1112	2018	1	1	5	30	1.29	0	26
1112	2018	1	1	6	0	1.28	0	26
1112	2018	1	1	6	30	1.28	0	26
1112	2018	1	1	7	0	1.28	0	26
1112	2018	1	1	7	30	1.29	0	26
1112	2018	1	1	8	0	1.29	0	26

Table 5 - Example of SIRMIP downloaded data

Anno	Mese	Giorno	Date	Date value	h	m	Time	Time value	Time tot
2018	1	1	1/1/2018	43101.00	0	30	0:30	0.02	43101.02083
2018	1	1	1/1/2018	43101.00	1	0	1:00	0.04	43101.04167
2018	1	1	1/1/2018	43101.00	1	30	1:30	0.06	43101.0625
2018	1	1	1/1/2018	43101.00	2	0	2:00	0.08	43101.08333
2018	1	1	1/1/2018	43101.00	2	30	2:30	0.10	43101.10417
2018	1	1	1/1/2018	43101.00	3	0	3:00	0.13	43101.125
2018	1	1	1/1/2018	43101.00	3	30	3:30	0.15	43101.14583
2018	1	1	1/1/2018	43101.00	4	0	4:00	0.17	43101.16667
2018	1	1	1/1/2018	43101.00	4	30	4:30	0.19	43101.1875
2018	1	1	1/1/2018	43101.00	5	0	5:00	0.21	43101.20833

Table 6 - Transformation of date in serial numbers

As mentioned before, data are available as original data and validated data: the first one are the data just measured by the sensors, whereas the latter are the same, but filtered after a check, which aims to offer a set of data without any unreliable data, that can be caused by any kind of breaks of the sensor, as well as by obstructions that the sensor could undergo.

This implies that the validated data have a percentage of missing data larger than the original data: as example, the hydrograph of the year 2015 is reported in Figure 33.

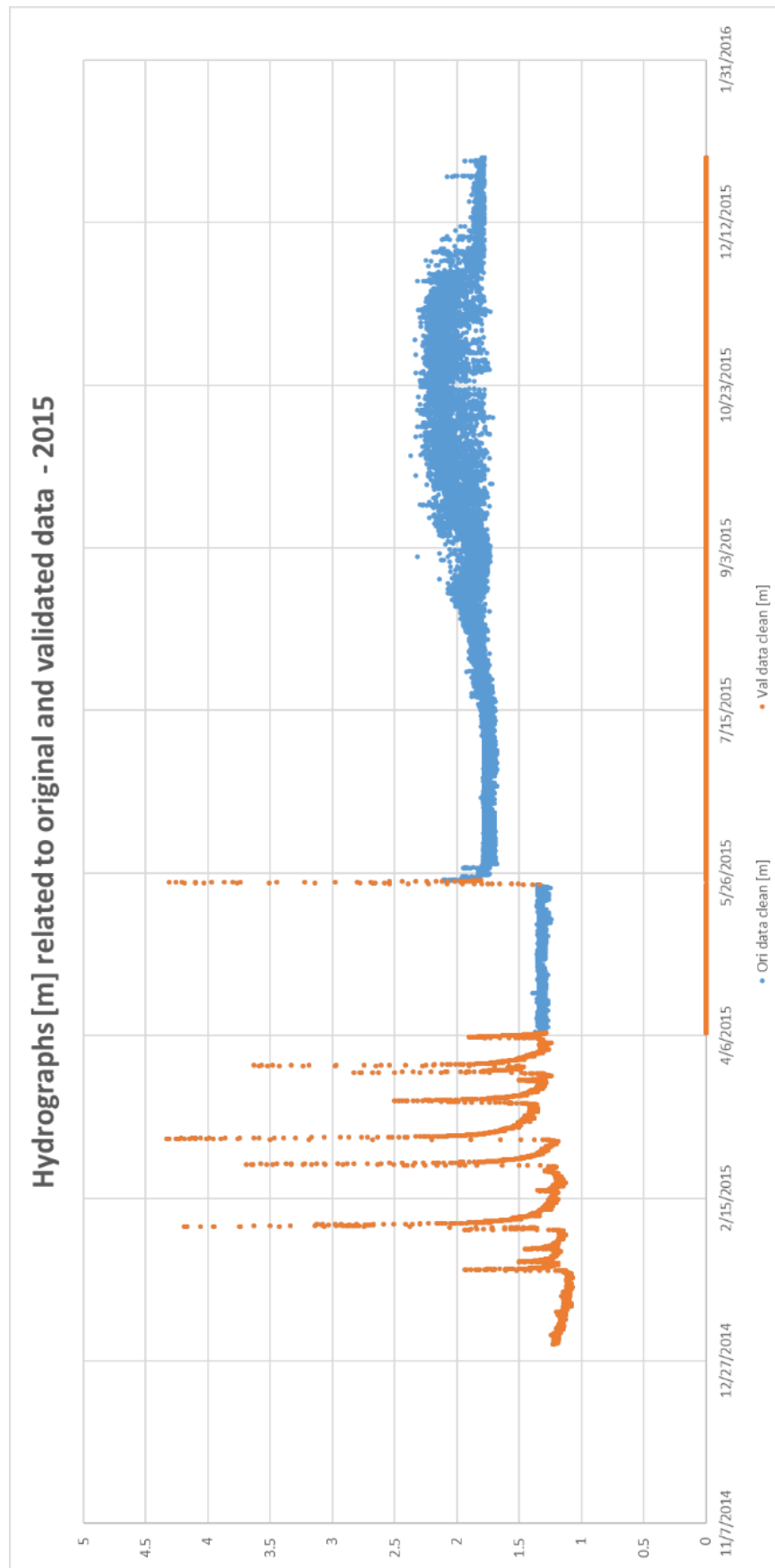


Figure 33 - Comparison between original data and validated data, 2015

The blue points are the original data, and they are overlapped by the orange points, the validated data, when available. The unusual distribution, almost constant at with higher values of the expected ones (that should be comparable to the dry periods of the first part of the year) suggest that some errors in the measurements have occurred, thus these data have been discarded.

For these reasons, the percentages of the missing values, both for original and validated data have been calculated and are reported in Table 7.

Year	Ori data miss		Val data miss	
	#	%	#	%
2003	16	0.09	17520	100.00
2004	290	1.65	17521	99.73
2005	2209	12.61	2300	13.13
2006	3908	22.31	3908	22.31
2007	7	0.04	7	0.04
2008	5	0.03	1773	10.09
2009	4	0.02	1934	11.04
2010	259	1.48	860	4.91
2011	54	0.31	13962	79.69
2012	1137	6.47	9051	51.52
2013	419	2.39	3830	21.86
2014	17	0.10	829	4.73
2015	0	0.00	12861	73.41
2016	2	0.01	12339	70.24
2017	5	0.03	3744	21.37
2018	0	0.00	0	0.00
2019	0	0.00	827	4.72
2020	0	0.00	7623	43.39

Table 7 - Percentages of missing data: the colour scale is proportional to the percentage of missing data

As the validated data have been considered for the selection of the typical year, only the years with a percentage of missing values lower than 25% have been considered as eligible, though the RMSEs have been calculated for them as well (except for the first

two years, 2003 and 2004, for which the duration curves were not calculated, as almost no data were available).

At this point, the discharge values referred to each stage value have been computed by means of the rating curves, reported Table 1 (chapter 1.4.1).

Then, the rating curves have been used for the calculation of the discharge for each time interval of the dataset, and the daily averages have been found and reported on a new table (Table 8).

In Figure 34, both the stage hydrograph and the flow hydrograph of 2018 relative to Bettolle station are reported as example.

Time tot	Hydr. Level [m]	Discharge Q [m ³ /s]	daily aver [m ³ /s]
43101	1.29	1.79	1.85
43101.02083	1.29	1.79	
43101.04167	1.29	1.79	
43101.0625	1.28	1.69	
43101.08333	1.28	1.69	
43101.10417	1.29	1.79	
43101.125	1.28	1.69	
43101.14583	1.28	1.69	
43101.16667	1.28	1.69	
43101.1875	1.29	1.79	
43101.20833	1.29	1.79	
43101.22917	1.29	1.79	
43101.25	1.28	1.69	
43101.27083	1.28	1.69	
43101.29167	1.28	1.69	
43101.3125	1.29	1.79	
43101.33333	1.29	1.79	
43101.35417	1.28	1.69	
43101.375	1.29	1.79	
43101.39583	1.28	1.69	
43101.41667	1.27	1.59	
43101.4375	1.28	1.69	
43101.45833	1.27	1.59	
43101.47917	1.27	1.59	
43101.5	1.27	1.59	
43101.52083	1.27	1.59	
43101.54167	1.27	1.59	
43101.5625	1.27	1.59	
43101.58333	1.27	1.59	
43101.60417	1.25	1.41	
43101.625	1.27	1.59	
43101.64583	1.28	1.69	
43101.66667	1.3	1.89	
43101.6875	1.32	2.11	
43101.70833	1.33	2.22	
43101.72917	1.34	2.33	
43101.75	1.34	2.33	
43101.77083	1.33	2.22	
43101.79167	1.33	2.22	
43101.8125	1.32	2.11	
43101.83333	1.33	2.22	
43101.85417	1.33	2.22	
43101.875	1.32	2.11	
43101.89583	1.33	2.22	
43101.91667	1.33	2.22	
43101.9375	1.33	2.22	
43101.95833	1.33	2.22	
43101.97917	1.33	2.22	

Table 8 - Discharge calculations, for every 30 minutes and daily averaged

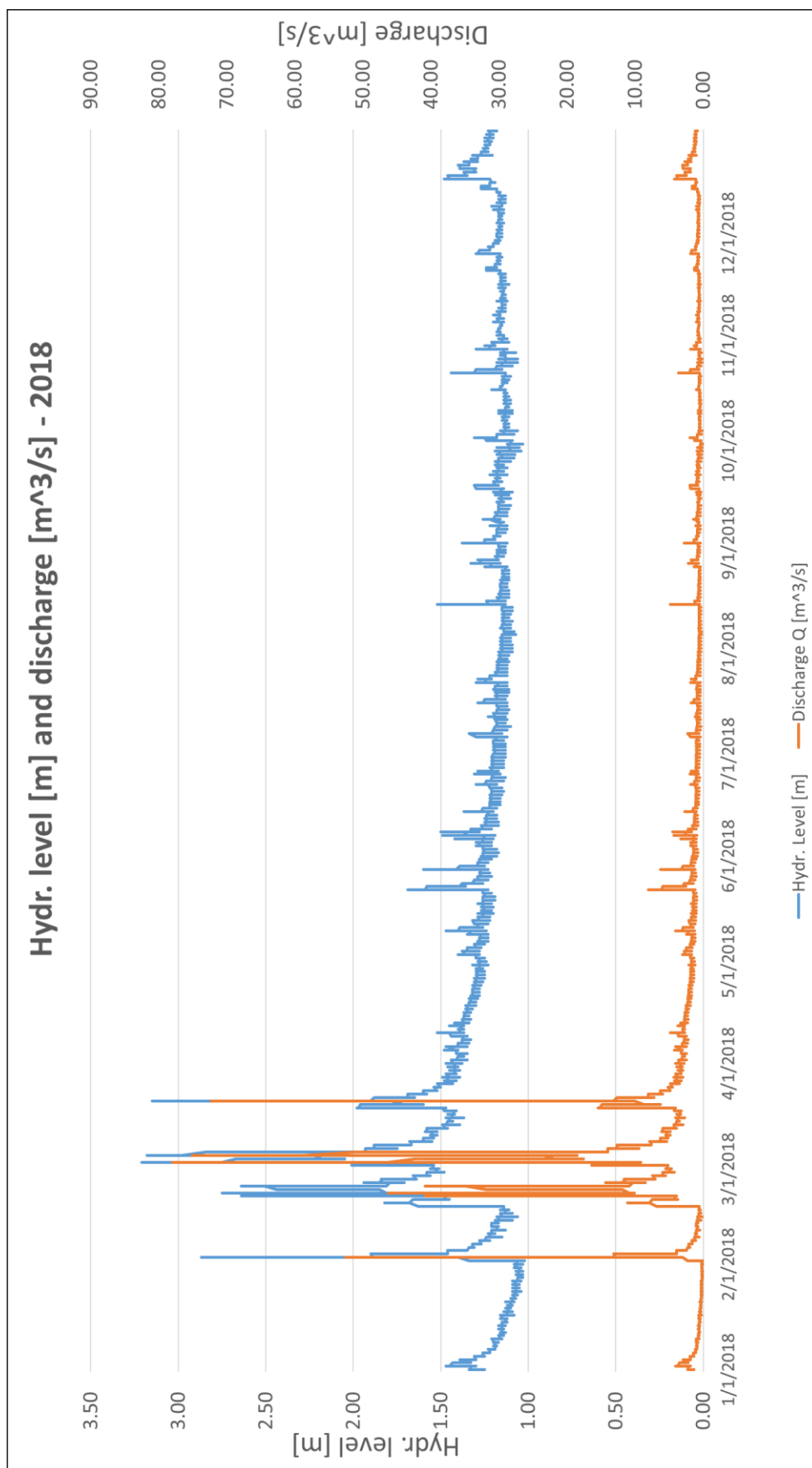


Figure 34 - Hydrometric level (m). on the left axis, and discharge (m³/s), on the right axis, year 2018

At this point, the duration curves, based on the daily average discharge, have been plotted, with the following procedure:

1. subdivide the daily average discharge into classes; the division have been realized with classes from 0 to 100 m³/s, with steps of 0.5 m³/s;
2. for each year, the number of days with at least the lower value of the class interval have been counted, obtaining directly the cumulative totals of each class;
3. calculate the percentages of the cumulative totals;
4. plot the data with the discharge on the x axis, in respect of the probability of exceedance, on y axis.

Furthermore, the average duration curve has been calculated, averaging the cumulative totals of the different years and calculating the percentages of these averages.

In Table 9, part of the calculations is reported as example.

Year	2018			2019			2020			Average	
C.i. Low Bound	#d>c.i. low	%d>c.i. low	σ ² -i (#)	#d>c.i. low	%d>c.i. low	σ ² -i (#)	#d>c.i. low	%d>c.i. low	σ ² -i (#)	#d>c.i. low	%d>c.i. low
>4.5	32	8.8	14.1	16	4.6	63.0	10	4.8	59.9	37.69	12.52
>4	33	9.0	26.7	19	5.4	76.8	12	5.7	71.7	42.77	14.21
>3.5	43	11.8	21.2	23	6.6	95.9	15	7.2	84.7	49.31	16.38
>3	50	13.7	33.1	29	8.3	124.1	18	8.6	117.4	58.54	19.45
>2.5	67	18.4	32.1	40	11.5	157.8	21	10.0	195.3	72.31	24.02
>2	83	22.7	56.9	60	17.2	171.4	27	12.9	301.5	91.15	30.28
>1.5	115	31.5	79.2	134	38.4	4.0	41	19.6	432.1	121.62	40.40
>1	172	47.1	44.5	173	49.6	17.8	63	30.1	559.4	161.92	53.80
>0.5	344	94.2	409.5	230	65.9	65.7	194	92.8	353.9	222.77	74.01
>0	365	100.0	0.0	349	100.0	0.0	209	100.0	0.0	301.00	100.00

Table 9 - Duration curves calculations

As shown, there is a column for the calculation of the variance σ^2 of each class in respect to the average value; the sum of all the variances was useful in order to find out the RMSE of each year.

All the duration curves are reported in Figure 35, in which the colours of the curves are different, relating to the number of the missing data of every year: in particular, they are:

- Green, for years with a percentage of missing data lower than 10%;
- Yellow, for years with a percentage of missing data between 10% and 25%;
- Red, for years with a percentage of missing data higher than 25%.

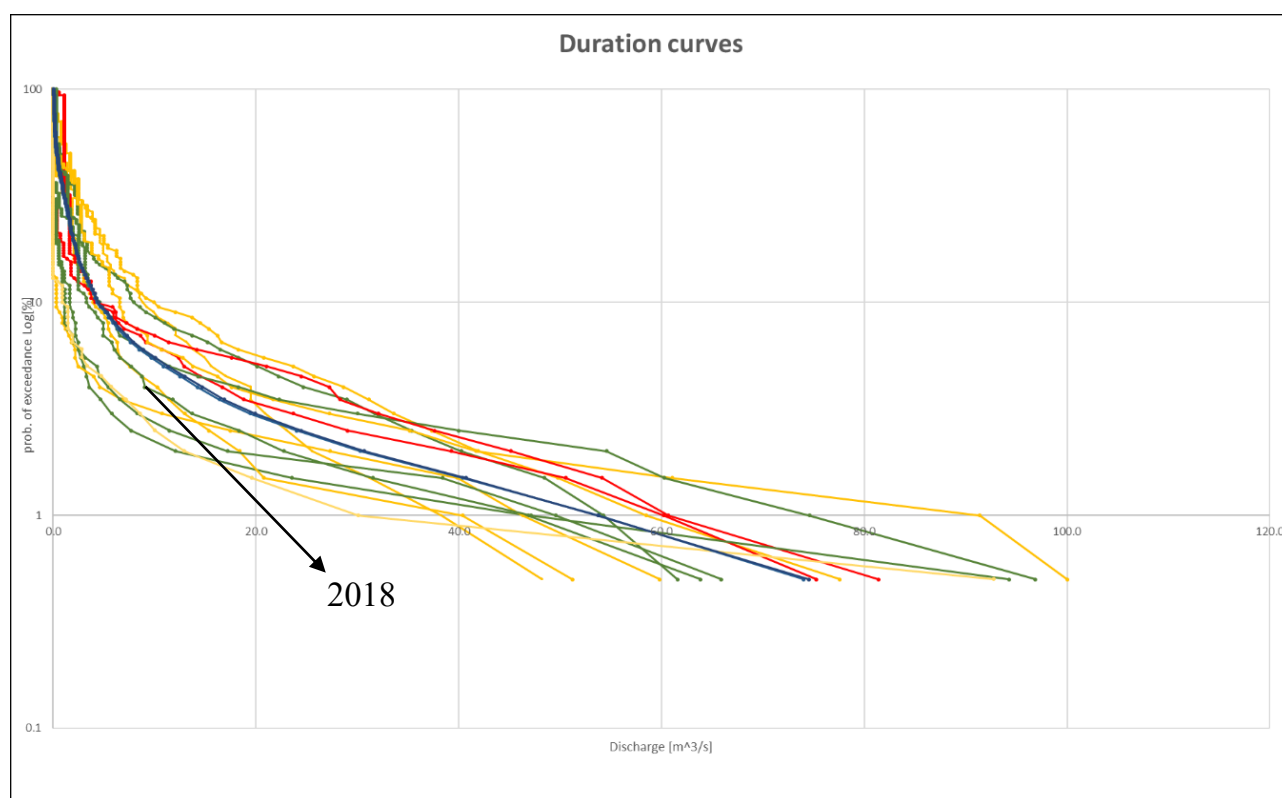


Figure 35 - Duration curves from 2005 to 2020 - Bettolle station

Then, in Table 10 the RMSEs of each year are reported: in the second column, the colour scale is proportional, from green to red, to the values of RMSE, from the lower

to the higher, respectively; in the third, instead, the scale is proportional to the percentage of missing data, recalling the results of Table 7.

Year	RMSE	% data miss
2005	2.92	13.13
2006	3.63	22.31
2007	3.13	0.04
2008	2.67	10.09
2009	2.47	11.04
2010	2.80	4.91
2012	1.41	51.52
2013	3.92	21.86
2014	3.44	4.73
2017	2.83	21.37
2018	1.98	0.00
2019	2.44	4.72
2020	3.65	43.39

Table 10 - RMSEs of investigated years, compared with data accuracy (as percentage of missing data)

The resulting RMSEs suggest that 2012 should be the typical year, but as it has a percentage of about 50% of missing data, it has been discarded as considered unreliable: for this reason, the 2018 have been selected as typical year for the further modelling and simulation part.

Now that the typical year has been chosen, the data of the hydrometric level of Ponte Garibaldi have been downloaded only for the year 2018, because they have been used as check values for the output data of the simulation, in order to evaluate the calibration accuracy.

3.2 Model implementation and calibration

The numerical modelling started from an already developed project, carried out in the recent years at UNIVPM (Ilari, 2021; Martinelli, 2021), which was, in turn, based on a previous model of the Civil Protection (2001). In this thesis, the available model has been improved by adjusting geometric characteristics and boundary conditions, and a systematic calibration process has been performed.

In order to have a better understanding of the calibration phases, a brief summary of the initial inputs is here reported.

3.2.1 Model setup

For this work, the input parameters, which have been adjusted in the calibration steps, essentially are:

- Geometric data: DTM terrain files, cross-sections geometry, bathymetry of the estuary and Manning coefficients;
- Boundary conditions: flow hydrograph and stage hydrograph for the initial boundary condition (i.e. at Bettolle cross-section), tidal stage for the final boundary condition (i.e. river estuary at Senigallia).

HEC-RAS software allows to implement other input parameters, but only the one mentioned have been taken into account in the model calibration.

3.2.1.1 Geometric data inputs

The starting point for the geometry definition is the DTM terrain implementation: for this purpose, topographic and bathymetric data have been requested to the Ministero dell'Ambiente e della Tutela del Territorio e del Mare.

In particular, the requested files were:

- Digital Terrain Model (DTM);
- Digital Surface Model first return (DSM first);
- Digital Surface Model last return (DSM last);
- point cloud in *.xyz format.

All the files were referred to a 2008 survey.

The DTM defines a generic statistic surface on which at a defined couple of points (X, Y), is attributed an elevation value (Z). The main difference between a DTM and a DSM lies on the fact that the former accounts only for the natural trend on the soil, whereas the latter considers also the objects that are present on the ground surface, such as anthropic elements (buildings) or natural ones (trees). The DSM first and DSM last indicate the impulses derived from the Lidar laser rays which are reflected in relation to the met objects, while the cloud point in *.xyz format, is the raw result of the laser acquisition, and it is composed of all the points collected by the Lidar provided with spatial coordinates. The DTM (Figure 36) has been used to define the geometry of the numerical model (Ilari, 2021; Martinelli, 2021).

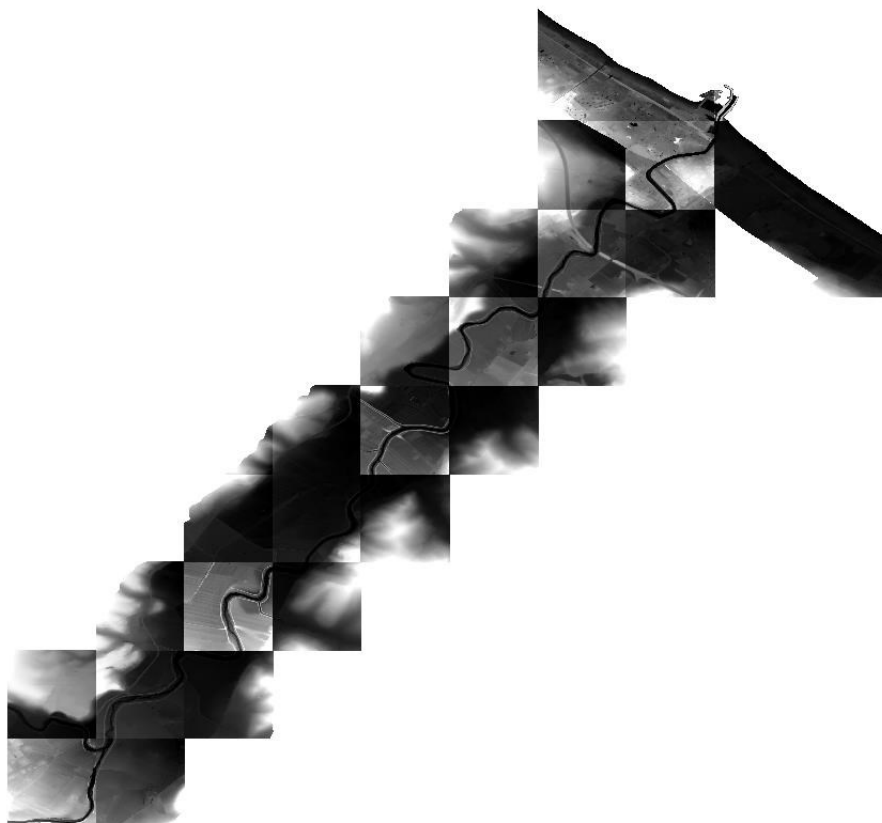


Figure 36 - DTM files used in the project

The DTM files, projected in EPSG: 32633 reference system, have been implemented into the software through the command “New terrain layer” (Figure 37).

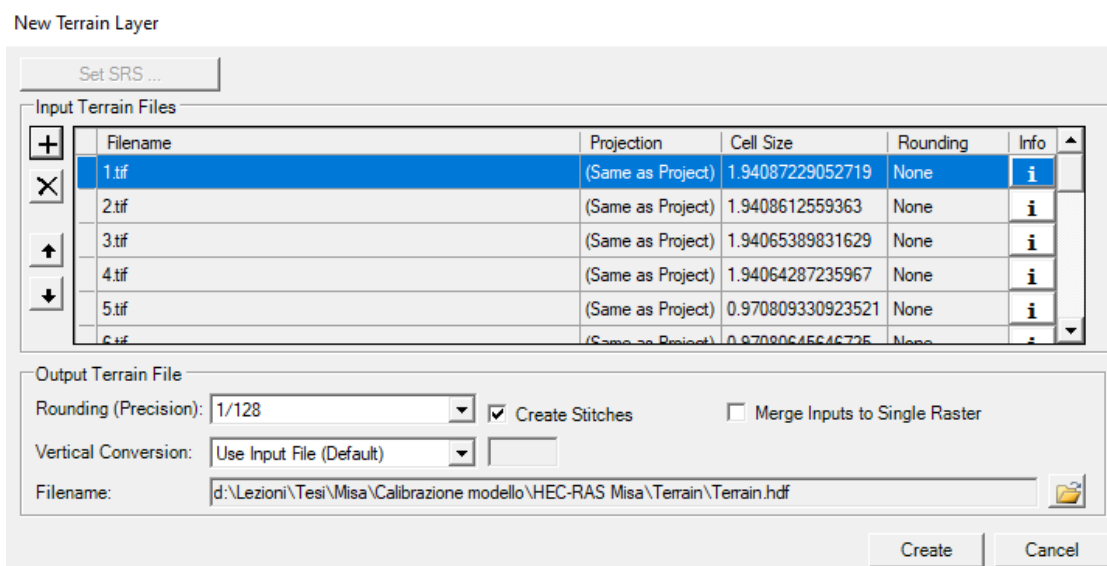


Figure 37 - DTMs implementation

The different characteristics of the DTM such as the cell size (resolution of the DTM) and the Rounding, which indicates the elevation precision of the new terrain data layer, have been left as default.

As said, the DTM terrains are a key aspect of the modelling, as the geometric data of the HEC-RAS model are built on its basis: the river flow direction, the bank lines, the flow path (which stands for the extension of the floodplain) and the desired cross-sections have been directly drawn on the terrain (Figure 38 and 39) by means of the dedicated tools.

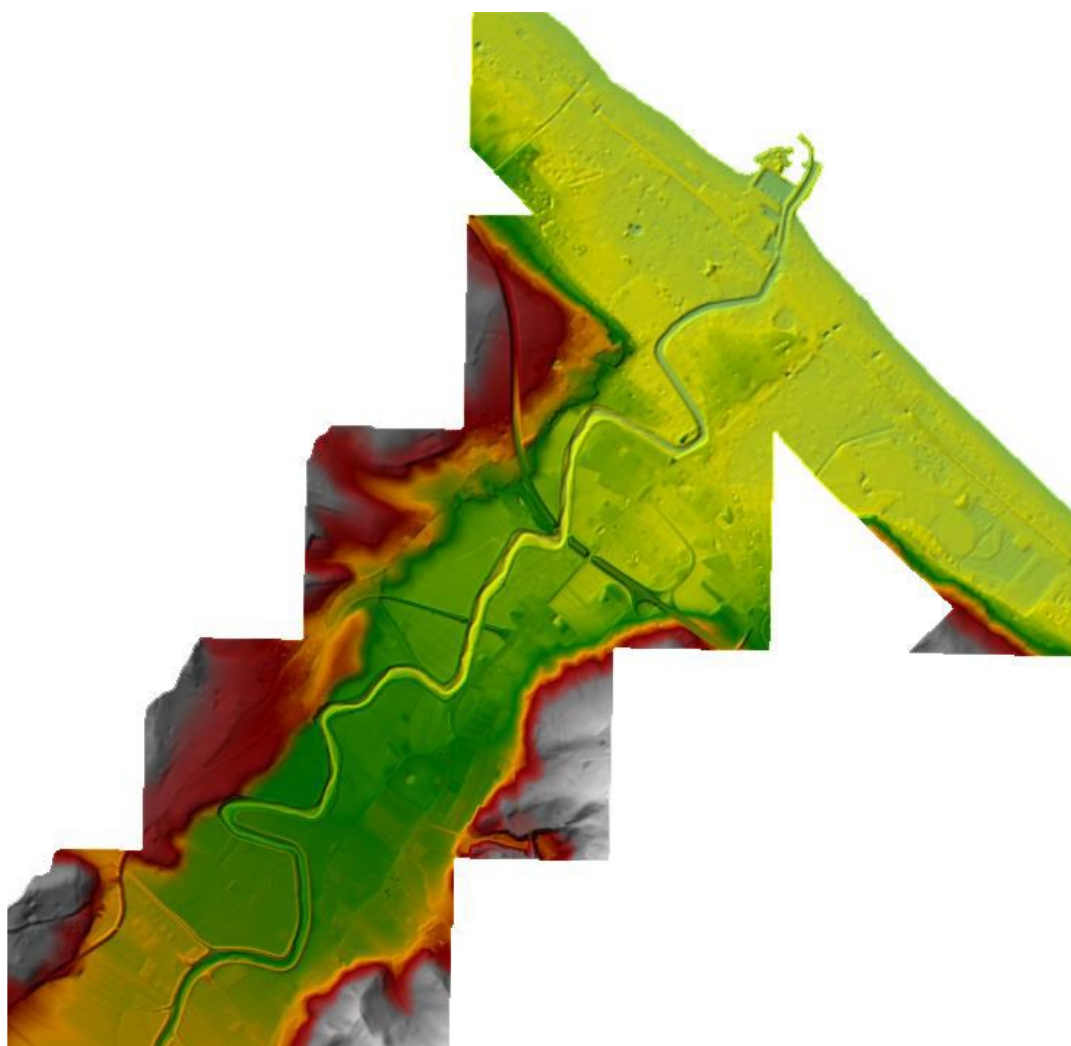


Figure 38 - Misa River DTM in HEC-RAS

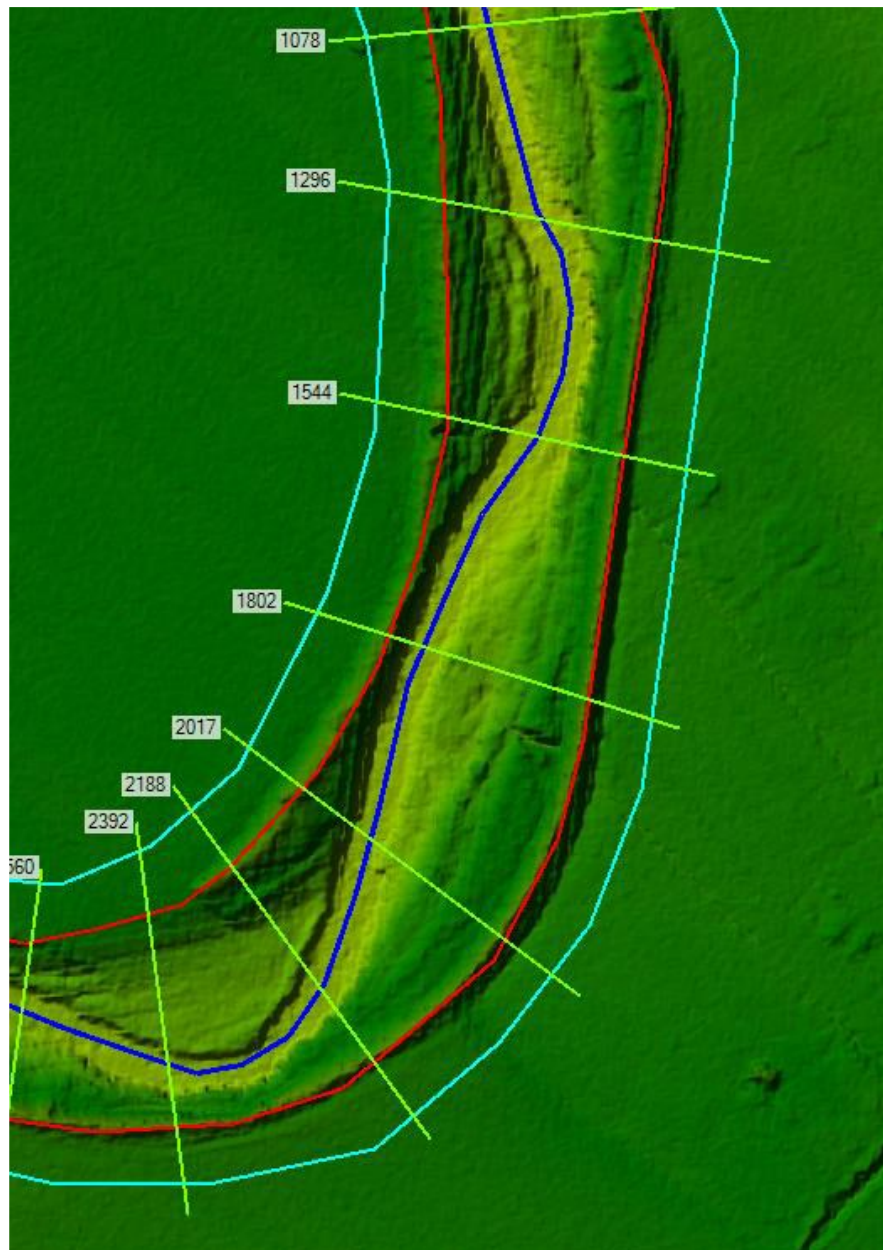


Figure 39 - Misa River geometry in RAS Mapper. In blue the river flow direction, in red the bank lines and in cyan the flow path

The cross-sections, in particular, have been extrapolated from the RAS terrain files, through the tool “Cut from terrain” available in the software (Figure 40). In general, the cross-sections have been evenly spaced along the river path, but they have been increased in number in correspondence of curves and cross-section variations (Figure 39). Moreover, some cross-sections (including Bettolelle and Ponte Garibaldi) have been implemented using more accurate and recent data dating back to 2019. This

dataset includes both data provided by the Civil Protection and data surveyed by UNIVPM (around the Ponte Garibaldi area).

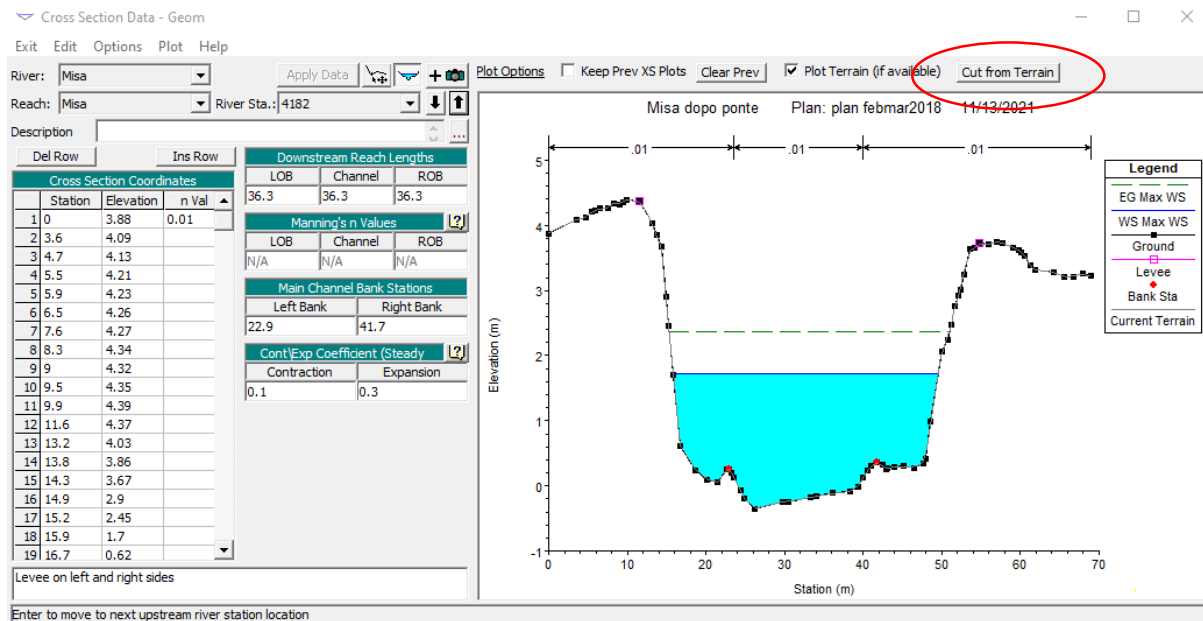


Figure 40 - Example of cross-section - Cut from terrain tool

The next step has been the interpolation of the geometry (Figure 41 and 42), which allows to link different points within consecutive cross-sections of the DTMs in order to have a continuity of the terrain (Ilari, 2021; Martinelli, 2021).

This operation has been done in RAS Mapper and it consists in:

- Selection of the desired cross-section to interpolate;
- Extraction of them into GeoTiff file that accounts for main channel and overbanks;
- Selection of the size with which the terrain will be extracted, considering that a lower size corresponds a higher definition but also a higher computation time and vice versa (for this reason, a size of 0.5 m has been selected);

- Implementation of the extracted GeoTiff file as “New terrain layer”, paying attention to let the extracted file as first file in order to maintain its characteristic.

Note that every change in any cross-section of the model implies a new interpolation of the cross section before any simulation run, in order to make effective the possible change in cross section parameters (geometry of the cross-section, levee position, Manning coefficient, etc.).

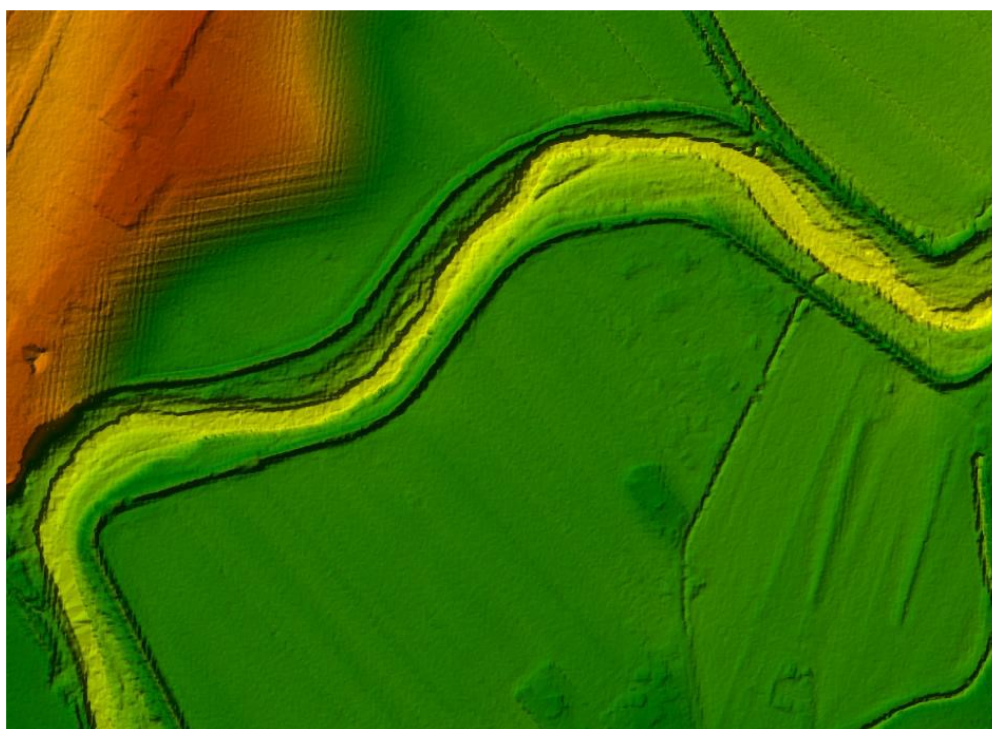


Figure 41 - River geometry before interpolation

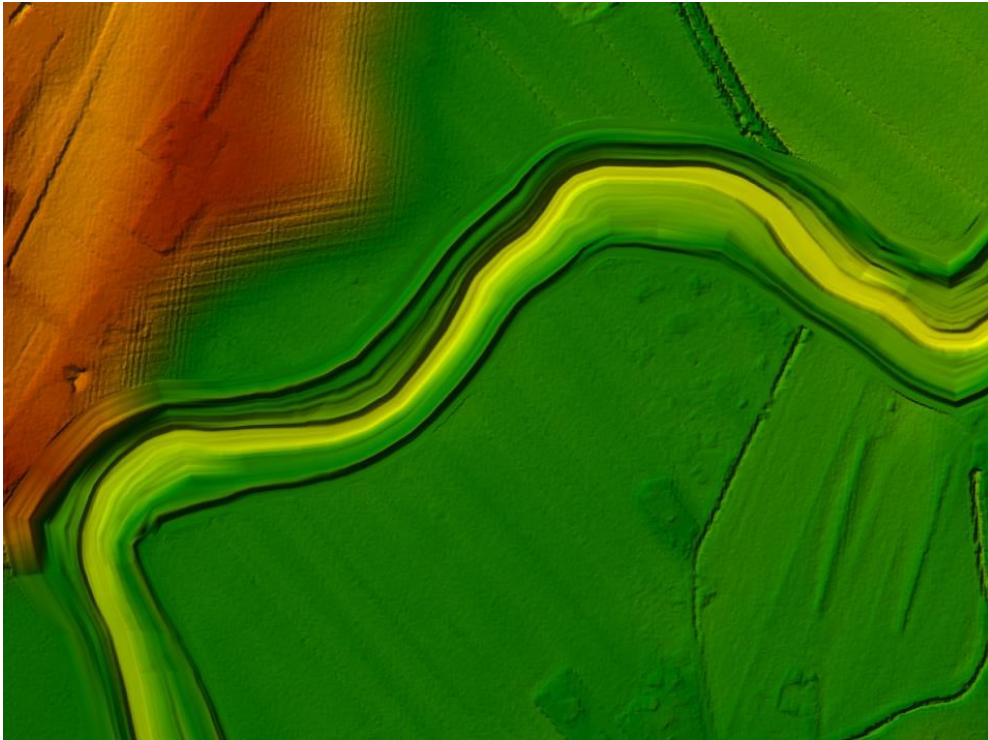


Figure 42 - River geometry after interpolation

The next step has been the addition of bridges, which have been added into the model by taking into consideration the dimensions found in the project developed by the Civil Protection in 2001, arranged with the new geometry of the cross section (Ilari, 2021; Martinelli, 2021).

Final step of the geometric data input has been the implementation of the bathymetry of the estuary (Ilari, 2021; Martinelli, 2021).

The bathymetric data, owned by the DICEA department, were in *.xyz format: by means of the use of CloudCompare software, the cloud point files are transformed into raster file, which can be added to the RAS Mapper in order to modify the geometry (i.e. the cross-sections) in proximity of the estuary (Figure 43).

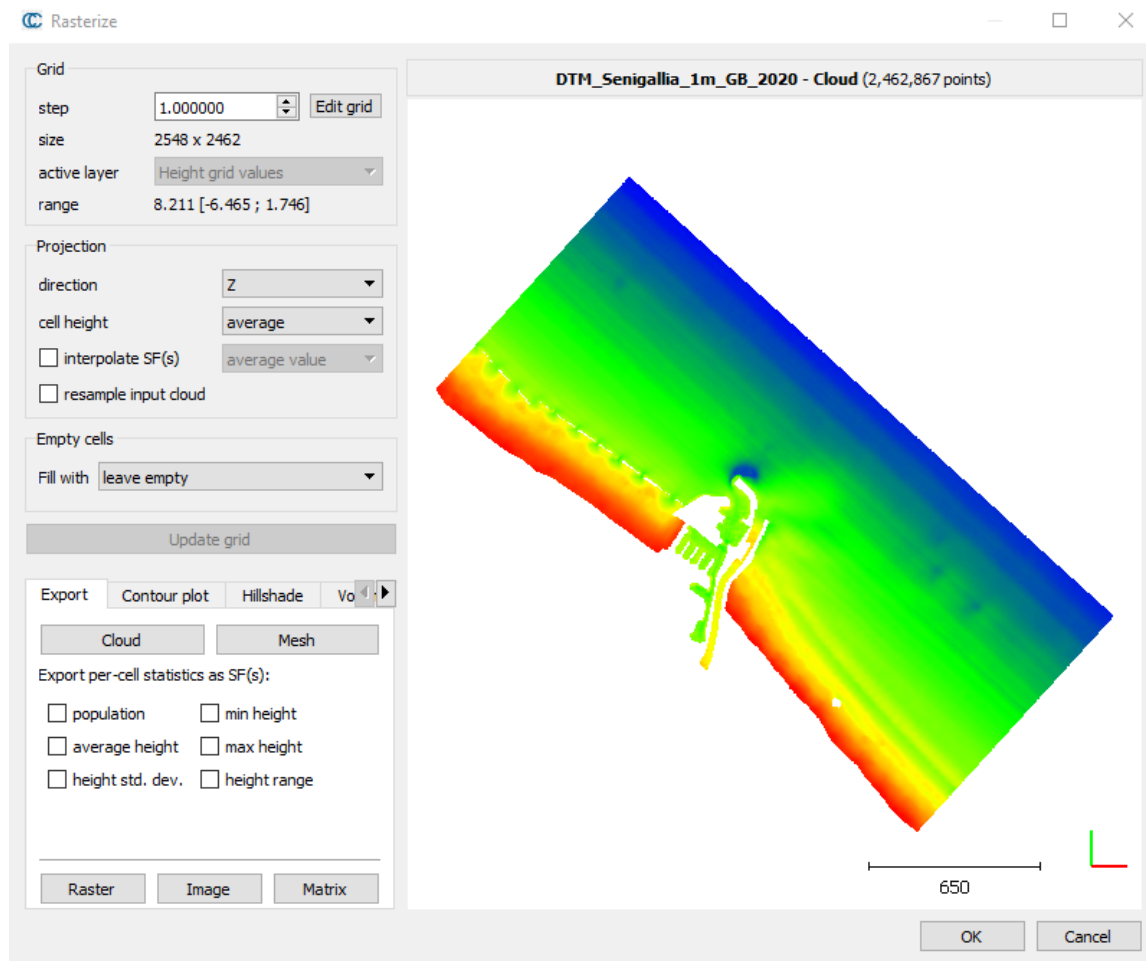


Figure 43 - CloudCompare rasterization operation

3.2.1.2 Boundary conditions input

Regarding the upstream boundary conditions (“BC” in the following), they can be given both in terms of flow and stage: the software will calculate the discharge automatically in respect to the first cross-section geometry in case of stage hydrograph input (Figure 44).

Flow Hydrograph

River: Misa Reach: Misa RS: 39110

☐ Read from DSS before simulation Select DSS file and Path

File:

Path:

☒ Enter Table Data time interval: 30 Minute

Select/Enter the Data's Starting Time Reference

☐ Use Simulation Time: Date: 04FEB2017 Time: 0000

☒ Fixed Start Time: Date: 04FEB2017 Time: 0000

No. Ordinates Interpolate Missing Values Del Row Ins Row

Hydrograph Data			
	Date	Simulation Time (hours)	Flow (m3/s)
1	03Feb2017 2400	00:00	5.266
2	04Feb2017 0030	00:30	5.266
3	04Feb2017 0100	01:00	5.266
4	04Feb2017 0130	01:30	5.428
5	04Feb2017 0200	02:00	5.428
6	04Feb2017 0230	02:30	5.428
7	04Feb2017 0300	03:00	5.594
8	04Feb2017 0330	03:30	5.428
9	04Feb2017 0400	04:00	5.107
10	04Feb2017 0430	04:30	5.594
11	04Feb2017 0500	05:00	5.763
12	04Feb2017 0530	05:30	5.428
13	04Feb2017 0600	06:00	5.266
14	04Feb2017 0630	06:30	5.266
15	04Feb2017 0700	07:00	5.266

Time Step Adjustment Options ("Critical" boundary conditions)

☐ Monitor this hydrograph for adjustments to computational time step

Max Change in Flow (without changing time step):

Min Flow: Multiplier:

Plot Data OK Cancel

Figure 44 - Upstream boundary condition example - Flow hydrograph

Similarly, the downstream boundary condition is added as the tidal stage, i.e. as stage hydrograph in the last cross section.

All the stage levels have been referred to the a.s.l., in agreement with software inputs and outputs.

Hence, SIRMIP stage values have been adapted:

- At Bettolle, SIRMIP values were increased by 19.18 m;
- At Ponte Garibaldi, SIRMIP values were lowered by 0.41 m.

3.2.2 Calibration of the model

The calibration of the model has been performed by means of comparison between the HEC-RAS results in respect of SIRMIP stage values at Ponte Garibaldi cross-section.

The selected year for the model calibration is 2018, which was the typical year that came out from the data analysis: more in specific, the calibration has been initially performed considering a rainy period occurred in the time period between February 18th and March 7th. Finally, the entire 2018 has been verified.

The calibration phase has followed a number of “steps”: starting from “Step 1” (the base model). For each step will be reported:

- Any change in the input data in respect to the previous step;
- The comparison between hydrographs of HEC-RAS results and SIRMIP values;
- The scatter plot of the HEC-RAS results and the SIRMIP data and relative RMSE value, calculated as follows:

$$RMSE = \sqrt{\sum_i^n \frac{(h_{Mi} - h_{Si})^2}{n}} \quad (17)$$

Where h_M and h_S are the stage values from the model and from the SIRMIP data, respectively, and n is the number of time intervals (787 in this case);

- Comments and critical analysis of the results.

3.2.2.1 Step 1 – Base model

The input data of the initial model (Ilari, 2021; Martinelli, 2021) were:

Geometry

- RAS terrains, referring to the DTM obtained from 2008 surveys, with implementation of 2019 surveys;
- A number of cross-section upstream in respect of Bettollelle, coming from 2001 Civil Protection modelling;
- A series of Manning coefficient, named “Series 1”, coming from the 2001 Civil Protection model;
- Estuary bathymetry relative to 2020

Boundary conditions

- Flow hydrograph, applied to the most upstream section, which was about 2.5 km upstream in respect to Bettollelle;
- Tidal stage of Ancona tide gauge, applied at the most downstream section.

Furthermore, Manning coefficients of the cross-section upstream in respect of Bettollelle cross-section (i.e. 8 cross-sections, Figure 47) have been artificially modified in order to obtain results similar to SIRMIP measurements at Bettollelle cross-section in terms of discharge.

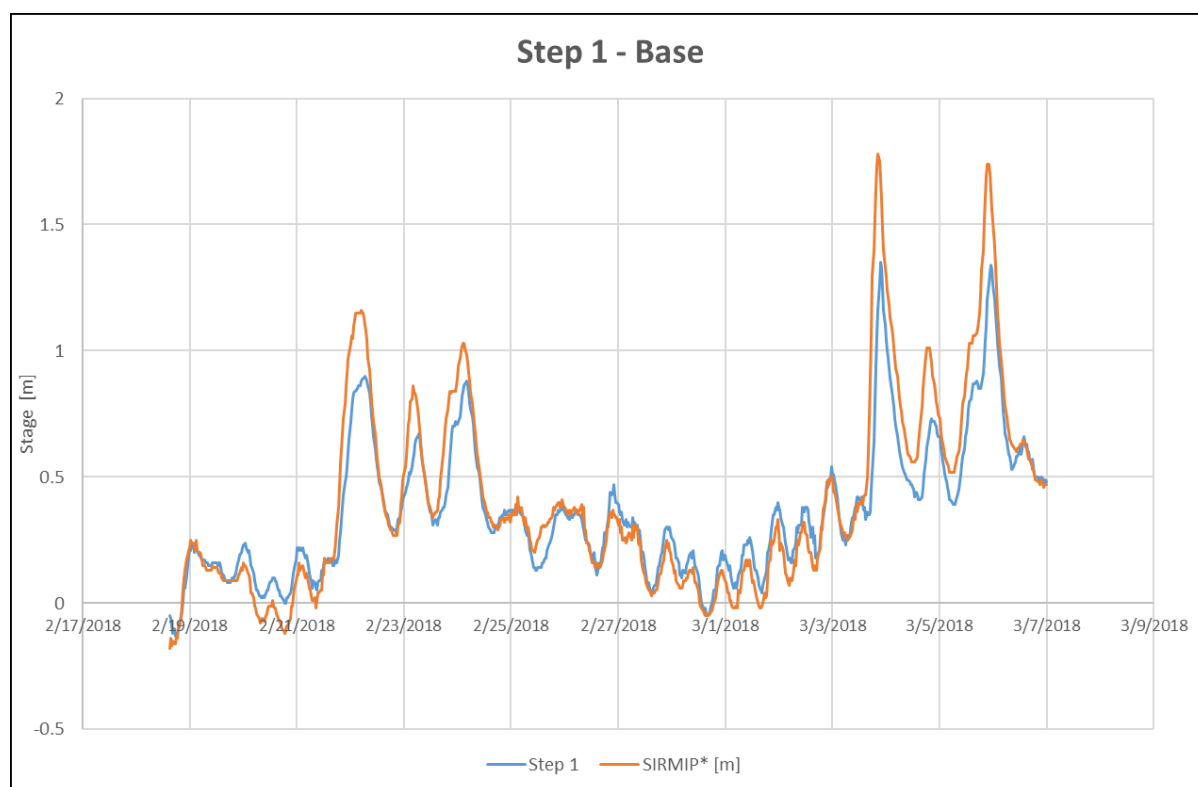


Figure 45 - Step 1 hydrograph of Ponte Garibaldi: stage (m) HEC-RAS results vs SIRMIP values

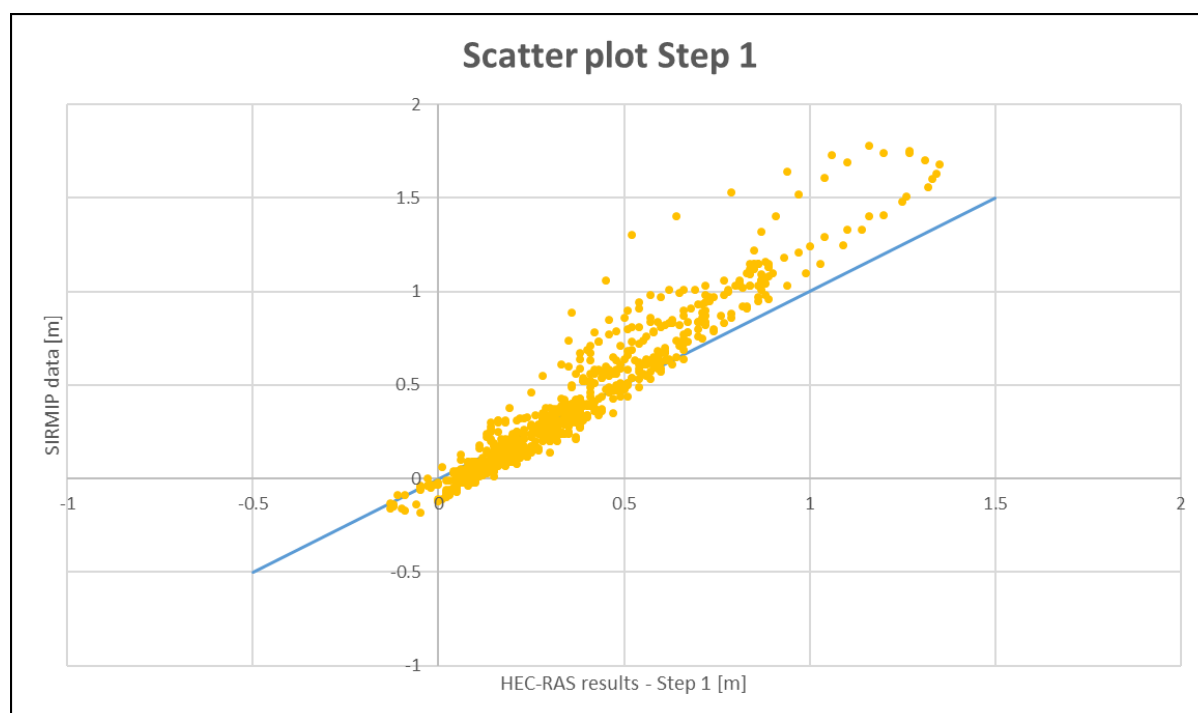


Figure 46 - Scatter plot relative to Step 1

The RMSE of this step is equal to 0.1465 m.

As shown in the graphs (Figure 45 and 46), there are important differences between the two curves, in particular in the peak periods.

3.2.2.2 Step 2 – Upstream cross-sections removal

In this step, the stretches upstream of Bettolle cross-section have been removed: in particular, 8 cross-sections have been removed, as shown in Figure 47.

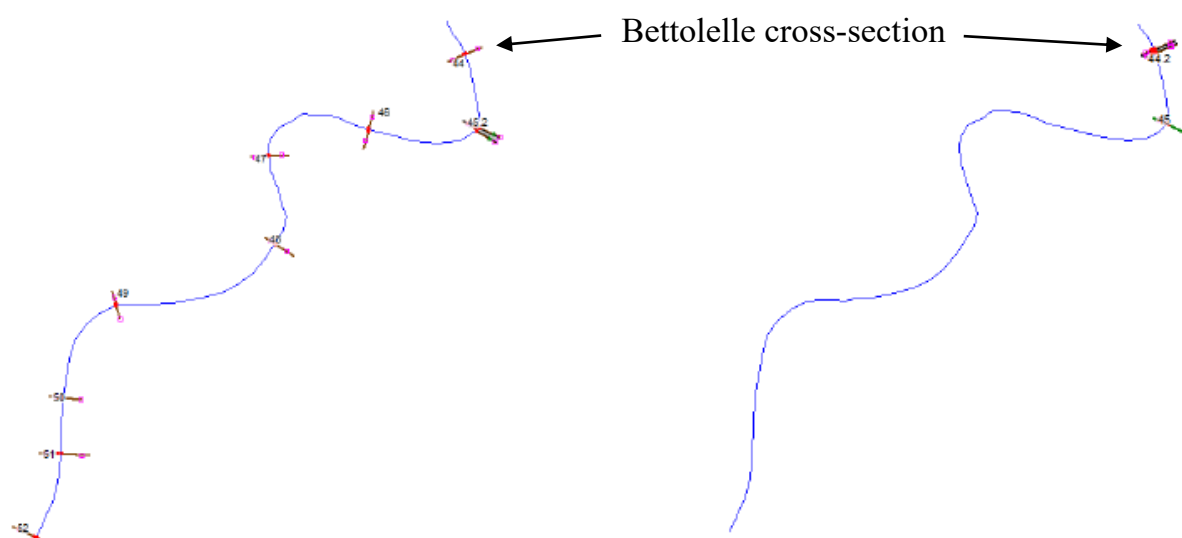


Figure 47 - Step 2: cross-sections removal

In this way, the initial boundary condition could be applied at Bettolle, where the measurements of the SIRMIP are available.

Moreover, the levees position of all cross-sections have been checked (Figure 48 and 49): this adjustment is likewise linked to the Manning coefficients, since without a correct setting of the levees, the water that was supposed to run along the main channel would have flowed also in the floodplain region, with the subsequent alteration of the river flow dynamics.

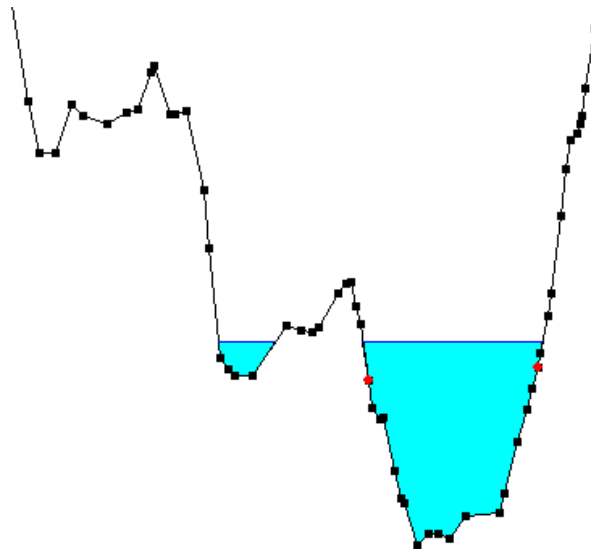


Figure 48 - Cross-section without levees

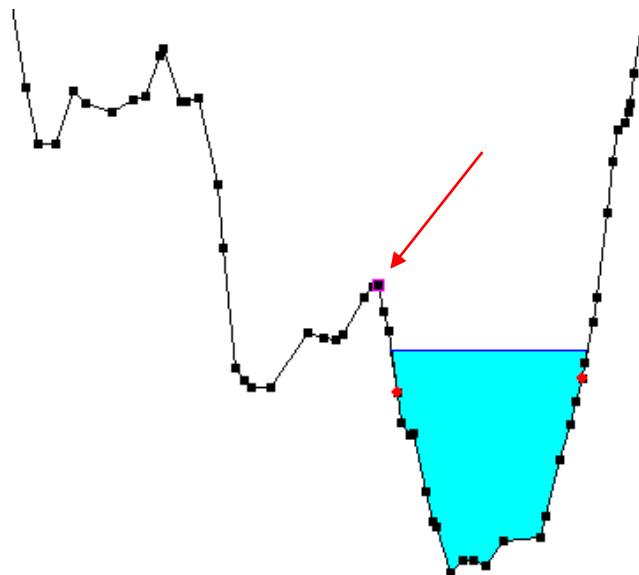


Figure 49 - Cross-section with levees assigned

Although, almost all the levees have been kept as they were in the initial model (Step 1) and not significant result changes were expected due to this operation.

The other setup parameters have been left as they were in Step 1.

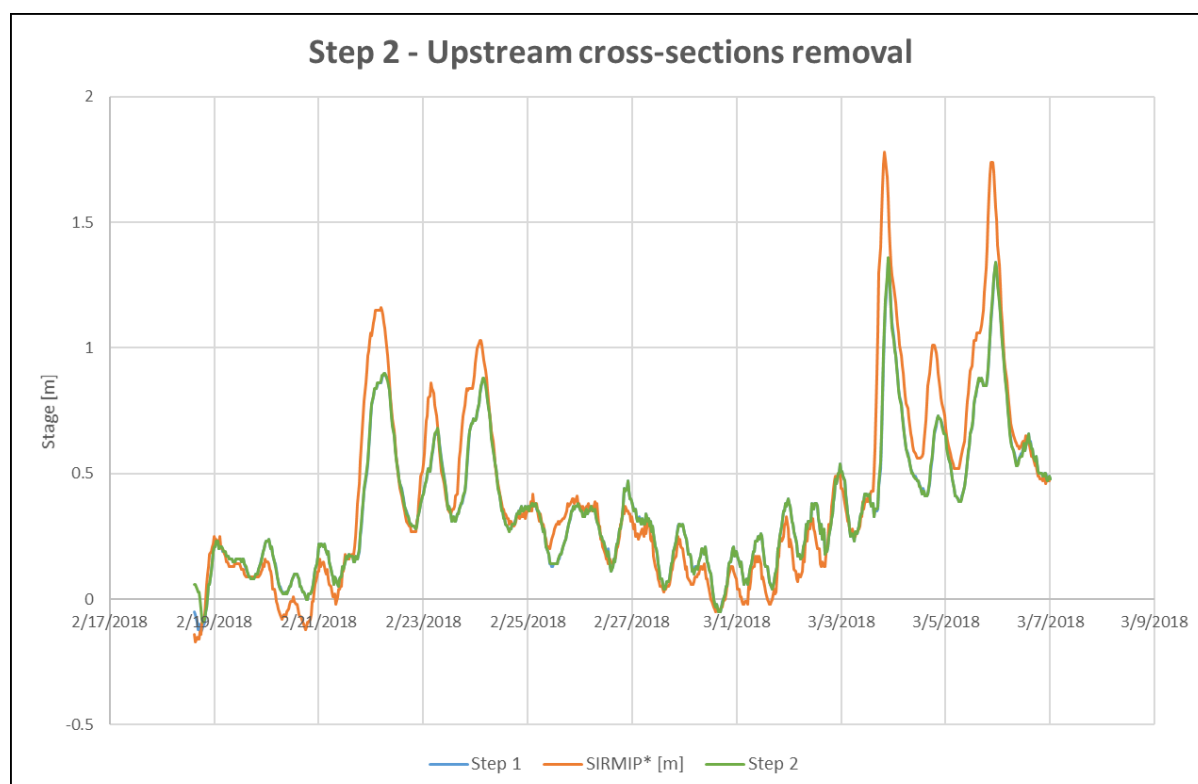


Figure 50 - Step 2 hydrograph of Ponte Garibaldi: stage (m) HEC-RAS results vs SIRMIP values

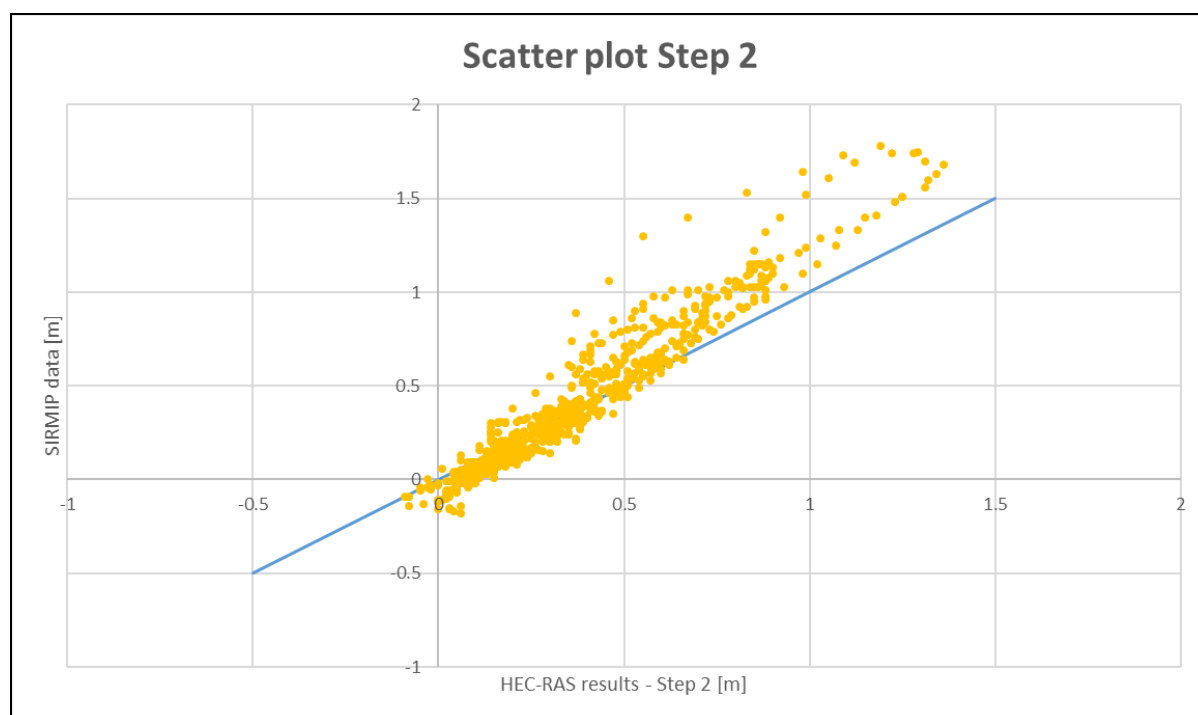


Figure 51 - Scatter plot relative to Step 2

The RMSE of this step is equal to 0.1449 m.

As shown in the graphs (Figure 50 and 51), no appreciable changes could be seen in this step (Step 1 and Step 2 curves are overlying): the reason is that, as said, the model was calibrated to have the same initial conditions at Bettolle. This step was made in order to have a more accurate and feasible model, with the right position of the boundary conditions.

3.2.2.3 Step 3 – Stage hydrograph BC input

In this step, the flow hydrograph, initial BC of Bettolle, was substituted by the stage hydrograph (Figure 52), in order to avoid any kind of rounding (or mistakes) of calculation passing from the stage to flow discharge by means of rating curve: in this way, this task is entrusted directly to the software.

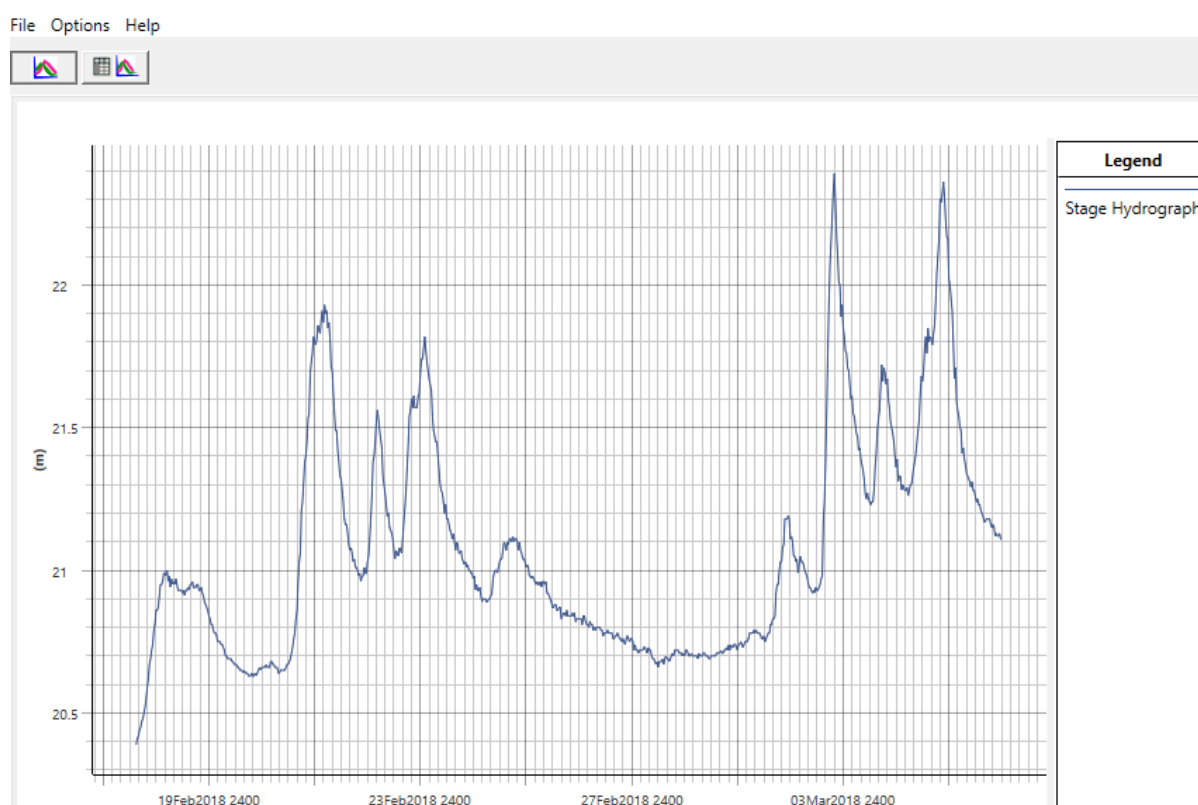


Figure 52 - Initial BC, Bettolle stage hydrograph

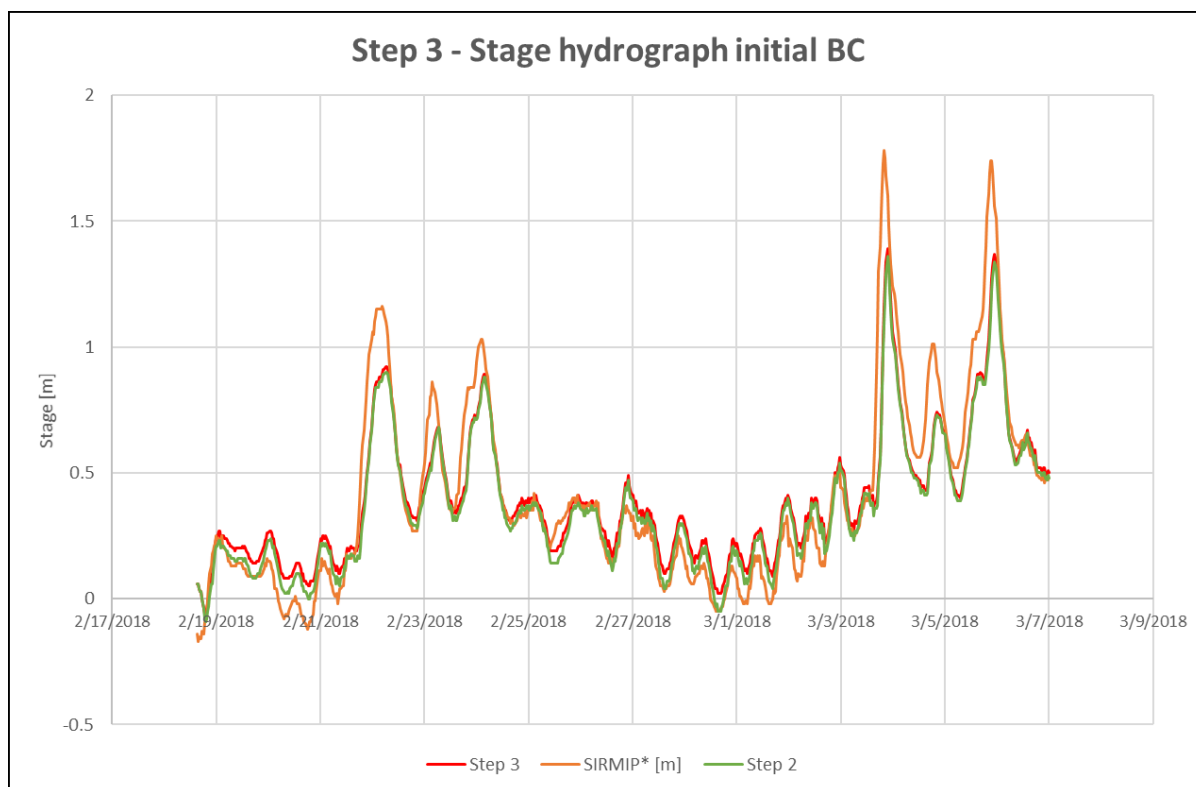


Figure 53 - Step 3 hydrograph of Ponte Garibaldi: stage (m) HEC-RAS results vs SIRMIP values

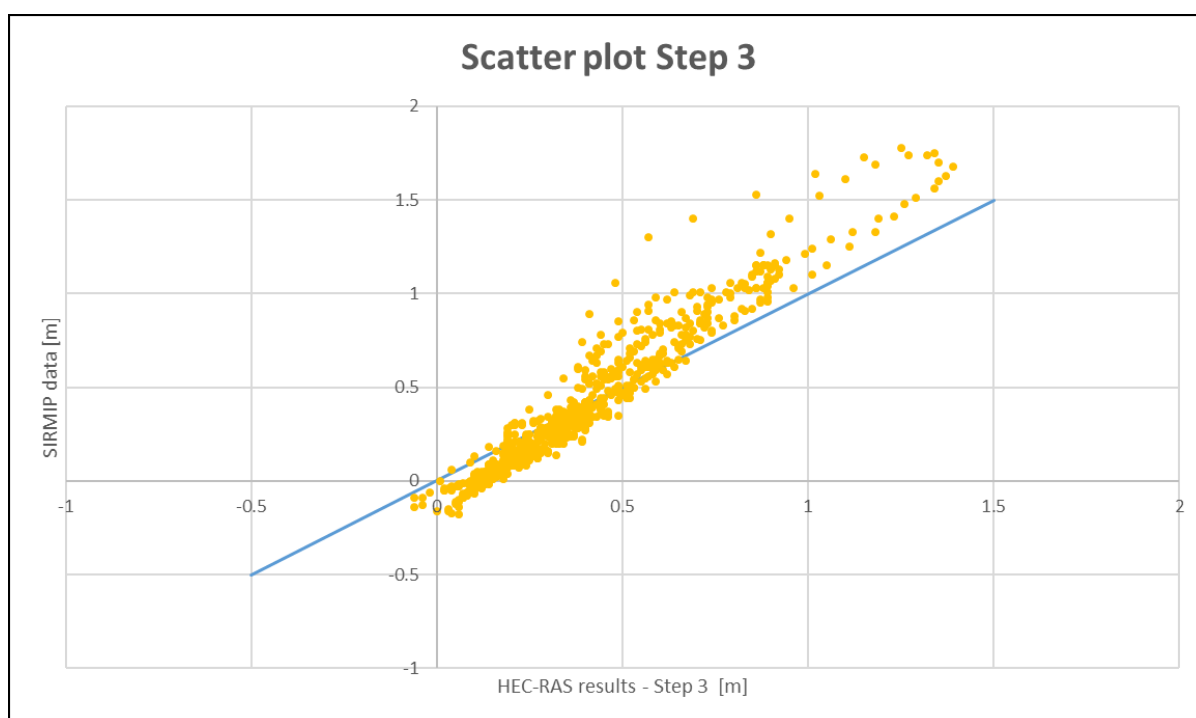


Figure 54 - Scatter plot relative to Step 3

The value of the RMSE of this step is 0.1441 m.

As shown in the hydrograph, results did not improve significantly, but still there are some differences between step 2 (green curve in Figure 53) and step 3 hydrograph (red line in Figure 53): this is caused probably by a different rating curve of the programme in respect to the rating curve provided by the SIRMIP, through which the previous flow hydrograph was calculated.

3.2.2.4 Step 4 – Bathymetry 2018 implementation

Moving to step 4, the 2018 bathymetry referring to the lower portion of the Misa River has been implemented: the *.xyz cloud point file, available at UNIVPM, has been opened with software CloudCompare and then rasterized; the raster file was added as new terrain file (ordered as first in the terrain file editor in order to superimpose the old one, Figure 55) into the model and then the relative cross-sections have been modified cutting them from the terrain. Further cross-sections interpolation has been done and the simulation started again, with all other inputs kept as in step 3.

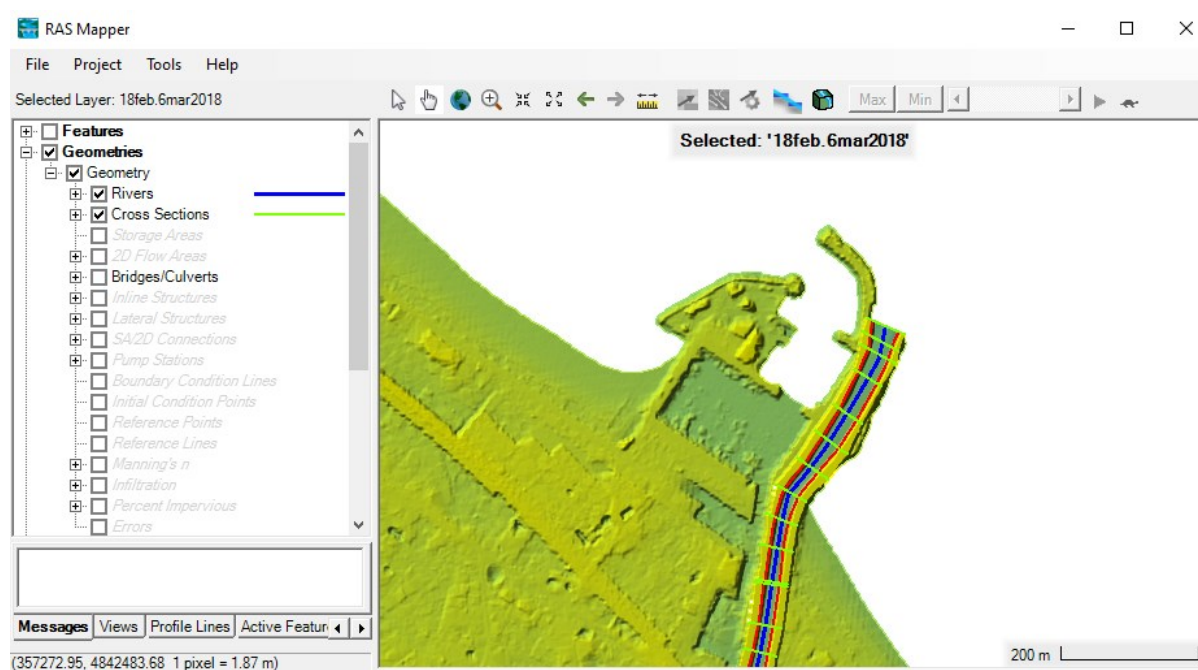


Figure 55 - 2018 bathymetry implementation

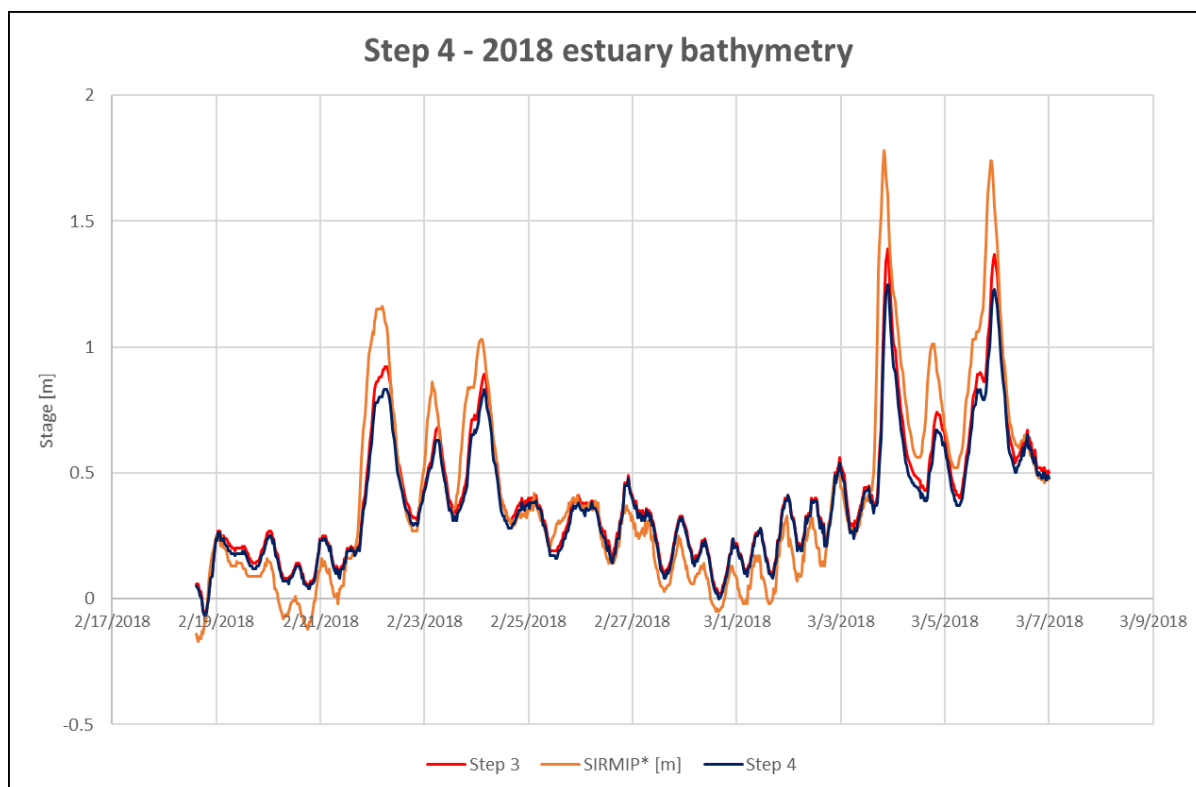


Figure 56 - Step 4 hydrograph of Ponte Garibaldi: stage (m) HEC-RAS results vs SIRMIP values

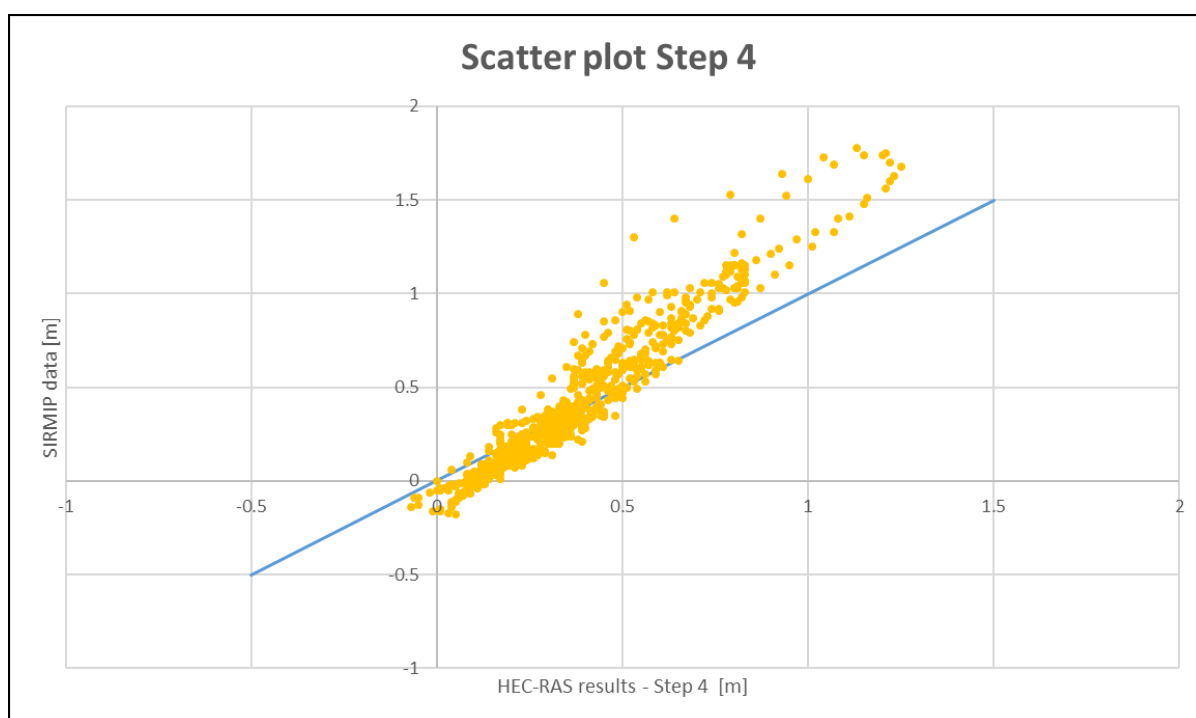


Figure 57 - Scatter plot relative to Step 4

The RMSE for this step is equal to 0.1677 m.

In this step, the results are worse respect those of step 3, which is evident from a visual analysis of graphs (Figure 56 and 57) and from the value of RMSE.

However, this was an obliged step, as the bathymetry related to 2018 must be chosen: the reason stands probably on the fact that the Manning values of the previous step were calibrated on a different bathymetry, which results to have a significant influence on the simulation results.

3.2.2.5 Step 5 – Manning value calibration

In this step, a new set of Manning coefficient (called “series 2”) substituted the previous Manning values: this new set of values (Figure 58) has been deduced from a critical analysis of the terrain from satellite views and substituted the old set of values coming from the 2001 Civil Protection survey.

Edit Manning's n or k Values

River: ☒ Edit Interpolated XS's Channel n Values have a light green background

Reach:

Selected Area Edit Options

	River Station	Frctn (n/K)	n #1	n #2	n #3
1	37747	n	0.03	0.04	0.03
2	37457	n	0.03	0.04	0.03
3	37195	n	0.03	0.04	0.03
4	36920	n	0.03	0.04	0.03
5	36469	n	0.03	0.04	0.03
6	36219	n	0.03	0.04	0.03
7	35789	n	0.03	0.04	0.03
8	35302	n	0.03	0.04	0.03
9	34983	n	0.03	0.04	0.03
10	34536	n	0.03	0.04	0.03
11	34102	n	0.03	0.04	0.03
12	33886	n	0.03	0.04	0.03
13	33599	n	0.03	0.04	0.03
14	33227	n	0.03	0.04	0.03
15	32966	n	0.03	0.04	0.03
16	32816	n	0.03	0.04	0.03
17	32587	n	0.03	0.04	0.03
18	32425	n	0.03	0.04	0.03
19	32261	n	0.03	0.04	0.03
20	32028	n	0.03	0.04	0.03

Figure 58 - Manning value "series 2" dataset for main and side channels

This step encloses a number of attempts, needed to reach the results showed in the following graphs (Figure 59 and 60).

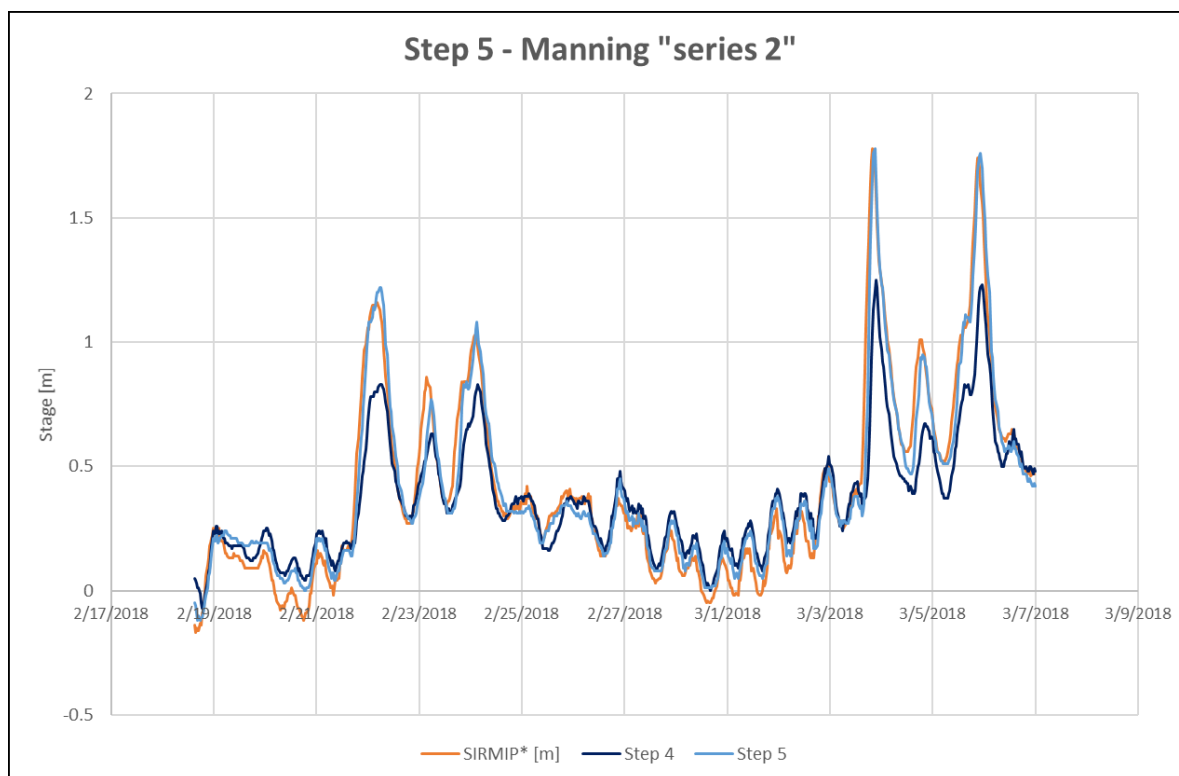


Figure 59 - Step 5 hydrograph of Ponte Garibaldi: stage (m) HEC-RAS results vs SIRMIP values

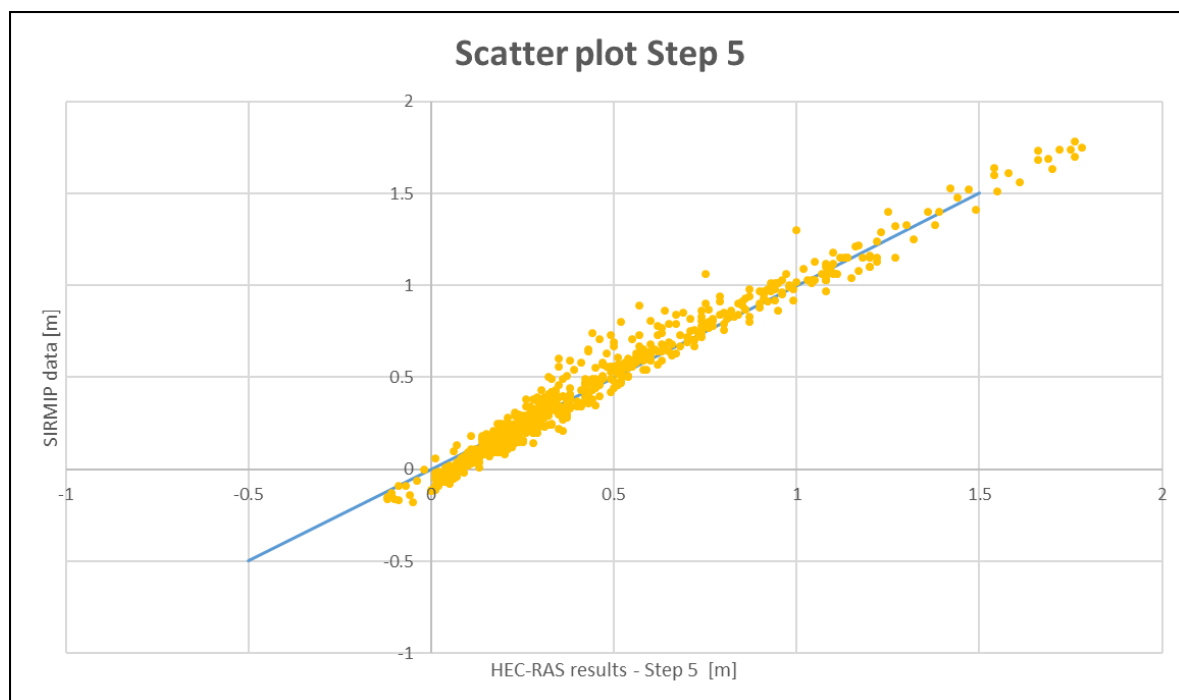


Figure 60 - Scatter plot relative to Step 5

The RMSE of this step is 0.06961 m.

As shown, it is possible to clearly see the influence of Manning coefficients in the model simulation: there is an important improvement in the results, well represented by the RMSE value. The peaks of this hydrograph (green curve, Figure 59) are much closer to the peak of the SIRMIP hydrograph in respect to step 4.

Still, there is a lack of accuracy, in particular way in the dry periods.

3.2.2.6 Sub-steps 5.1 to 5.6– Dry periods Manning calibration

A number of attempts have been done in order to improve the results for the dry periods, in particular in the period of time between July 1st and July 14th.

The steps, with relative RMSEs, consisted of changing in main channel and/or overbanks, increasing/decreasing Manning values; they are summed in Table 11.

Step	Manning Dataset	RMSE
Step5.1	Manning "series 2"	0.139609
Step5.2	Manning "series 1"	0.150753
Step5.3	Manning "series 2.1"	0.139538
Step5.4	Manning "series 2.2"	0.186824
Step5.5	Manning "series 2.3"	0.166156
Step5.6	Manning "series 2.4"	0.141433

Table 11 - Dry periods calibration attempts

Starting from step 5.1, in which Manning values were the same of step 5 (series 2), a first attempt has been made using the Manning “series 1” of step 1 to 4; then, new datasets of Manning value (series 2.1 to 2.4) have been used in the following attempts.

Note that the values of RMSE is not supposed to be compared with the ones of previous steps, as here there is another period of time: in fact, it is just used to evaluate the effect of the changes of n values in respect of these steps only.

As shown, no improvements can be appreciated and it was concluded that the mismatch of the dry periods is not due to Manning values: in the next steps, the dataset of “series 2” was kept as it was.

As example, for brevity issues, a couple of graphs related to these attempts are reported (Figure 61 and 62).



Figure 61 - Step 5.3 hydrograph vs SIRMIP hydrograph

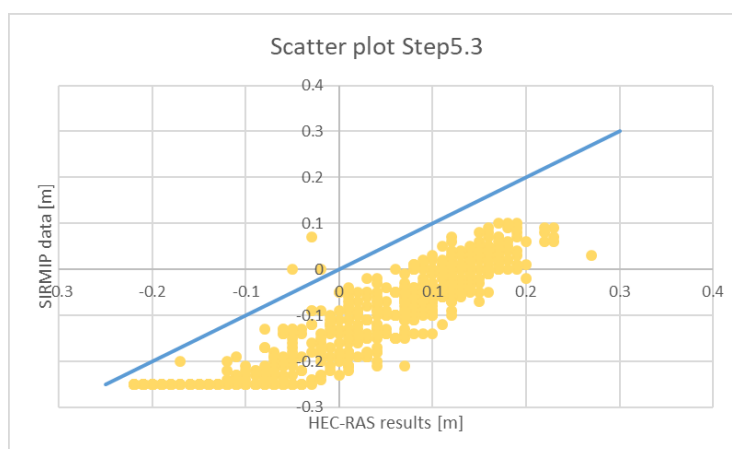


Figure 62 - Scatter plot relative to Step 5.3

3.2.2.7 Step 6 – Tidal stage BC of Senigallia tide gauge

In this final step of the calibration, the tidal stage hydrograph of Senigallia (Figure 63) substituted the Ancona one, used in the previous step.

Select Location in table then select Boundary Condition Type

	River	Reach	RS	Boundary Condition
1	Misa	Misa	37747	Stage Hydrograph
2	Misa	Misa	3	Stage Hydrograph

Stage Hydrograph

River: Misa Reach: Misa RS: 3

☐ Read from DSS before simulation Select DSS file and Path

File:

Path:

☒ Enter Table Data time interval: 30 Minute

Select/Enter the Data's Starting Time Reference

☐ Use Simulation Time: Date: 01JAN2018 Time: 0030

☒ Fixed Start Time: Date: 01JAN2018 Time: 0030

No. Ordinates Interpolate Missing Values Del Row Ins Row

Hydrograph Data			
	Date	Simulation Time (hours)	Stage (m)
1	01Jan2018 0030	00:00:00	0.01
2	01Jan2018 0100	01:30:00	0
3	01Jan2018 0130	01:00:00	-0.02
4	01Jan2018 0200	02:30:00	-0.04
5	01Jan2018 0230	02:00:00	0.01
6	01Jan2018 0300	03:30:00	0
7	01Jan2018 0330	03:00:00	-0.04
8	01Jan2018 0400	04:30:00	-0.01
9	01Jan2018 0430	04:00:00	0.05
10	01Jan2018 0500	05:30:00	0.04
11	01Jan2018 0530	05:00:00	0.1
12	01Jan2018 0600	06:30:00	0.11
13	01Jan2018 0630	06:00:00	0.16
14	01Jan2018 0700	07:30:00	0.17
15	01Jan2018 0730	07:00:00	0.16
16	01Jan2018 0800	08:30:00	0.17

Plot Data OK Cancel

Figure 63 - Tide stage of Senigallia tide gauge implementation

Figure 64 and 65 show the hydrographs and the scatter plot of step 6.

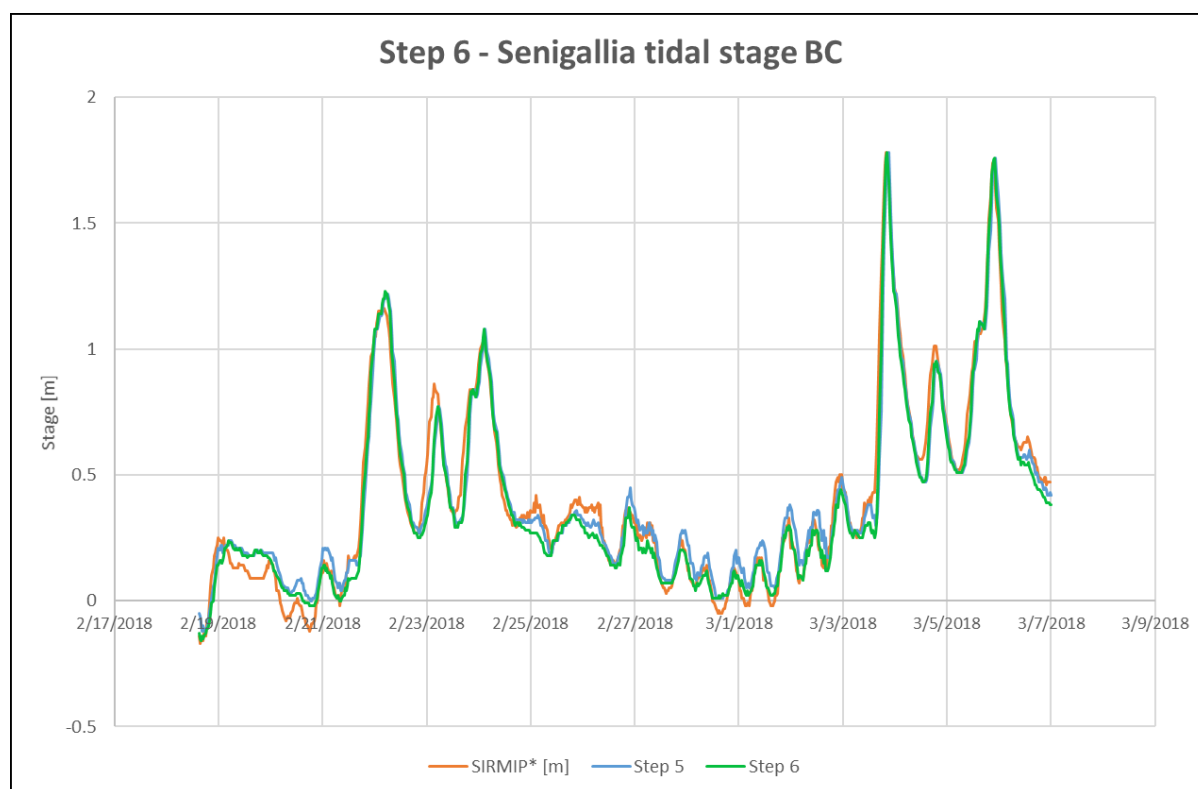


Figure 64 - Step 5 hydrograph of Ponte Garibaldi: stage (m) HEC-RAS results vs SIRMIP values

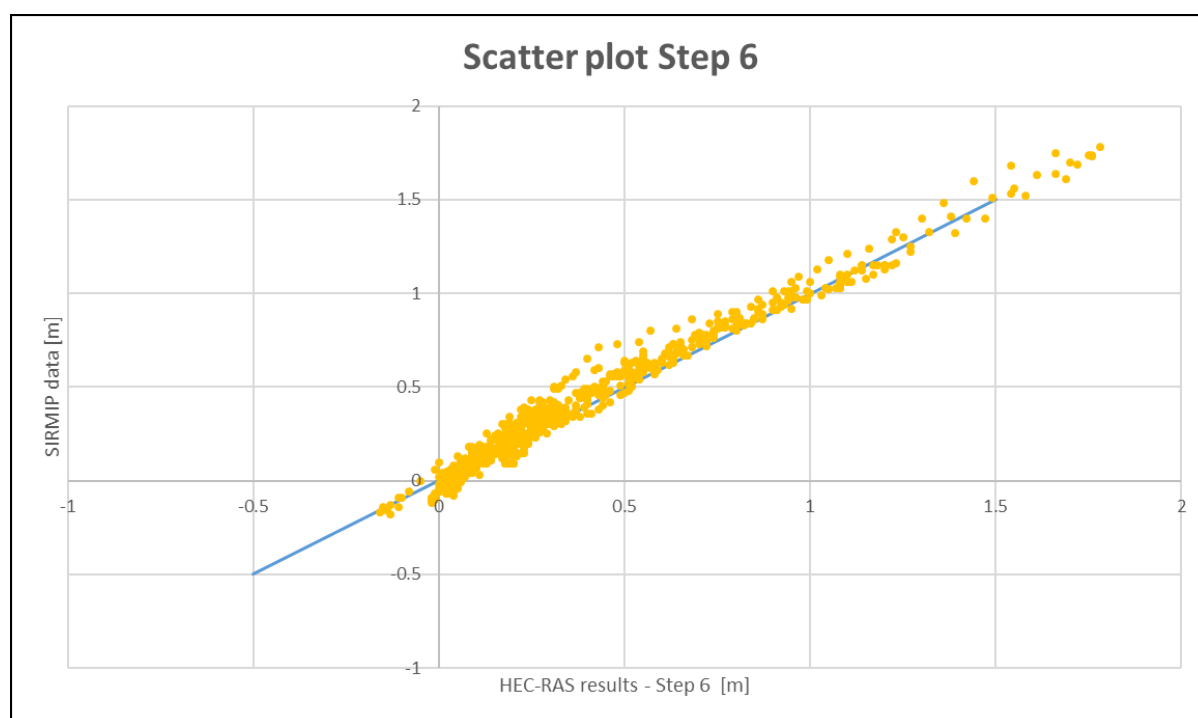


Figure 65 - Scatter plot relative to Step 6

The RMSE of this step is 0.0649 m.

This value has been considered small enough to end the calibration phase, as it shows an adequate accuracy for the aim of the present work.

Lastly, considering the mismatch at the very beginning of every hydrograph of all the steps, which is related to the time needed to get the simulation up and running (which is, in this case, a period of about 7 hours), the simulation of the whole year 2018 has been setup with December 31st, 2017 as start time, in order to have the most accurate results possible.

In Figure 66 and 67, hydrograph related to the whole 2018 and relative scatter plot are reported.

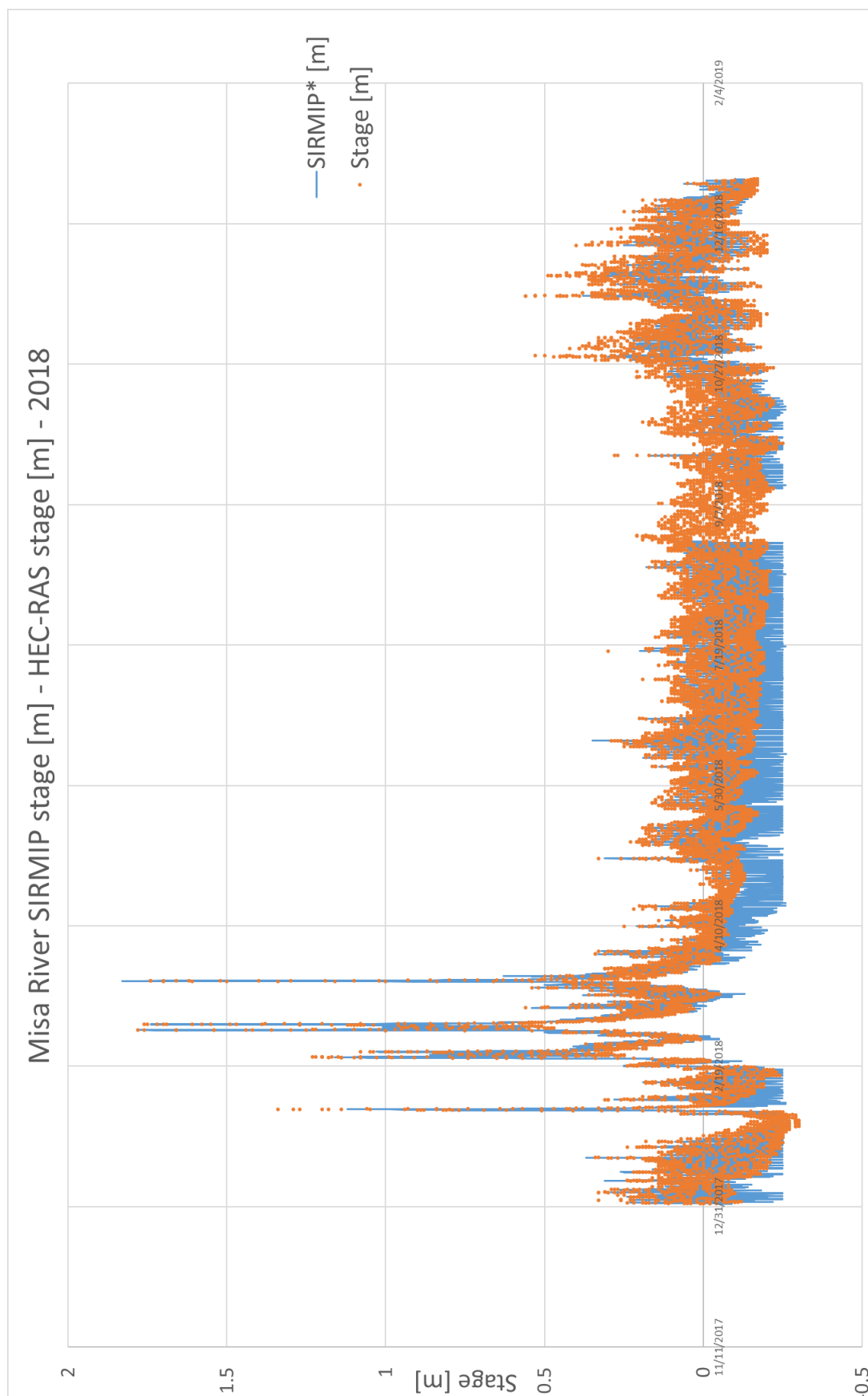


Figure 66 - Hydrograph of P. Garibaldi, year 2018: SIRMIP vs HEC-RAS values

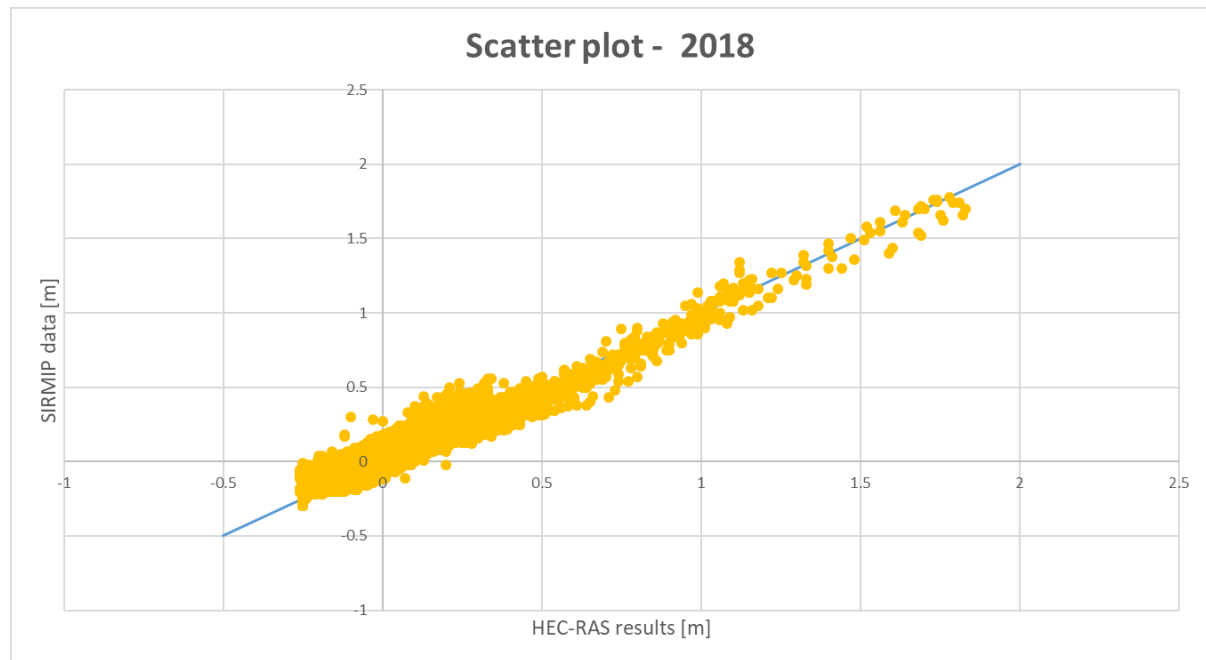


Figure 67 - Scatter plot relative to year 2018

From the 2018 hydrograph (Figure 66), it is shown that the simulation has good results for the wet periods (peaks), but there is a relevant lack of accuracy in the middle part of the graph, which are the dry periods, object of study in step 5.

This is probably due to the fact that, in this model, phenomena of groundwater discharge/recharge were not taken into account: in particular, in summer (in the middle of the hydrograph), when the groundwater is lower, there will be an important flux of water from river to the groundwater itself (losing-river condition), causing a lowering in river stage level. On the other hand, in autumn and winter, this flux should be lower or with opposite sign (gaining-river condition). A partial confirmation is the little difference in the hydrograph between measured values and simulation results of wet periods.

In Table 12, a summary of the calibration phase is reported, in which, for each step, is reported the input changes and the relative RMSEs.

Step#	Input changes	RMSE
Step 1	Base model:	0.1465
	First section more upstream than Bettollelle	
	Initial BC: Flow hydrograph	
	Final BC: Ancona tide stage	
	Bathymetry 2020	
	Manning value series 1	
Step 2	Upstream cross-sections removal	0.1449
Step 3	Initial BC: Stage hydrograph	0.1441
Step 4	Bathymetry relative to 2018	0.1667
Step 5	Manning series 2 implementation	0.0696
Step 5.1	Manning calibration for dry periods (RMSE not reported, as done in a different period of time)	
Step 5.2		
Step 5.3		
Step 5.4		
Step 5.5		
Step 5.6		
Step 6	Final BC: Senigallia tide stage	0.0649

Table 12 - Model calibration summary

3.3 Energetic analysis

Once the model has been calibrated, its results have been employed for the energetic production assessment. In particular, the average flow velocity and the water surface data, coming from the simulation, for all the cross sections of the model have been investigated, in order to evaluate suitable location for the installation of a hydrokinetic turbine system.

In Table 13, the yellow column “WS elev*” reports the water surface elevation referred to the channel bottom.

Date	Q tot [m ³ /s]	Min ch el [m]	WS elev [m]	WS elev* [m]	Chan vel [m/s]	Flow area [m ²]	XS Aver vel [m/s]
1/1/2018	10.87	0.4	1.4	1	0.45	24.71	0.440
1/1/2018	10.87	0.4	1.4	1	0.45	24.73	0.440
1/1/2018	10.78	0.4	1.39	0.99	0.45	24.6	0.438
1/1/2018	10.75	0.4	1.39	0.99	0.45	24.55	0.438
1/1/2018	10.73	0.4	1.39	0.99	0.45	24.54	0.437
1/1/2018	10.61	0.4	1.39	0.99	0.44	24.39	0.435
1/1/2018	10.5	0.4	1.38	0.98	0.44	24.22	0.434
1/1/2018	10.57	0.4	1.38	0.98	0.44	24.3	0.435
1/1/2018	10.58	0.4	1.39	0.99	0.44	24.34	0.435
1/1/2018	10.49	0.4	1.38	0.98	0.44	24.2	0.433
1/1/2018	10.47	0.4	1.38	0.98	0.44	24.18	0.433
1/1/2018	10.59	0.4	1.38	0.98	0.44	24.32	0.435
1/1/2018	10.71	0.4	1.39	0.99	0.45	24.5	0.437
1/1/2018	10.73	0.4	1.39	0.99	0.45	24.53	0.437
1/1/2018	10.61	0.4	1.39	0.99	0.44	24.38	0.435

Table 13 - Example of simulation results, data used for the energetic analysis

3.3.1 Cross sections selection

The selection of possible locations where to perform the evaluation of the available and extractable energy, are based on two main criteria:

- from a practical point of view, cross sections in which the installation of turbine could be easier and cheaper, i.e. cross sections located downstream of bridges;
- from an efficiency worthiness, cross sections with higher values of average velocity to maximize the available power and, by consequence, the energy production.

In both cases, cross sections evenly distributed among the whole river have been selected.

By means of qualitative analysis, the thematic map (Figure 68) of the maximum velocity results has been analysed, in order to evaluate some suitable cross section to be investigated.

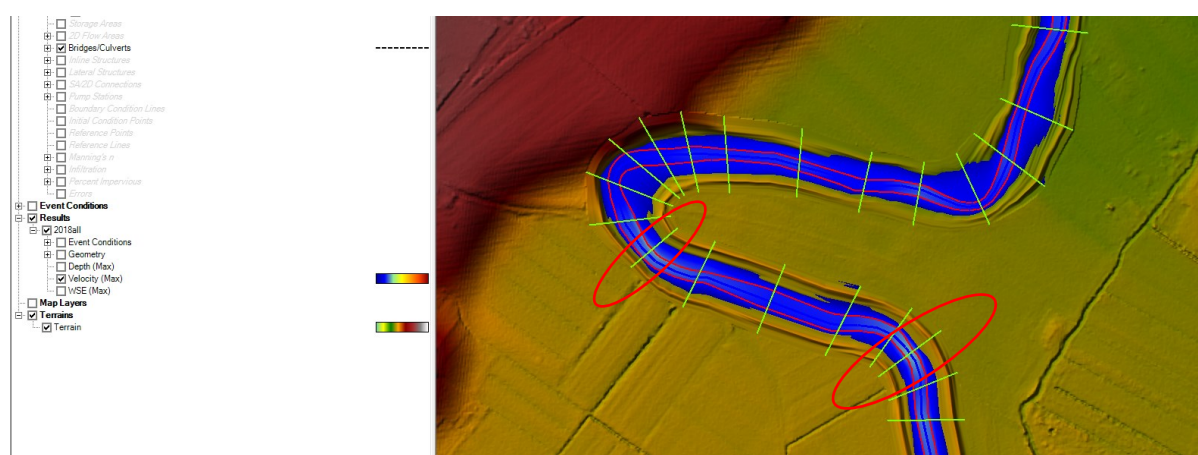


Figure 68 - Example of high velocity cross sections, circled in red

Following these criteria, the selected cross sections (named by a number, which represent the distance in meters from the estuary, calculated on the river flow direction, Figure 69 and 70) have been:

- Cross sections downstream the 4 bridges of the model, which are:
 XS 6052, “Ponte via Urbana”;
 XS 10569, “Ponte A14”;
 XS 13215, “Ponte Borgo Galluzzo”;
 XS 25806, “Ponte Cannella-Vallone”
- “High velocity cross sections, which are:
 XS 11134, XS 15292, XS 17487, XS 21008.



Figure 69 - Selected cross sections, part 1

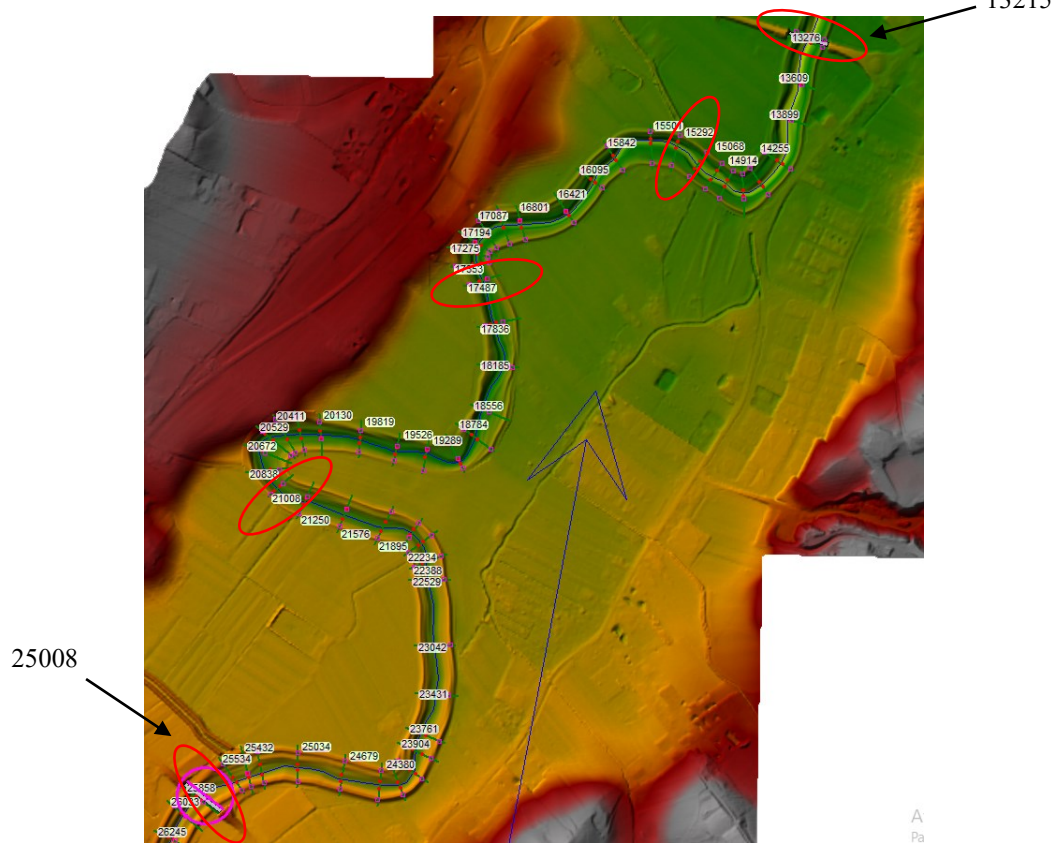


Figure 70 - Selected cross sections, part 2

3.3.1.1 High velocity sections evaluation

Some preliminary calculations have been performed, in order to evaluate if the “high velocity cross-sections” selected show a significant earning in terms of both power available above the whole cross-section and power available in case of application of a single turbine. In both cases, the velocity considered is the average velocity of the whole cross section (further considerations about the value of the velocity have been done in chapter 3.3.3).

Hence, recalling the equation of the available power P_a ,

$$P_a = \frac{1}{2} \rho A v^3$$

on the basis of the data of Table 13, the available power for each cross-section have been calculated, both for the whole cross section and for a single turbine, at each time interval.

The available power of the whole cross section (Table 15, 6th column) has been calculated considering:

- a value of 997 kg/m^3 for the water density;
- a flow area, in m^2 , directly from the results (Table 15, 5th column);
- the average velocity for the whole cross-section, coming from the results as well (Table 15, 4th column).

The power available for a single turbine has been calculated considering only an aligned configuration of a turbine with the maximum radius (i.e. the maximum area and the maximum power available), because in this phase the aim is to compare different types of cross-sections and not different types of turbine configurations.

In order to evaluate the maximum radius, duration curves of the water surface elevation of each cross-section have been constructed, analogously what done in chapter 3.3.1.

In this way, the value of water surface elevation with 90% probability of exceedance (“WS_{90%}”) has been calculated for each cross-section: this value, for this step and the further energy production assessment, has been considered as minimum activation threshold of the turbine (for each configuration).

As an example, the duration curve of the water surface elevation of the cross-section 6052 (location shown in the upper part of Figure 69) is reported in Figure 71.

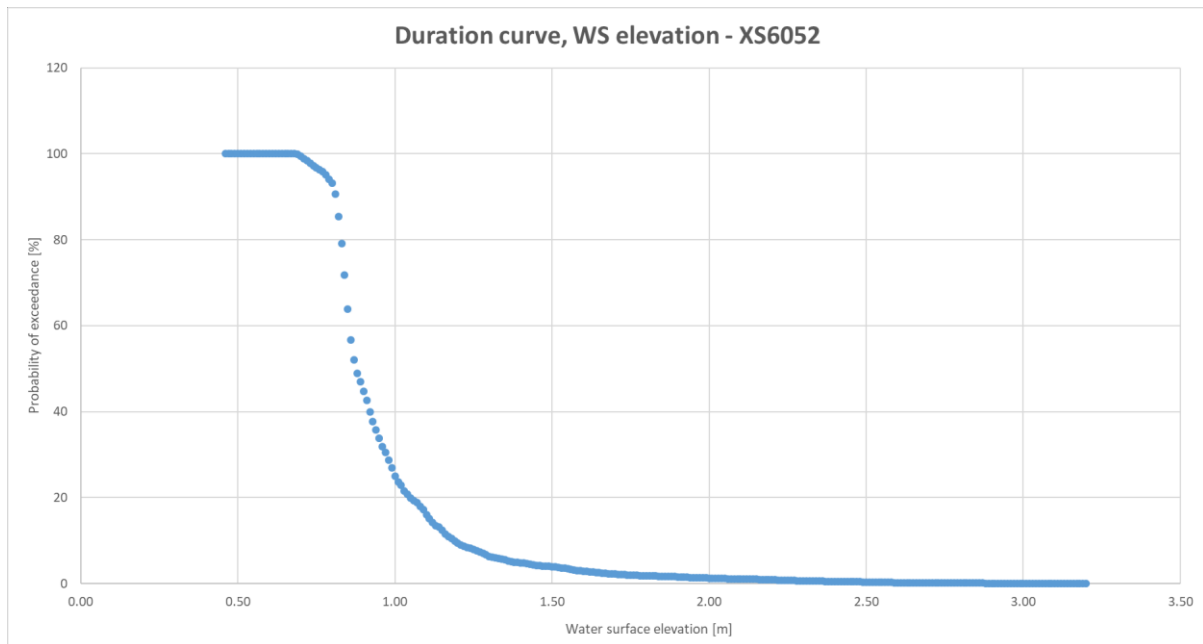


Figure 71 - Water surface duration curve - Cross section 6052

In this case, the value with a probability of exceedance of 90% is equal to 0.81 m.

In order to avoid problems of sediment transport near the river bottom and velocity reduction due to friction effects of the river bottom, each possible turbine configuration should be located at least 0.2 m far from the river bed. So, in this case, we can evaluate a maximum radius for a turbine “ R_{\max} ” equal to 0.3 m.

The procedure reported above has been repeated for all the selected cross-sections and a summary of the minimum activation threshold “ $WS_{90\%}$ ” and the values of the maximum radius of the turbine “ R_{\max} ” at each cross section is reported in Table 14.

Note that use of turbines with $R > R_{\max}$ is still possible, but they will have a higher activation threshold.

Cross section	WS90%	Rmax
XS 6052	0.81 m	30 cm
XS 10569	0.60 m	20 cm
XS 13215	0.79 m	29 cm
XS 25806	0.67 m	23 cm
XS 11134	0.59 m	19 cm
XS 15292	0.51 m	15 cm
XS 17487	0.51 m	15 cm
XS 21008	0.71 m	25 cm

Table 14 - Summary of cross-sections parameters for energetic analysis

Following these assumptions, calculations of the available power for each time interval and for each selected cross-section have been done. As an example, a part of the results for the cross-section 6052 is reported in Table 15.

Time interval	Q tot [m ³ /s]	WS elev* [m]	Chan vel [m/s]	Flow area [m ²]	XS Pav [W]	Turb P av [W]
43101.021	10.87	1	0.45	24.71	1048.60	12.84
43101.042	10.87	1	0.45	24.73	1046.90	12.84
43101.063	10.78	0.99	0.45	24.6	1031.93	12.84
43101.083	10.75	0.99	0.45	24.55	1027.51	12.84
43101.104	10.73	0.99	0.45	24.54	1022.62	12.84
43101.125	10.61	0.99	0.44	24.39	1000.89	12.01
43101.146	10.5	0.98	0.44	24.22	983.75	12.01
43101.167	10.57	0.98	0.44	24.3	996.96	12.01
43101.188	10.58	0.99	0.44	24.34	996.51	12.01
43101.208	10.49	0.98	0.44	24.2	982.56	12.01
43101.229	10.47	0.98	0.44	24.18	978.57	12.01
43101.250	10.59	0.98	0.44	24.32	1000.98	12.01
43101.271	10.71	0.99	0.45	24.5	1020.24	12.84
43101.292	10.73	0.99	0.45	24.53	1023.46	12.84
43101.313	10.61	0.99	0.44	24.38	1001.71	12.01
43101.333	10.48	0.98	0.44	24.2	979.76	12.01
43101.354	10.47	0.98	0.44	24.18	978.57	12.01
43101.375	10.59	0.98	0.44	24.32	1000.98	12.01
43101.396	10.7	0.99	0.45	24.48	1019.05	12.84
43101.417	10.63	0.99	0.44	24.4	1005.74	12.01
43101.438	10.61	0.99	0.44	24.36	1003.36	12.01
43101.458	10.57	0.98	0.44	24.33	994.50	12.01

Table 15 - Available power calculations for whole cross-section (column 6) and in case of a single turbine (column 7)

Finally, the available energy of the entire year, for both the whole cross-section and for the single turbine, has been calculated using equation (18):

$$E_{av} = \sum_i P_{av-i} \Delta t \quad (18)$$

Where P_{av-i} is the available power at the time interval i and Δt the value of the time interval, i.e. 30 minutes in this case.

A summary of the results for each selected cross-section is reported in Table 16, in which the coloured part represents the “High velocity cross-sections”.

XS	Qav	Av stage a.s.l.	Min ch el	Av Stage* [m]	Vav [m/s]	XS E av [kWh]	Flow area av [m ²]	Turb E av [kWh]
6052	11.45	1.36	0.40	0.96	0.44	24407.57	23.70	171.31
10569	11.45	3.03	2.27	0.76	0.97	59957.57	11.08	536.66
13215	11.45	4.47	3.51	0.96	1.10	84933.03	9.61	1761.01
25806	11.45	12.13	11.32	0.81	1.21	109945.01	8.67	1525.47
11134	11.45	3.26	2.52	0.74	0.76	47886.00	13.78	264.62
15292	11.45	5.61	4.96	0.65	1.08	93854.66	9.70	466.64
17487	11.45	6.97	6.32	0.65	1.31	121221.88	8.06	770.77
21008	11.45	9.21	8.38	0.83	1.12	109209.33	9.29	1528.29

Table 16 - Summary of cross-sections parameters

We can observe that:

- comparing the cross-sections with similar distance from the estuary (recalling that the name of each cross-section represents such distance), there are no significant differences in the average velocities between the first four sections of the table and the latter ones (except for cross-section 6052, in which there is the smallest hydraulic gradient);
- the flow area increases in proximity to the estuary, i.e. increase the average stage level.

The latest aspect is crucial in the available energy assessment: if, on one side, the velocities are higher for the cross-sections in yellow (and the available power scales

with the cube of this value), on the other hand the flow area is lower, as well as the average stage too. This implies that, even if the available energy is higher - in general - for the last four sections, the available energy of a single turbine is lower: this is due to the fact that higher values of average stage imply higher activation thresholds and allows for higher R_{\max} of the turbines.

Hence, the four sections selected for their higher values of flux velocity (highlighted in yellow in Table 16) have been discarded for the further analysis, because the complex mooring for the installation of the turbines in those zones would not provide any benefit in energy production.

3.3.2 Turbines configuration

Before performing the energy production calculations, some assumptions were needed in order to make a more accurate assessment, both in terms of feasibility and in terms of parametric choices.

A floating hydrokinetic turbine (Archimedes screw turbine) configuration has been chosen, anchored to the bridge pillars and with supports for the river-bed. The anchorage system has been chosen so that turbines could be easily installed and maintained, and, in terms of calculations, kept near the surface, where higher velocities are reached; the supports instead are supposed to keep the turbine always above a distance of 0.20 m from the river-bed, to avoid sediments transport problems and velocity oscillations due to turbulence, as previously mentioned.

A hypothetical configuration is reported in Figure 72 (note that the supports are not sketched).

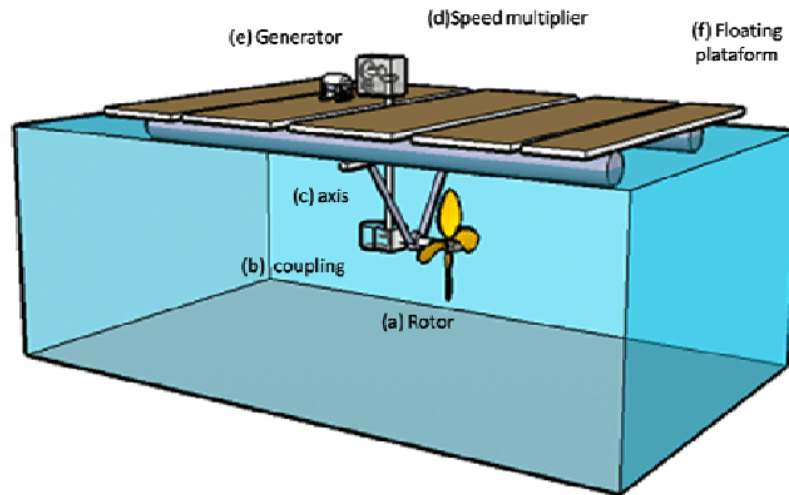


Figure 72 - Turbines configuration scheme (Filho, Bardelli de Rossi, & Mambeli Barros, 2010)

Furthermore, both an aligned configuration and an inclined configuration were assumed. For both cases, maximum values of efficiency C_{pB} , which depends on pitch angle θ and TSR, have been used, assuming an optimal control of the turbine angular velocity.

In particular, recalling the values of Table 4:

- for aligned configuration ($\theta = 0^\circ$), $C_{pB0^\circ} = 0.238$ for $TSR = 0.75$;
- for inclined configuration has been chosen $\theta = 40^\circ$, hence $C_{pB40^\circ} = 0.313$ for $TSR = 1$.

In both cases the value of the efficiency is defined in order to allows the evaluation of the available power using the cross-sectional area of the turbine on a plane perpendicular to the turbine axis, which will allow easier calculations in the following.

Talking about the flux velocity, considering a typical velocity distribution in rivers, reported in Figure 73, the average velocity is considered as the velocity of the flux at a distance of 60% of the whole depth from the water surface. As, for the chosen

configuration, the 60% of the stage is very close to the height of the turbine centre in every case (for each cross-section and at any time interval), the average channel velocity has been considered suitable for the energy calculations phase and assumed as constant.

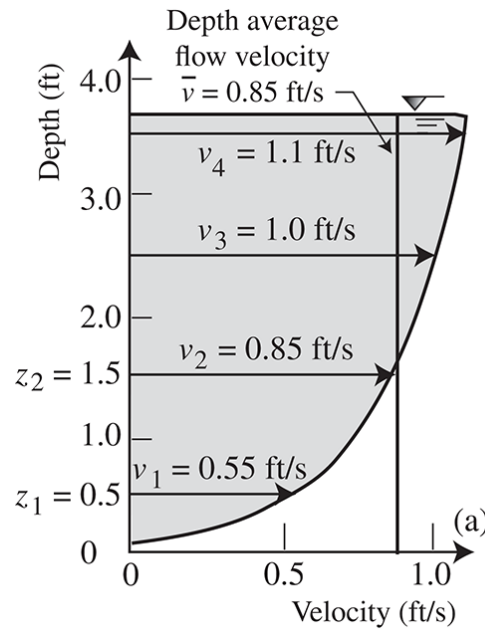


Figure 73 - Typical velocity distribution in rivers

Finally, both aligned and inclined configurations were constituted of a number of turbines in parallel: in order to satisfy the condition of undisturbed flux of the Betz' law, they have been placed at a distance of at least $6R$, between turbine centres in the cross-section plane. In inclined configuration, the distance of $6R$ in the cross-section plane has been ensured between the centre of the front of each turbine and the centre of the rear of the next turbine.

3.3.3 Energetic production calculations

The produced energy has been evaluated for both aligned and inclined configurations, for each cross-section and for different turbines characterized by different radii: $R = 0.20$ m, 0.25 m and $R = 0.30$ m.

Those configurations, after exporting from HEC-RAS the selected cross-sections, have been elaborated in AUTOCAD and are reported in Figure 74 to Figure 81.

For each sketch, the dashed yellow line represents the minimum distance of the turbine from the river bottom, whereas the red line represents the minimum water surface elevation and, lastly, the green line represents the activation threshold the R_{\max} of the specific cross-section.

For each specific turbine, a minimum water surface elevation has been defined: in every time interval in which the water surface does not reach that value, the turbine does not activate and, in terms of calculations, the flux velocity has been taken as null, i.e. a null power contribution has been considered. In such conditions, most probably some power would be extracted actually, i.e. taking those values as null is a conservative measure in terms of energetic production assessment.

The red circle, when present, represent the minimum elevation that the turbine could reach and was useful to calculate the activation threshold of each turbine.

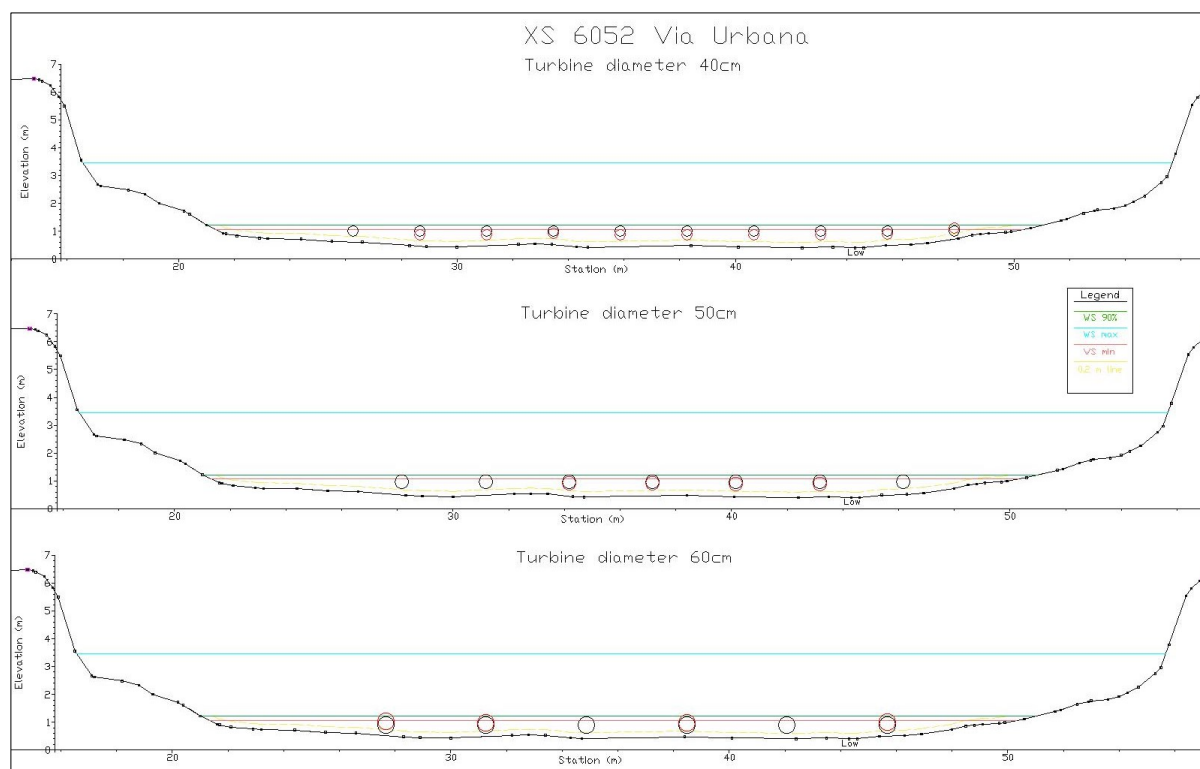


Figure 74 - XS 6052, aligned configurations ($R=0.20$ m, 0.25 m and 0.30 m)

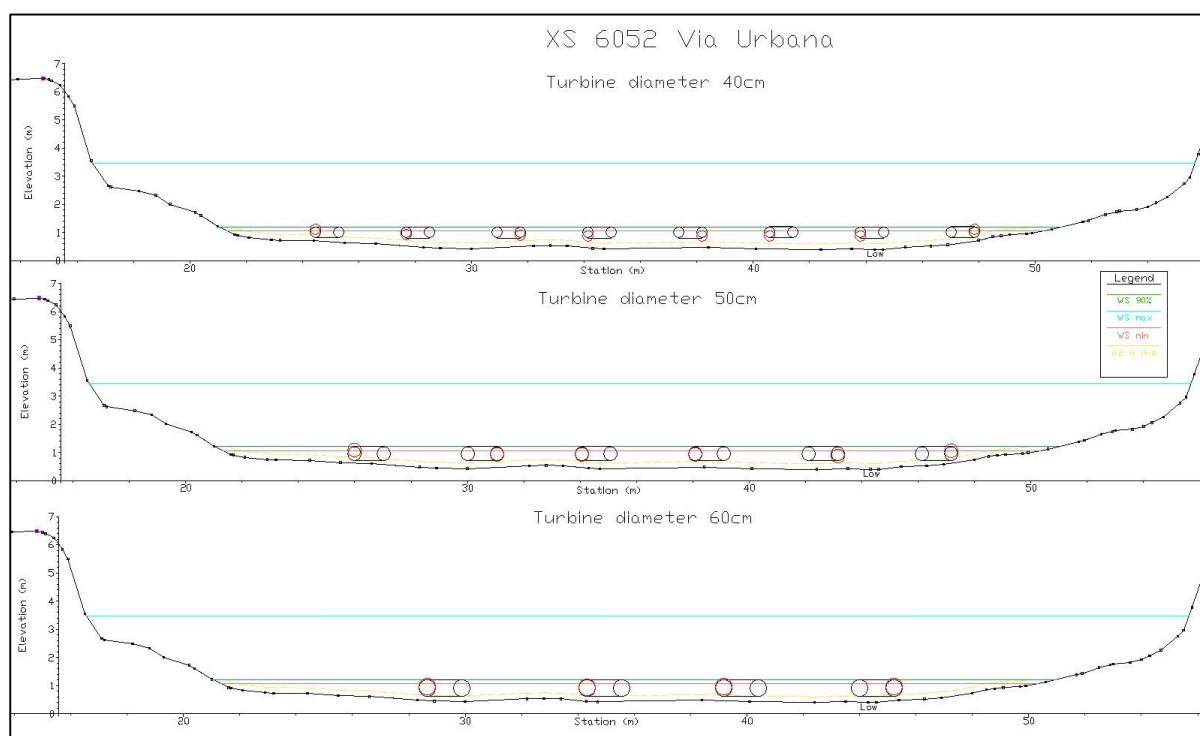


Figure 75 - XS 6052, inclined ($\theta = 40^\circ$) configurations ($R=0.20$ m, 0.25 m and 0.30 m)

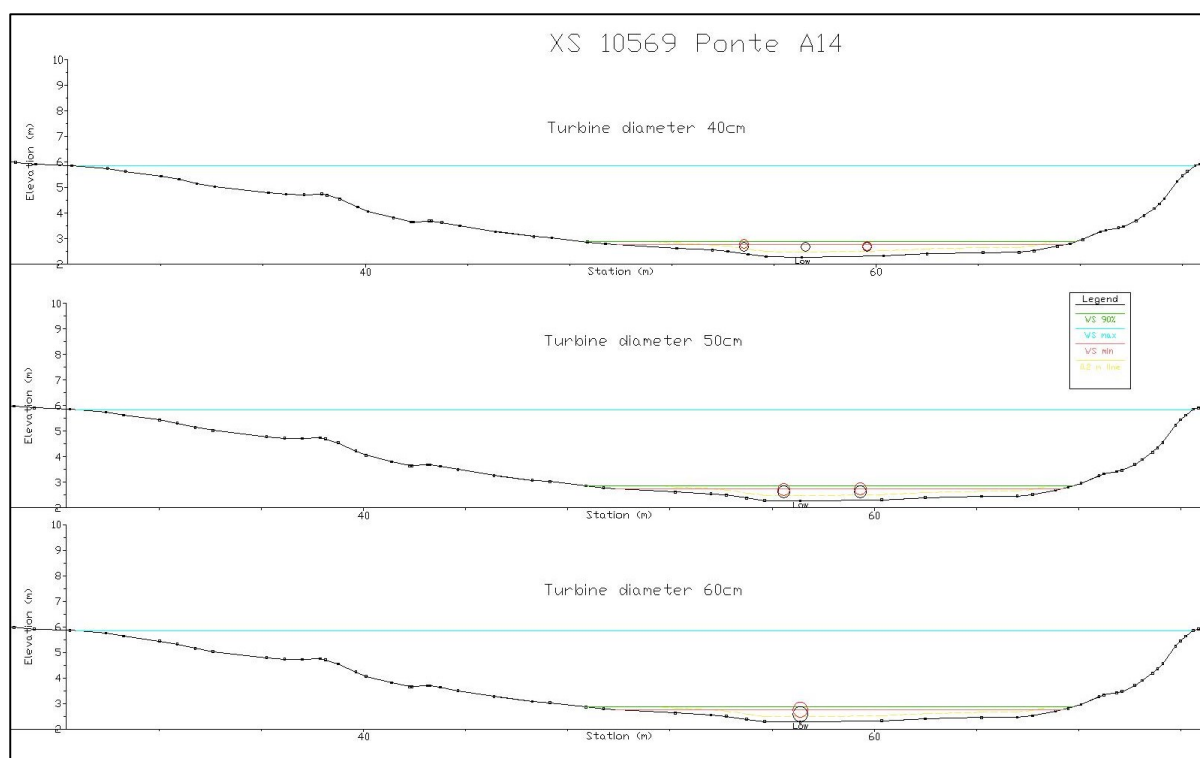


Figure 76 - XS 10569, aligned configurations ($R=0.20$ m, 0.25 m and 0.30 m)

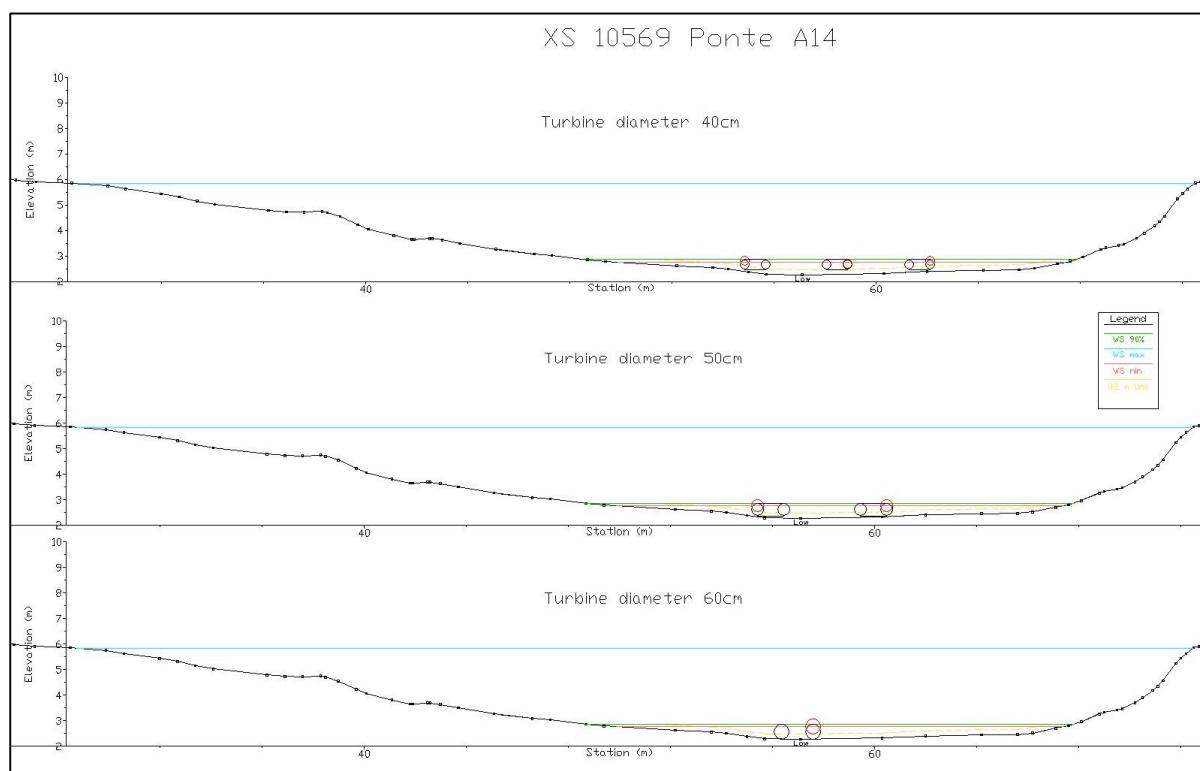


Figure 77 - XS 10569, inclined ($\theta = 40^\circ$) configurations ($R=0.20$ m, 0.25 m and 0.30 m)

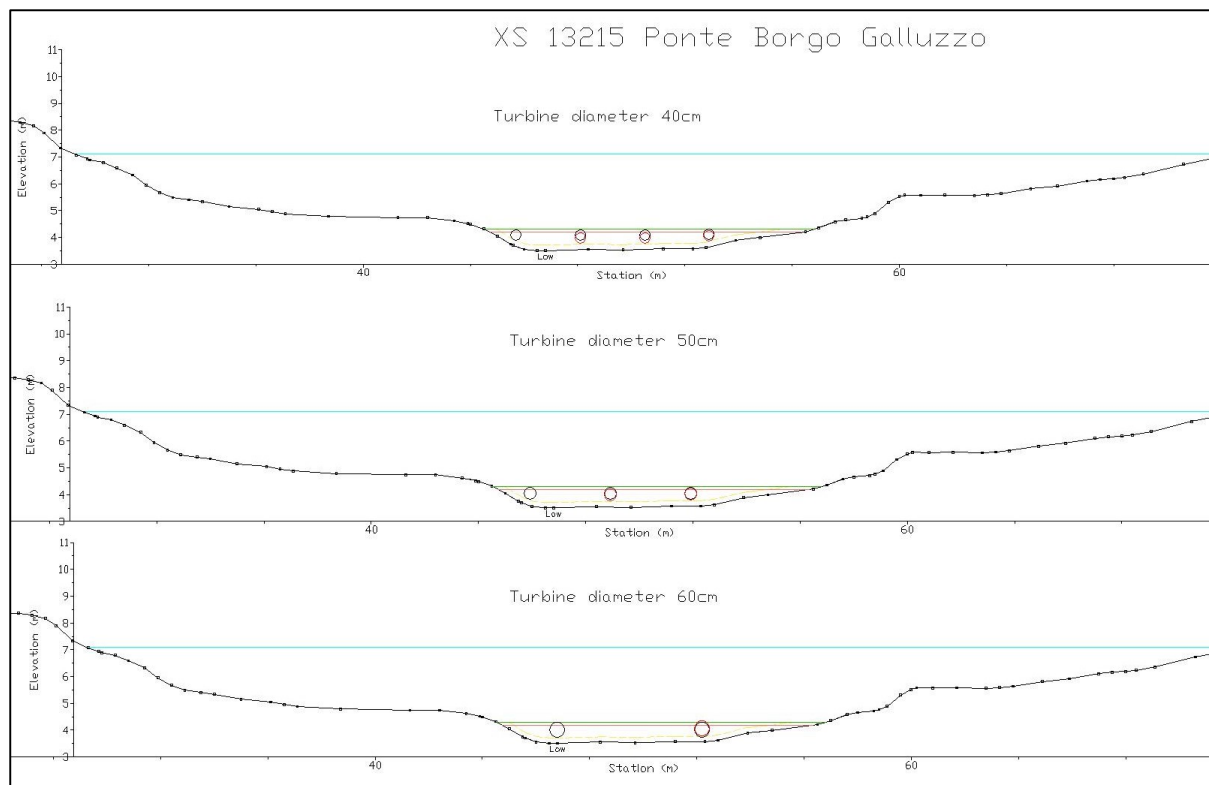


Figure 78 - XS 13215, aligned configurations ($R=0.20\text{ m}$, 0.25 m and 0.30 m)

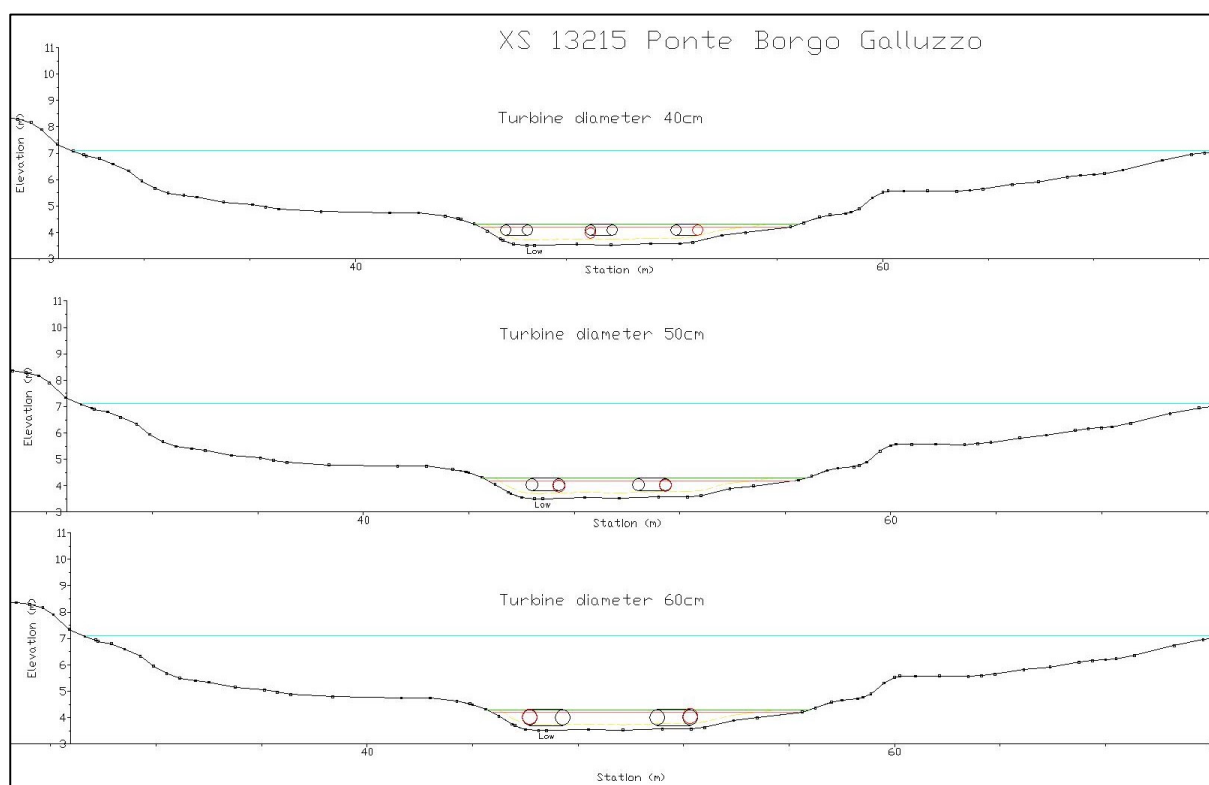


Figure 79 - XS 13215, inclined ($\theta = 40^\circ$) configurations ($R=0.20\text{ m}$, 0.25 m and 0.30 m)

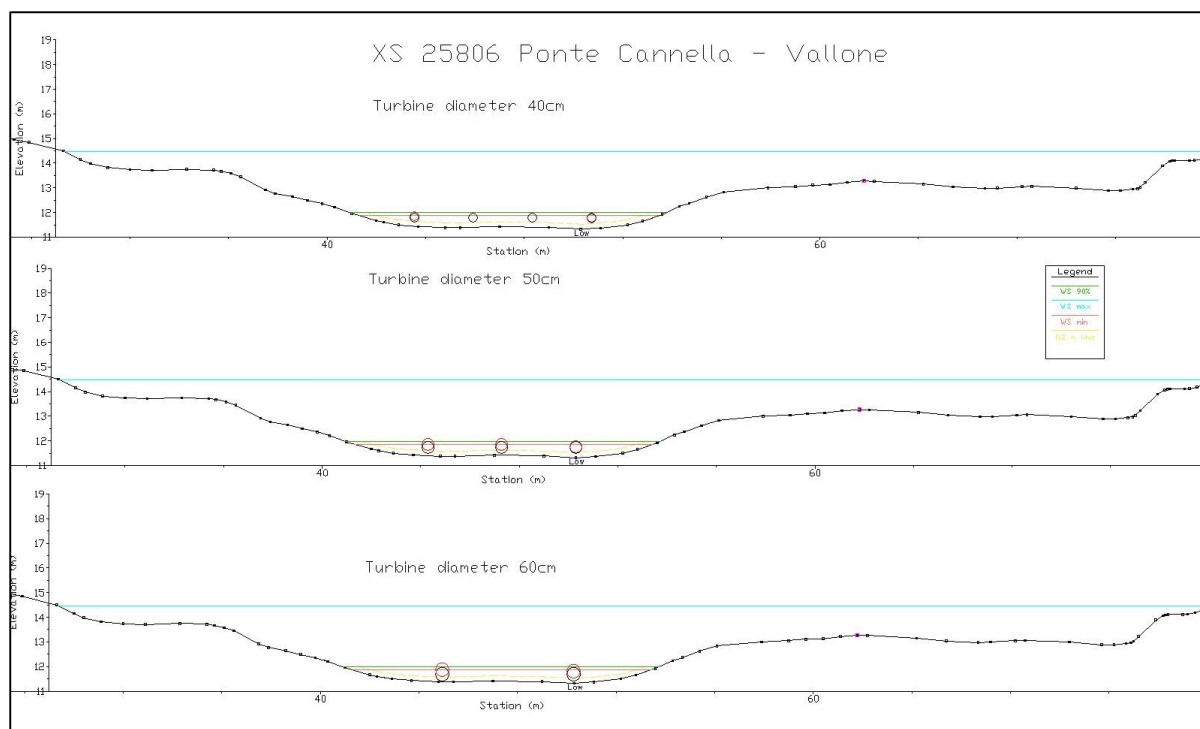


Figure 80 - XS 25806, aligned configurations ($R=0.20$ m, 0.25 m and 0.30 m)

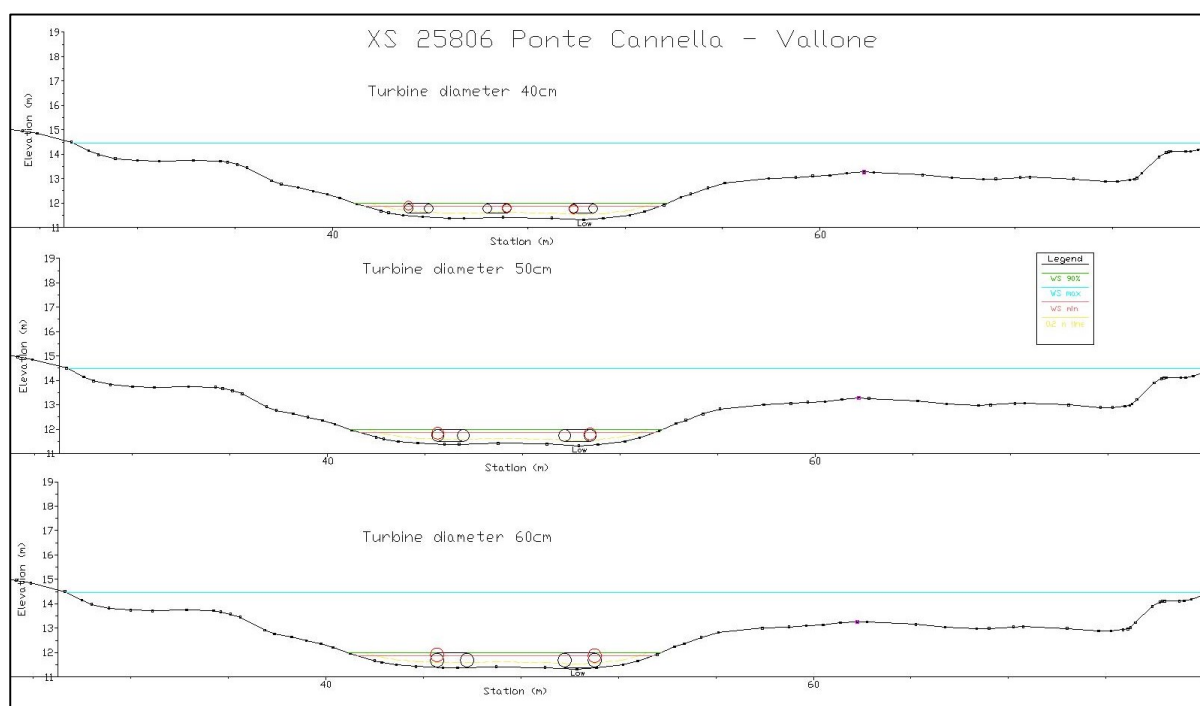


Figure 81 - XS 25806, inclined ($\theta = 40^\circ$) configurations ($R=0.20$ m, 0.25 m and 0.30 m)

Cross-sections 6052, which has low values of average velocities and hydraulic gradient, differently from the other ones, has a high value of average width, which allows to use a large number of turbines, from 4 ($R = 0.30$ m, inclined configuration, Figure 75) up to 10 turbines ($R = 0.20$ m, aligned configuration, Figure 74).

The other cross-sections, instead, are narrower in respect to the previous one, i.e. less turbines could be positioned in such locations, in general from 4 (for $R = 0.20$ m) up to 1 in case of $R = 0.30$ m.

Last thing to observe is that, in some configurations, where radius $R > R_{\max}$ are used, the activation thresholds are higher (position of the red circles reflects this aspect) and its effects in terms of power production will be evaluated; in cross-section 25806, configuration $R = 0.30$ m inclined, this aspect could be observed clearly (Figure 81).

Hence, power production assessment has been performed: as an example, a part of calculation is reported in Table 17, in particular for the inclined configuration of cross-section 25806. For each turbine the column called “Vact” reports the channel velocity if the stage value is higher than the activation water surface threshold, zero otherwise.

Then, the power extracted by each turbine is calculated analogously to the power available, which is multiplied by the power coefficient C_{pB} , which is 0.313 in this case.

Finally, the energy extracted among the whole year is calculated multiplying each contribution of power extracted for the time interval, (30 minutes) and then summing them.

SECTION	minWS	val90%	Configuration R=20cm						Configuration R=25cm						Configuration R=30cm					
			T20.1		T20.2		T20.3		T25.1		T25.2		T30.1		T30.2					
Date	WS elev*	Chan vel [m/s]	Vact[m/s]	Pext[W]	Vact[m/s]	Pext[W]	Vact[m/s]	Pext[W]	Vact[m/s]	Pext[W]	Vact[m/s]	Pext[W]	Vact[m/s]	Pext[W]	Vact[m/s]	Pext[W]				
1/1/2018	0.55	0.67	1.22	35.604	1.220	35.604	1.220	35.604	1.220	55.631	1.220	55.631	0.000	0.000	1.220	80.109				
1/1/2018	0.85	1.22	1.220	35.604	1.220	35.604	1.220	35.604	1.220	55.631	1.220	55.631	0.000	0.000	1.220	80.109				
1/1/2018	0.85	1.22	1.220	35.604	1.220	35.604	1.220	35.604	1.220	55.631	1.220	55.631	0.000	0.000	1.220	80.109				
1/1/2018	0.84	1.21	1.210	34.736	1.210	34.736	1.210	34.736	1.210	54.274	1.210	54.274	0.000	0.000	0.000	0.000				
1/1/2018	0.83	1.21	1.210	34.736	1.210	34.736	1.210	34.736	1.210	54.274	1.210	54.274	0.000	0.000	0.000	0.000				
1/1/2018	0.84	1.22	1.220	35.604	1.220	35.604	1.220	35.604	1.220	55.631	1.220	55.631	0.000	0.000	0.000	0.000				
1/1/2018	0.85	1.22	1.220	35.604	1.220	35.604	1.220	35.604	1.220	55.631	1.220	55.631	0.000	0.000	1.220	80.109				
1/1/2018	0.85	1.22	1.220	35.604	1.220	35.604	1.220	35.604	1.220	55.631	1.220	55.631	0.000	0.000	1.220	80.109				
1/1/2018	0.84	1.21	1.210	34.736	1.210	34.736	1.210	34.736	1.210	54.274	1.210	54.274	0.000	0.000	0.000	0.000				
1/1/2018	0.83	1.21	1.210	34.736	1.210	34.736	1.210	34.736	1.210	54.274	1.210	54.274	0.000	0.000	0.000	0.000				
1/1/2018	0.84	1.22	1.220	35.604	1.220	35.604	1.220	35.604	1.220	55.631	1.220	55.631	0.000	0.000	0.000	0.000				
1/1/2018	0.85	1.22	1.220	35.604	1.220	35.604	1.220	35.604	1.220	55.631	1.220	55.631	0.000	0.000	1.220	80.109				
1/1/2018	0.85	1.22	1.220	35.604	1.220	35.604	1.220	35.604	1.220	55.631	1.220	55.631	0.000	0.000	1.220	80.109				
1/1/2018	0.84	1.21	1.210	34.736	1.210	34.736	1.210	34.736	1.210	54.274	1.210	54.274	0.000	0.000	0.000	0.000				
1/1/2018	0.83	1.21	1.210	34.736	1.210	34.736	1.210	34.736	1.210	54.274	1.210	54.274	0.000	0.000	0.000	0.000				
1/1/2018	0.84	1.22	1.220	35.604	1.220	35.604	1.220	35.604	1.220	55.631	1.220	55.631	0.000	0.000	0.000	0.000				
1/1/2018	0.85	1.22	1.220	35.604	1.220	35.604	1.220	35.604	1.220	55.631	1.220	55.631	0.000	0.000	1.220	80.109				
1/1/2018	0.84	1.21	1.210	34.736	1.210	34.736	1.210	34.736	1.210	54.274	1.210	54.274	0.000	0.000	0.000	0.000				
1/1/2018	0.83	1.21	1.210	34.736	1.210	34.736	1.210	34.736	1.210	54.274	1.210	54.274	0.000	0.000	0.000	0.000				
1/1/2018	0.82	1.2	1.200	33.882	1.200	33.882	1.200	33.882	1.200	52.940	1.200	52.940	0.000	0.000	0.000	0.000				
1/1/2018	0.82	1.2	1.200	33.882	1.200	33.882	1.200	33.882	1.200	52.940	1.200	52.940	0.000	0.000	0.000	0.000				
1/1/2018	0.82	1.2	1.200	33.882	1.200	33.882	1.200	33.882	1.200	52.940	1.200	52.940	0.000	0.000	0.000	0.000				
1/1/2018	0.82	1.2	1.200	33.882	1.200	33.882	1.200	33.882	1.200	52.940	1.200	52.940	0.000	0.000	0.000	0.000				
1/1/2018	0.82	1.2	1.200	33.882	1.200	33.882	1.200	33.882	1.200	52.940	1.200	52.940	0.000	0.000	0.000	0.000				
1/1/2018	0.8	1.19	1.190	33.042	1.190	33.042	1.190	33.042	1.190	51.627	1.190	51.627	0.000	0.000	0.000	0.000				
1/1/2018	0.81	1.2	1.200	33.882	1.200	33.882	1.200	33.882	1.200	52.940	1.200	52.940	0.000	0.000	0.000	0.000				
1/1/2018	0.83	1.21	1.210	34.736	1.210	34.736	1.210	34.736	1.210	54.274	1.210	54.274	0.000	0.000	0.000	0.000				
1/1/2018	0.85	1.23	1.230	36.487	1.230	36.487	1.230	36.487	1.230	57.010	1.230	57.010	0.000	0.000	0.000	0.000				
1/1/2018	0.88	1.24	1.240	37.384	1.240	37.384	1.240	37.384	1.240	58.412	1.240	58.412	0.000	0.000	0.000	0.000				
1/1/2018	0.89	1.25	1.250	38.296	1.250	38.296	1.250	38.296	1.250	59.837	1.250	59.837	0.000	0.000	0.000	0.000				
1/1/2018	0.9	1.26	1.260	39.272	1.260	39.272	1.260	39.272	1.260	61.285	1.260	61.285	0.000	0.000	0.000	0.000				

In Table 18, a summary of the results is reported.

The configurations highlighted in yellow are the ones for $R = R_{\max}$, in order to better evaluate the influence of the value of the activation threshold in the annual energy production.

	Configurations											
XS	Aligned (θ=0°)						Inclined (θ=40°)					
	R =20 cm		R =25 cm		R =30cm		R =20 cm		R =25 cm		R =30cm	
6052	N turb	E ext [kWh]	N turb	E ext [kWh]	N turb	E ext [kWh]	N turb	E ext [kWh]	N turb	E ext [kWh]	N turb	E ext [kWh]
	1	17.29	1	27.52	1	30.82	1	18.30	1	28.15	1	44.22
	2	18.12	2	27.52	2	32.68	2	23.70	2	36.74	2	48.49
	3	18.12	3	28.03	3	39.62	3	23.76	3	36.81	3	45.28
	4	18.05	4	28.03	4	33.06	4	23.83	4	36.74	4	44.22
	5	18.12	5	28.16	5	39.62	5	23.83	5	37.08		
	6	18.12	6	28.20	6	32.27	6	23.83	6	28.59		
	7	18.12	7	27.52			7	23.83				
	8	18.12					8	18.30				
	9	18.12										
	10	13.91										
	TOT	176.09	TOT	194.96	TOT	208.08	TOT	179.38	TOT	204.10	TOT	182.21
	E/turb	17.61	E/turb	27.85	E/turb	34.68	E/turb	22.42	E/turb	34.02	E/turb	45.55
10569	N turb	E ext [kWh]	N turb	E ext [kWh]	N turb	E ext [kWh]	N turb	E ext [kWh]	N turb	E ext [kWh]	N turb	E ext [kWh]
	1	58.88	1	102.41	1	108.38	1	77.44	1	111.53	1	132.66
	2	120.56	2	92.01			2	140.28	2	111.53		
	3	95.77					3	80.05				
	TOT	275.22	TOT	194.41	TOT	108.38	TOT	297.77	TOT	223.07	TOT	132.66
	E/turb	91.74	E/turb	97.21	E/turb	108.38	E/turb	99.26	E/turb	111.53	E/turb	132.66
13215	N turb	E ext [kWh]	N turb	E ext [kWh]	N turb	E ext [kWh]	N turb	E ext [kWh]	N turb	E ext [kWh]	N turb	E ext [kWh]
	1	191.65	1	299.45	1	431.20	1	252.04	1	407.37	1	494.38
	2	199.34	2	308.33	2	326.38	2	262.16	2	402.15	2	429.23
	3	199.34	3	305.79			3	256.29				
	4	196.71										
	TOT	787.04	TOT	913.57	TOT	757.58	TOT	770.49	TOT	809.53	TOT	923.61
E/turb	196.76	E/turb	304.52	E/turb	378.79	E/turb	256.83	E/turb	404.76	E/turb	461.80	
25806	N turb	E ext [kWh]	N turb	E ext [kWh]	N turb	E ext [kWh]	N turb	E ext [kWh]	N turb	E ext [kWh]	N turb	E ext [kWh]
	1	197.77	1	265.15	1	327.66	1	239.66	1	364.35	1	398.15
	2	262.18	2	258.51	2	361.67	2	286.68	2	406.40	2	430.92
	3	262.18	3	309.02			3	354.74				
	4	269.74										
	TOT	991.88	TOT	832.67	TOT	689.33	TOT	881.08	TOT	770.75	TOT	829.06
E/turb	247.97	E/turb	277.56	E/turb	344.67	E/turb	293.69	E/turb	385.38	E/turb	414.53	

Table 18 - Energetic analysis results summary referring to one year

Table 19 the percentages of the total annual energy extracted from every configuration in respect to the total available energy of the whole cross-section are reported; the scale of colour highlights greatest percentages (in green) to the worst ones (in red).

XS	$\theta=0^\circ$		$\theta=40^\circ$	
	R	% of all XS	R	% of all XS
6052	20	0.721	20	0.7349313
	25	0.799	25	0.8362273
	30	0.853	30	0.7465455
10569	20	0.459	20	0.496632
	25	0.324	25	0.3720401
	30	0.181	30	0.2212582
13215	20	0.927	20	0.9071731
	25	1.076	25	0.9531345
	30	0.892	30	1.087455
25806	20	0.902	20	0.8013813
	25	0.757	25	0.7010338
	30	0.627	30	0.7540722

Table 19 - Percentage of energy extracted of each configuration

4 DISCUSSION

Analysing the summary of the energy production (Table 18), the first thing to highlight is that the best results, in terms of extracted energy/turbine, are for configurations with $R = 30$ cm, even if use of turbine with value $R > R_{\max}$, determined for each cross-section in chapter 3.3.1 (Table 14), would lower the activation threshold.

Hence, cross-sections with high average stage value are more flexible to different configurations, have higher value of available energy (Table 16) and are more efficient in terms of extracted energy by the turbine above the whole cross-section (Table 19).

In Figure 82 to 85, the comparisons of energy production between all the configuration for each cross-section are reported.

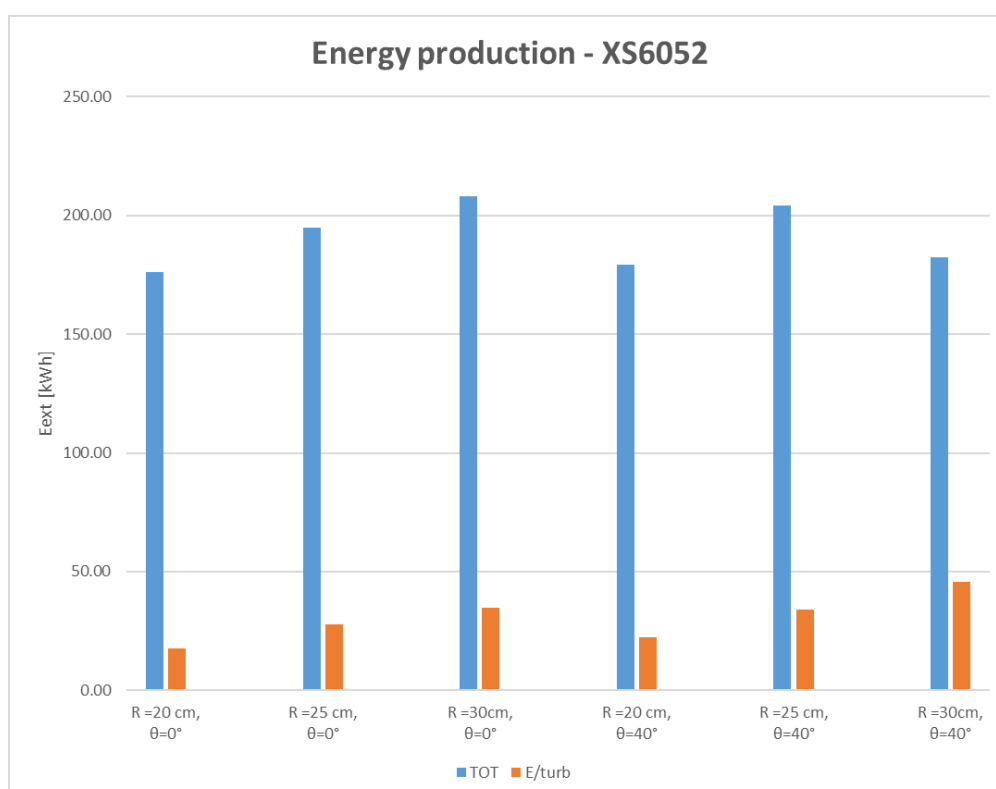


Figure 82 - Energy production, all configurations – XS6052

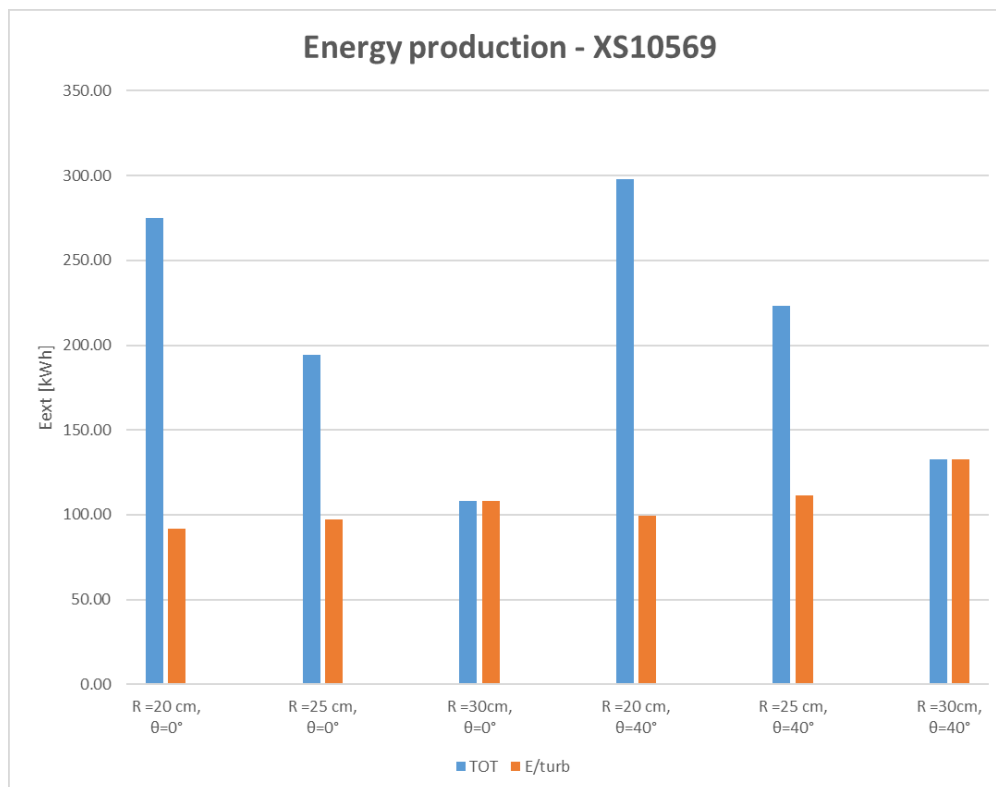


Figure 83 - Energy production, all configurations – XS10569

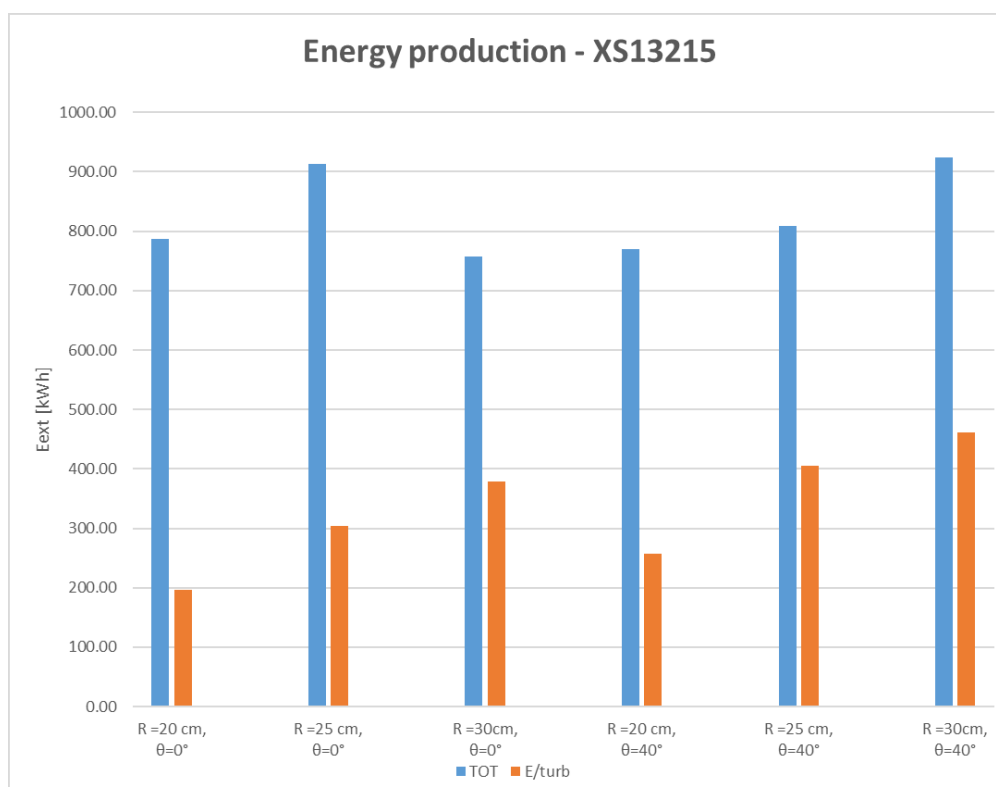


Figure 84 - Energy production, all configurations - XS13215

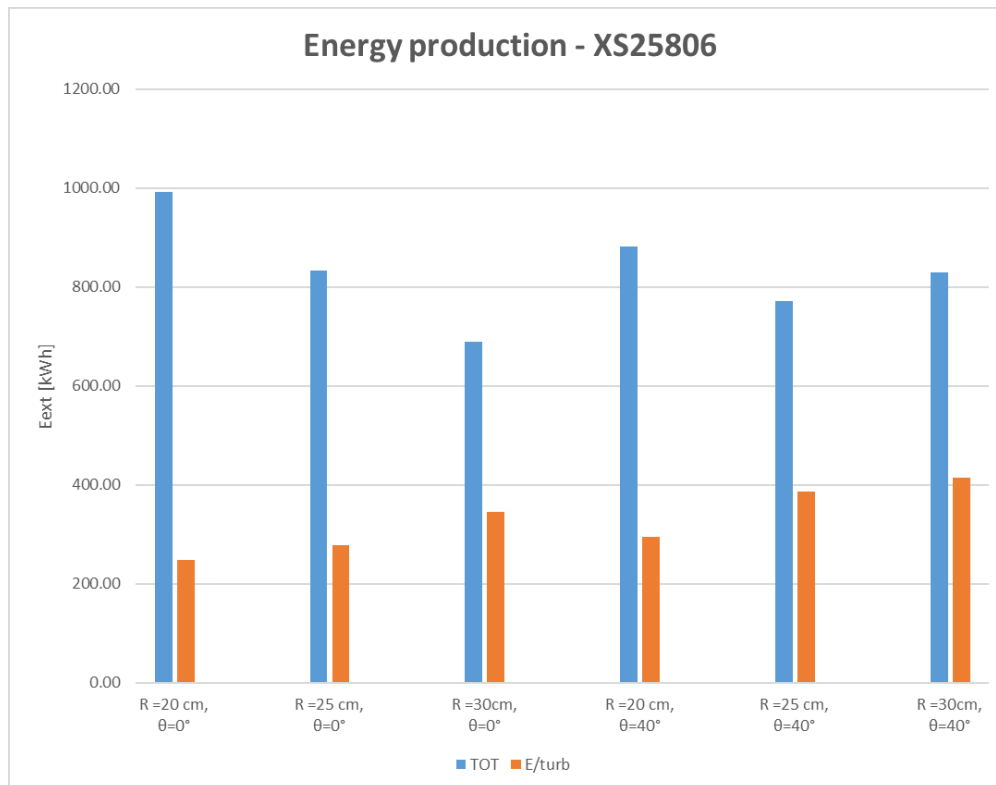


Figure 85 - Energy production, all configurations – XS25806

As shown, the trend of extracted energy per turbine (orange columns) is the same in all case, i.e. the higher is the radius of the turbine, the higher is the extracted energy.

On the other hand, another important aspect is such that the total extracted energy does not have a common trend in all cases. This is due to the fact that in each specific configuration, a variable number of turbine can be used and, for the same cross-section, in some configurations with lower value of $E_{\text{ext}}/\text{turb}$ leads to a greater amount of total extracted energy.

Considering the inclination of the turbine, comparing configurations with the same radius, the inclined configurations have higher values of $E_{\text{ext}}/\text{turb}$ but not always greater amounts of total extracted energy, due to the fact that they need to be set with wider spacing, (i.e., in some cases, fewer turbines can be used if inclined).

Moreover, when installing the turbine, the value of the activation threshold has to be considered, because it leads to longer working periods of the turbine during the year, avoiding “dead periods”.

Furthermore, the higher amounts of extracted energy are for cross-sections located more upstream, due to higher hydraulic gradients (i.e. higher average velocities) and narrower geometries, which lead to higher values of average stage.

It is important to keep in consideration one more aspect: if the absolute value of extracted energy is important in terms of energy harvesting, on the other hand the specific extracted energy per turbine is a key parameter when evaluating the worthiness of each configuration. This aspect is very important under the economic point of view, as the cost of the investments strongly depends by the number of turbine used.

As an example, possible gaining in 5 years have been assessed, considering an energy cost of 0.501 €/kWh (market price at present days).

Cross-section	Configuration	Earning [€]	# of turbines	€/turbine
6052	R =30cm, $\theta=0^\circ$	521.25	6	86.87
10569	R =20 cm, $\theta=40^\circ$	745.91	3	248.64
13215	R =30cm, $\theta=40^\circ$	2313.64	2	1156.82
25806	R =20 cm, $\theta=0^\circ$	2484.65	4	621.16

Table 20 - Possible gaining - best configuration for each XS

5 CONCLUSIONS

This thesis focused on the assessment of the potential power production of a hydrokinetic turbine, already object of study in the Hydraulics laboratory of UNIVPM, in a hypothetical application along the final stretch of Misa River, on the basis of the results coming from a hydraulic numerical model constructed through the use of the HEC-RAS software. By analysing the hydrometric data coming from the Civil Protection of the Marche Region website (SIRMIP), a preliminary statistical study has been performed in order to select a typical year, for which the data to build up the model have been extracted. The statistical study consisted of the construction of duration curves of all the available years, i.e. from 2005 to 2020, and following calculation of the their RMSEs of the probability of exceedance in respect to the average duration curve. The year 2012 show the lower value of RMSE (1.41%) but, considering the lack of data (about 50 %), it has been considered unreliable and 2018, which has the second lower value of RMSE (1.98%) and, for which, all the data were available, has been selected as typical year. Afterwards, the model has been calibrated, acting mostly on input parameters, such as Manning coefficients and boundary conditions. The calibration has been performed on a three-weeks period, between February and March 2018, following a series of steps, some dependent on year selection, some based on considerations done during the work. For each step, the RMSE, found using the modelled stage coming from the software and the measured stage from SIRMIP, has been calculated: the calibration has been considered over once it reached the value 0.0649 m, which was lower enough for the accuracy this work needed. Finally, the

results of the simulated year, such as channel velocity and river stage along the whole river stretch, have been used to choose possible locations and configurations of different systems of hydrokinetic turbines (specifically, the Archimedes screw turbine) and to perform an energy production assessment. In particular, four sections have been chosen, each of them related to the four bridges present in the simulated river stretch. Calculations have been done for configurations characterized by different radii ($R = 0.20 \text{ m}$, 0.25 m and 0.30 m), as well as by either aligned turbines or inclined (with $\theta = 40^\circ$) turbines, in order to both look for the best configuration above all the cross sections, and to analyse the influence of the two parameters (R and θ) in the power production. In details, a larger radius corresponds to higher value of extracted power (even it leads to a higher activation threshold, i.e. to more inactive periods of the turbine). On the other hand, inclined configurations give a higher value of extracted energy per single turbine, but, as they need more spacing, this does not lead to higher values of total energy production, because less turbines could be used if compared to aligned configurations (in the same section).

Among all the studied configurations, the best cases resulted to be the ones relative to cross sections with higher average velocities and average stages, in particular:

- Cross-section 13215, with $R = 0.30 \text{ m}$, $\theta = 40^\circ$, $E_{\text{ext}} = 923.61 \text{ kWh}$ in 1 year;
- Cross-section 25806, with $R = 0.20 \text{ m}$, $\theta = 0^\circ$, $E_{\text{ext}} = 991.88 \text{ kWh}$ in 1 year.

From an economic perspective, the possible saving in 5 years using such configurations are similar (about 2500 €, considering the actual market energy price of 0.501 €/kWh), but, as the first configuration produces a similar amount of energy using only 2 turbines

(the latter is made by 4 turbines), it results to be the best configuration. Still, the energy production is relatively low in respect to typical energy consumption of developed countries; however, this technology could be useful in other scenarios: specifically, little rural communities with relatively small energy demand could benefit from the energy generated by Archimedes screw turbines, whose production is in line with the consumption of some community services (e.g., electricity for schools, kindergartens, churches, hospitals), as evaluated for rural areas of developing and least developed countries (Kirubi, Jacobson, Kammen, & Mills, 2009).

6 REFERENCES

- Brocchini, M., Calantoni, Postacchini, M., Sheremet, A., Staples, T., Smith, J., . . . Soldini, L. (2017). Comparison between the wintertime and summertime dynamics of the Misa River estuary.
- Filho, G., Bardelli de Rossi, & Mambeli Barros, R. (2010). "Poraque" hydrokinetic turbine.
- Ilari, M. (2021). Hydrodynamic modeling of the final reach of the Misa River (Senigallia, Italy): the role of sea action and bed forms.
- ISPRA. (s.d.). *Rete mareografica nazionale*. Tratto da <https://www.mareografico.it/>
- Khan, B. I. (2009). Hydrokinetic energy conversion systems and assessment of horizontal and vertical.
- Kirubi, C., Jacobson, A., Kammen, D., & Mills, A. (2009). Community-Based Electric Micro-Grids Can Contribute to Rural Development: Evidence from Kenya.
- Martinelli, J. (2021). Hydrodynamic modeling of the final reach of the Misa River (Senigallia, Italy): model setup and calibration.
- Postacchini M., Z. G. (2021). Slides of the course.
- Postacchini, M., & Zitti, G. (2021). Slides of the course.
- Pritchard, D. (1967). What is an estuary: physical viewpoint.
- Regione Marche - Autorità di Bacino Regionale. (2016). *Assetto di progetto media e bassa valle del Fiume Misa*.

SIRMIP. (s.d.). *Sistema Informativo Regionale Meteo-Idro-Pluviometrico*. Tratto da

SIRMIP

ONLINE:

<http://app.protezionecivile.marche.it/sol/registrazione.sol?lang=it>

US Army Corps of Engineers Institute for Water Resources Hydrologic Engineering centre. (2020). HEC-RAS Reference manual, version 6.0.

Vermaak, K. K. (2013). Status of micro-hydrokinetic river technology in rural applications: review of literature.

Wikipedia. (s.d.). *River channels*. Tratto da Wikipedia, the free encyclopedia: <https://en.wikipedia.org/wiki/River>

Zitti, G., Fattore, F., Brunori, A., Brunori, B., & Brocchini, M. (2019). Efficiency evaluation of a ductless Archimedes turbine: Laboratory experiments and numerical simulations.

Zitti, G., Fattore, F., Brunori, A., Brunori, B., & Brocchini, M. (2019). Numerical investigation on the effects of the pitch angle on the efficiency of an Archimedean-type turbine.

7 ACKNOWLEDGMENTS

I would like to express all my gratitude to my advisor, Dr. Matteo Postacchini, and to my co-advisors, Dr. Gianluca Zitti and Dr. Eleonora Perugini, who guided me during the internship first and then during the drafting of this thesis, for their assistance at every stage of the research project and for their insightful comments and suggestions.

Then, I wish to express my warmest thanks to my parents, Federico and Alba, and to my brother Tommaso, for always (at least almost always) having supported me through my university course, trusted me in spite of everything.

Special thanks to my grandparents, in particular way to my grandmother Giovanna, who has always encouraged me, who would have been so proud to see me today – finally- and who could not for so little.

Last but not the least, I would like to extend my sincerest thanks to everybody else that has been, is and will be part of my life: my Uncles, Aunts, Cousins and all my Friends as well, for making me who I am (“Not such a great job” I would say, but still... but you have to go with it!).